System Flexibility and AI Computational Enhancement for Day-Ahead Power System

Operations

by

Arun Venkatesh Ramesh

A report submitted to the Department of Electrical and Computer Engineering,

Cullen College of Engineering

in partial fulfillment of the requirements for the degree of

Doctor of Philosophy

in Electrical and Computer Engineering

Chair of Committee: Dr. Xingpeng Li

Committee Member: Dr. Kaushik Rajashekara

Committee Member: Dr. Harish Krishnamoorthy

Committee Member: Dr. Lei Fan

Committee Member: Dr. Jian Shi

University of Houston

December 2022

ACKNOWLEDGMENT

I would like to express my sincere gratitude to Dr. Xingpeng Li for providing me the opportunity to conduct my Ph.D. studies at the Renewable Power Grid lab at the University of Houston. His mentorship, advice, and encouragement throughout the past four years have been invaluable for the development of this research. I would like to thank Prof. Kaushik Rajasekhara for the continuous support and encouragement through my program. I would also like to thank Dr. Harish Krishnamoorthy, together with Dr. Lei Fan, and Dr. Jian Shi, for being part of my dissertation committee and providing valuable insights on how to improve this dissertation.

I would also like to thank already graduated students Dr. Amin Sadat, Dr. Yu Yao, Dr. Shilei Jiao, and Dr. Jean de Lobo Fonseca together with current students Mingjian Tuo, Cunzhi Zhao, Thuan Pham, Jin Lu, Jesus Silva, Vinay Rathore, and Hussain Sayed, for the supportive discussions and camaraderie while pursuing this program.

I would like to thank my parents, Ramesh Arunachalam and Mythili Ramesh, for all their love, support, and patience in the last four years of my academic life. Finally, I would like to dedicate this work to Deepak Ramesh (in memoriam), brother, and mentor who always encouraged me to pursue academic excellence.

ABSTRACT

Smart grids play a critical part in today's world and is paramount to optimize the usage of energy and to address the increasing penetration of renewable energy sources (RES). The power system is a complicated network of electrical elements and requires efficient operation. The day-ahead operations use the security-constrained unit-commitment (SCUC) to provide a reliable, secure, and least-cost solution while clearing the market for forecasted demand. However, existing power system operations do not use available system flexibility in the form of transmission network or demand response exhaustively. Operators rely on experience to use these resources and disregard the economic benefit of such technologies. Hence, the importance of strategies such as corrective network reconfiguration (CNR) and corrective demand response (CDR) as an economic tool are initially explored.

Network reconfiguration is considered for superior economic incentive. In addition, it enables integration of RES, efficient utilization of energy storage, and reducing carbon emission in high penetration systems. This is implemented by reducing curtailment of RES and relieving system congestion, while also addressing reducing carbon emissions. However, due to the complexity added to existing SCUC model, such solutions are not scalable to practical systems.

To address computational efficiency to SCUC, considering substantial economic incentive tools like CNR, two novel remedies are identified in this thesis:

(1) A purely optimization-based technique is shown by utilizing benders decomposition by breaking a large SCUC model into master problem and sub-problems. The proposed approach is iteratively solved by effectively screening non-critical sub-problems to handle the computational complexity. Simulation results points to scalability to large practical power system networks.

(2) A novel approach by leveraging machine learning (ML) to learn patterns between system demand profile and generator commitment schedule using historical information is developed. The ML would assist with innovative post-processing methods and create a feasibility layer to improve predictions that would result in a reduced model for problem size reduction of SCUC. The proposed approach with selective utilizing of ML predictions can bring substantial computational benefits. This is achieved without loss in solution quality while being easily extendible to any decomposed, heuristic, or sped-up algorithms for SCUC.

TABLE OF CONTENTS

LIST OF TABLES

LIST OF FIGURES

NOMENCLATURE

Sets and indices:

g	Generator index.
k	Transmission element (line or transformer) index.
t	Time period index.
n	Bus index.
c	Line contingency index.
C	Set of non-radial transmission contingencies.
$e(n)$	Set of ESS connected to bus n.
G	Set of generators.
G_c	Set of all generator contingencies.
$g(n)$	Set of generators connecting bus n.
K	Set of all transmission element.
K_c	Set of all non-radial line contingencies.
M	Total samples.
M^{test}	Test Samples.
M^{train}	Training Samples.
N	Set of all buses.
$N(g)$	Bus location of generator g.
T	Set of Time intervals.
W	Set of renewable units.
$w(n)$	Set of RES units connected to bus n.
$\delta^+(n)$	Set of lines with bus n as receiving bus.
$\delta^-(n)$	Set of lines with bus n as sending bus.
Ω^{cri}	Set of all critical sub-problems.
Ω_1^{inf}	Set of infeasible PCFC sub-problems.

Ω_2^{inf}	Set of infeasible NR-PCFC sub-problems.
ψ	Cut-set determined for all sub-problems.

Parameters:

b_k	Susceptance of line k.
c_g	Linear cost for generator g.
c_g^{NL}	No-load cost for generator g.
c_g^{SU}	Start-up cost for generator g.
c_n^{Ctg}	Cost of CDR at bus n.
c_w^{pen}	Penalty for energy curtailed for RES w.
$d_{n,t}$	Predicted demand of bus n in time period t.
$d_{n,t}^m$	Predicted demand of bus n in time period t for generated sample m.
$d_{n,t}^{ini}$	Initial nodal demand of bus n in time period t for a test system.
DT_g	Minimum down time for generator g.
ESS_e^{max}	Maximum energy capacity of ESS e.
M	A big real number.
P_g^{min}	Minimum capacity of generator g.
P_g^{max}	Maximum capacity of generator g.
P_k^{max}	Long-term thermal line limit for line k.
P_k^{emax}	Emergency thermal line limit for line k.
$Pmax_e^{cha}$	Maximum charging power for ESS e.
$Pmax_e^{dis}$	Maximum discharging power for ESS e.
$P_{w,s}^{max}$	Maximum capacity of RES w in scenario s.
R_g^{hr}	Regular hourly ramping limit of generator g.
R_g^{SU}	Start-up ramping limit of generator g.

R_g^{SD}	Shut-down ramping limit of generator g.
R_g^{10}	10-minute outage ramping limit of generator g.
$Rmax_e^{cha}$	Rate of charging for ESS e.
$Rmax_e^{dis}$	Rate of discharging for ESS e.
SOC_e^{max}	Maximum state of charge in percentage of ESS e.
SOC_e^{min}	Minimum State of charge in percentage of ESS e.
UT_g	Minimum up time for generator g.
$U_{m,g,t}^{ML}$	Machine learning predicted commitment status for generator g in period t for sample m.
Z_{max}	The maximum number of transmission elements that are allowed to switch off in each period.
π_s	Known probability of RES scenario s.

Variables:

$CDR_{n,c,t}$	Corrective demand response action at bus n in period t for contingency c
$F_{k,c,t}^{+}, F_{k,c,t}^{-}$	Dual variables of line k's contingent max and min limit constraints for contingency c and period t.
$E_{e,c,t,s}$	Energy level in ESS e in period t and scenario s after outage of line c.
$E_{e,t,s}$	Energy level in ESS e in period t and scenario s
$P_{e,c,t,s}^{cha}$	Charge power in ESS e in period t and scenario s after outage of line c.
$P_{e,t,s}^{cha}$	Charge power in ESS e in period t and scenario s
$P_{e,c,t,s}^{dis}$	Discharge power in ESS e in period t and scenario s after outage of line c.

$P_{e,t,s}^{dis}$	Discharge power in ESS in period t and scenario s.
$P_{g,t}$	Output of generator g in time period t.
$P_{g,t}^{MUC}$	Output of generator g in period t obtained from MUC.
$P_{g,t,s}$	Output of generator g in time period t and scenario s.
$P_{g,c,t,s}$	Output of generator g in time period t and scenario s after outage of line c
$P_{k,t}$	Lineflow of line k in time period t.
$P_{k,t,s}$	Lineflow of line k in time period t and scenario s.
$P_{k,t}^{MUC}$	Lineflow of line k in time period t obtained from MUC.
$P_{k,c,t}$	Flow in line k in period t after outage of line c.
$P_{k,c,t,s}$	Line flow of line k in time period t and scenario s after outage of line c
$P_{w,t,s}$	RES w output in time period t and scenario s.
$P_{w,c,t,s}$	Output of RES w in time period t and scenario s after outage of line c
$r_{g,t}$	Reserve from generator g in time period t.
$r_{g,t,s}$	Reserve from generator g in time period t.
$u_{g,t}$	Commitment status of generator g in time period t.
$u_{g,t}^{MUC}$	Generator g status in period t obtained from MUC.
$u_{g,t}^{m}$	Commitment status of generator g in time period t for generated sample m.
$u_{g,t}^{dn}$	Commitment status turned OFF from ON by feasibility layer for generator g in period t.
$u_{m,g,t}^{MF}$	Feasibility layer processed commitment status for generator g in period t for sample m.

$u_{g,t}^{up}$	Commitment status turned ON from OFF by feasibility layer for generator g in period t.
$v_{g,t}$	Start-up variable of generator g in time period t.
$v_{g,t}^{MUC}$	Generator g start-up in period t obtained from MUC.
$v_{m,g,t}^{MF}$	Feasibility layer processed start-up status for generator g in period t for sample m.
$S_{k,c,t}$	Dual variable of line k's contingent power flow constraint for contingency c and period t.
$z_{c,t}^{k}$	Line status variable of line k after outage of line c in time period t.
$z_{c,t,s}^{k}$	Line status variable of line k after outage of line c in time period t for scenario s.
$z_{k,c,t,s}^{CNR}$	CNR Line status variable of line k after outage of line c in period t.
$z_{k,t,s}^{PNR}$	PNR Line status variable of line k in period t.
$\beta_{g,c,t}^{+}, \beta_{g,c,t}^{-}$	Dual variables of generator g contingent reserve max and min constraint, for contingency c and period t.
$\theta_{i,t,s}$	Phase angle of bus i in time period t and scenario s.
$\theta_{o,t,s}$	Phase angle of bus o in time period t and scenario s.
$\theta_{n,t}$	Phase angle of bus n in time period t.
$\theta_{m,t}$	Phase angle of bus m in time period t.
$\theta_{n,t,s}$	Phase angle of bus n in time period t and scenario s.
$\theta_{m,t,s}$	Phase angle of bus m in time period t and scenario s.
$\theta_{m,c,t}$	Phase angle of bus m in period t after outage of line c.
$\theta_{n,c,t}$	Phase angle of bus n in period t after outage of line c.
$\theta_{n,c,t,s}$	Phase angle of bus n in time period t and scenario s after outage of line c.

$\theta_{m,c,t,s}$ Phase angle of bus m in time period t and scenario s after outage of line c.

$\theta_{ref,t}$ Phase angle of reference bus in time period t.

$\lambda_{n,c,t}$ Dual variable of bus n's power balance constraint for contingency c and period t.

1.   INTRODUCTION

1.1.   Background and motivation

Several national level directives in recent years stress on decarbonization to reduce emissions and battle climate change. This means retirement of carbon-based coal plants and increased investments in renewable energy portfolios. With the influx of renewable technologies and distributed generation, more advanced technologies are required to handle the unpredictability while ensuring system reliability. The resulting transfer of power is bi-directional, whereas traditional system was operated under the assumption that power is transferred from top-to-bottom, generation to consumption. Also, the expected increase in electric vehicles also changes the demand curve as they replace fossil-based cars to grid loads. The demand side also experiences significant changes over the years with increased demand patterns and addressing needs in uncertain situations such as weather anomalies etc.

Energy storage in the form of batteries is a form of flexibility to address these uncertainties, however it is still nascent and is not widely available. Another factor to consider is the high initial cost of energy storage, which requires optimal usage in the shorter term to perform price arbitrage while meeting system reliability standards. The long-term battery life depreciation by limiting cycles of operation or depth of discharge also needs to be considered. However, reliable storage exists in traditional systems in the form of hydropower which also requires optimal planning to maintain reservoir

level. Therefore, these complexities stress the importance of developing a smarter electrical grid which encompasses all the suite of technologies where the individual equipment operations can be optimally performed. Not only that, leveraging any existing system flexibility in the form network reconfiguration or demand response actions can address congestion in the network to lower the cost and increase reliability. Hence, the development of smarter algorithms is required to utilize the existing and future portfolio of power system equipment flexibly, efficiently, and reliably.

1.2. Operational Horizons

The power system operational and planning falls under the several time horizons. These time horizons provide guidelines for operations, the need of short-term planning, the need of the long-term maintenance, and for expansion. They can be broadly categorized in the following horizons:

- 5–40 years: power system expansion planning.

- 1–3 years: maintenance scheduling for large equipment, long-term bilateral contracts, generation capacity commitment.

- 1 day–1 week: maintenance scheduling for medium and small equipment; power system operational planning.

- 1 day: day-ahead scheduling.

- 5–30 minutes: contingency analysis, look-ahead dispatching.

- < 1 minute: system control, frequency regulation, stability.

From the above, the short-term operations based on the time period is implemented with day-ahead (24 hours), real-time (5–30 minutes), and regulation (<1 min) horizons. Fig. 1.1 shows the California independent system operator(ISO) timelines for short-term operation.
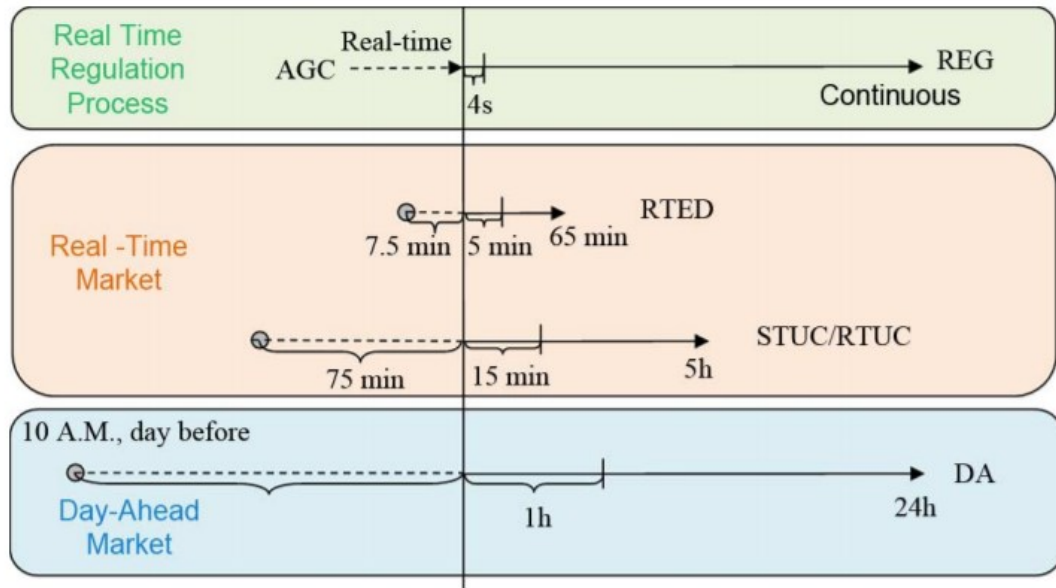
Fig. 1.1 California independent system operator short-term timeline [1].

1.3. Day-ahead markets

In the United States, the wholesale energy market is a look-ahead market and consists of day-ahead and real-time markets. Every day, the Independent system operators (ISOs) collect bids from generators and utilities. Following this, ISOs solve the Day-ahead markets (DAM) to provide the optimal commitment schedules and dispatch of generators to meet the predicted load for each hour of the next day. To

ensure reliability, the North American Electric Reliability Corporation (NERC) sets several standards for the ISOs to comply. Among them, the day-ahead solution must be N-1 compliant which implies that the system solution should be capable to handle a disturbance such as a line or a generator outage contingency [2]. This is handled by committing extra generators to support the system in the case of contingencies and maintaining reserve adequacy to handle an emergency.

DAM clears the bids and provides the least-cost solution of hourly generator commitment and dispatch for the bid-cleared demand. Typical time frame of DAM covers a period of 24 hours, from 00:00 am to 11:59 pm The SCUC requires several inputs such as load bids, generator offers, virtual bids, bilateral schedule, and self-scheduling as shown in Fig. 1.2. In addition, the network topology and parameters are required to optimize the system for a least-cost reliable commitment and dispatch solution based on a common-pricing model. The SCUC clears almost 93%–97% of the demand [3]–[6], following which a reliability unit commitment (RUC) is performed for meeting the forecasted loads.

Contingency analysis (CA), which is a sequence of power flow runs under different element outages, is performed by eliminating one element from the system at a time to identify any system violations for the day-ahead solution. If the CA fails, then an out of market correction is performed by committing additional generators and re-dispatching generators. The out of market correction is performed until all known violations are eliminated.
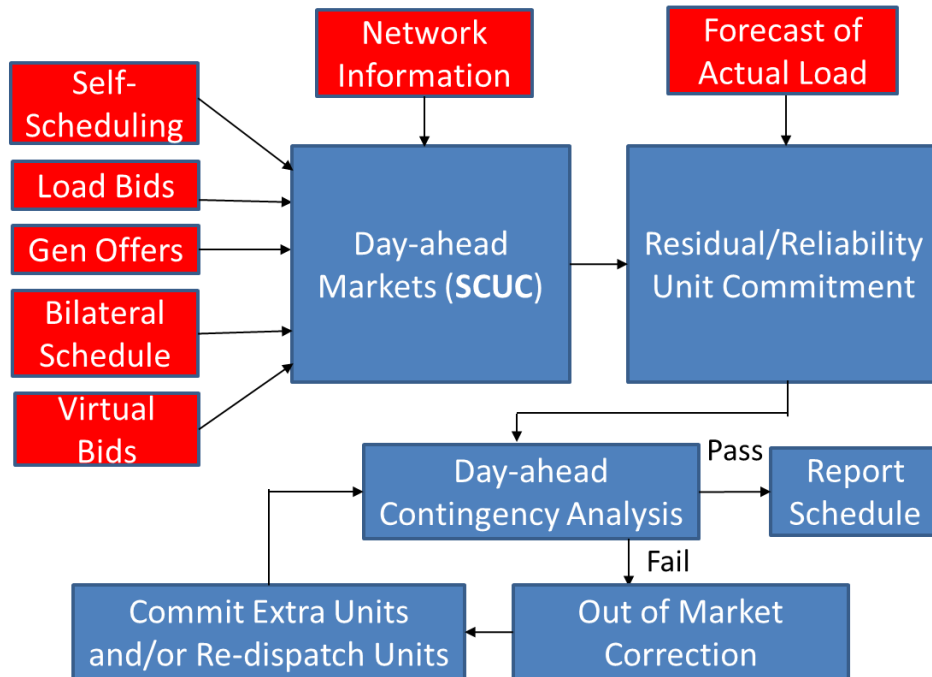
Fig. 1.2 ISO day-ahead market practice.

1.4.   **Industry Practices**

California ISO's DAM that collects bids for energy, ancillary services, reliability unit availability, self-scheduling, and virtual energy bids are open seven days prior to the operating day and closes for bids by 10:00 am on the day prior to the operating day. Once the bids are obtained, the DAM begins with market power mitigation to identify non-competitive constraints for energy bids. Following this, the integrated forward market will clear the bids using SCUC and the RUC is used to procure additional capacity for reliability. The results for the next operational day are posted by 13:00 pm [7].

New York ISO closes the DAM for bids by 05:00 am the day prior to the operational day. The load forecast is posted by 08:00 am and the generator schedules are determined by clearing the energy bids and posted by 11:00 am [8].

Midwest ISO's (MISO) DAM implements a co-optimized SCUC for energy offers and regulating reserves between 10:00 am–13:30 pm. MISO's DAM determines the commitment for about 1,500 resources totaling ~177,760 MW capacity, and the peak load is of ~127,125 MW [9]. After the SCUC, a rebidding is performed at 14:00 pm to run a simultaneously co-optimized security-constrained economic dispatch (SCED) for ancillary services and clearing energy prices [10].

ISO New England (ISO-NE) collects market inputs by 10:00 am and the results are posted by 13:30 pm, which publishes the generator schedules, locational marginal prices (LMP) and binding constraints. ISO-NE's network consists of more than 1,000 price nodes where LMPs are calculated. The reliability of the commitment schedule is verified using a contingency analysis embedded simultaneous feasibility test to identify out-of-merit dispatches [11].

The Energy Reliability Council of Texas (ERCOT) begins DAM at 06:00 am and ends by 18:00 pm. The information related to DAM is obtained by 06:00 am. Then, ERCOT performs pre-market activities. The DAM clears the SCUC between 10:00 am –13:30 pm. Once the results for the DAM are obtained for the next operation day, the RUC begins at 14:30 pm to commit additional units by considering more accurate

weather and load forecasts and updated network model. Finally, market adjustment is performed between 18:00 pm–0:00 am [12].

PJM's DAM collects market participant offers such as energy and regulation bids between 08:00 am –11:00 am. The day-ahead results are posted by 13:30 pm after processing all the market requests from bids. After the results are available, the re-bids are processed until 14:15 pm. These re-bids and updated forecasts are used in the reliability analysis for out-of-market corrections, which goes from 14:15 pm until midnight [13].

Southwest Power Pool's (SPP's) DAM posts the available generating reserves by 06:00 am following which SPP closes the generation offers and load bids by 09:30 am. Between 09:30 am–13:00 pm, the commitment and dispatch schedules are optimized using SCUC. RUC process begins at 13:45 pm after collecting re-bids. Finally, the results from RUC are posted at 16:15 pm [14].

1.5. Unit Commitment

Electric power needs to be generated, transferred, and utilized concurrently as there are limited bulk storage options. As a result, this process requires economical operational solutions. Moreover, the production of energy is governed by physical restriction of the generators, network, and transmission limits. Generators also have restrictions of ramping rates, minimum up-down time and reserve margins constraints. The production of energy is a multi-period (typically 24 hours) problem to meet the

hourly demand in a day-ahead scenario. This process of indicating the ON/OFF status of generators and dispatch points of generators for each interval of a fixed period of time T is known as unit-commitment (UC). Here, care is taken to maintain flexibility to meet the variation of demand in real-time.

Since the UC model is utilized in DAM, it requires a convex and linear model to ensure that a global solution can be obtained. Therefore, the UC is an optimization problem. Hence, constraints are required to model topology of the network and include the power flows in the lines since the power generated are delivered through the transmission network. However, it is of prime importance that the model is tractable and hence DC power flow constraints (an approximation of real power) are involved as opposed to AC power flow constraints. It can also be noted that the wholesale market/DAM only deals with real power trading which implies the binding requirement to energy price is the real power being traded. The resulting UC model is a mixed-integer linear program (MILP). A detailed model of UC along with all the security constraints is provided in Chapter 2.

1.6.   N-1 reliability

The guidelines of NERC (North American Reliability Council) standard 51 describes that the solution of the UC requires an *N*-1 reliability criterion [2]. This implies that the power system should be planned and operated in a way to supply all loads without issues when a generator or line contingency occurs. To satisfy this

standard, system operators usually use the security-constrained unit commitment (SCUC) to dispatch/commit generators. Due to the addition of security constraints, SCUC results in higher operation costs when compared to UC. To reduce the operational cost of SCUC system, flexibility can be leveraged through transmission, demand response, and energy storage. System costs also reduce when these actions are utilized as re-course actions in post-contingency scenario while adhering to the reliability standards.

1.7. Preventive and Corrective actions

The reliability in the system can be maintained by the combination of recourse actions to address the uncertainties in the system. Mainly they are divided into preventive action and corrective action. A preventive action is implemented prior to the contingency to avoid line flows exceeding emergency ratings following a contingency. This means the system is set to handle the contingency without any control actions such as re-dispatch following a contingency. A corrective action is implemented after the disturbance has occurred to move the system from emergency state to normal-secure or normal-insecure state.

1.8. System Flexibility

Ideally, the power system is engineered with reliability and future developments in mind. This implies that the system has existing flexibility in the form of additional transmission lines, fast-acting generation services, and demand response

capability. Also, with the addition of renewable sources, energy storage system is also available for providing transient or limited amount of energy, as needed. As a result, there are several ways that system flexibility can be leveraged to address short-term and long-term needs as well as congestion-relief methods when smart grids are operated efficiently. When system flexibility addressed in the form of network reconfiguration, demand response and energy storage can lead to additional benefits such as: (i) system reliability, (ii) congestion management, (iii) cost reduction, (iv) integration of renewable sources and (iv) contingency planning.

1.9.   Machine Learning

Machine learning (ML) is a field of science developed to learn relationships in data. It is also popularly known as artificial intelligence (AI) as it mimics the pattern of brain by using trained neurons in decision making. ML models leverage data to improve performance on decision-support, prediction and automation. ML algorithms are used to develop models that learn through sample data also known as training data to help in making predictions or decisions without being explicitly programmed. In this work, ML is used for predictive classification to identify ON/OFF status of generators given input data.

ML has two broad classes of problems namely, regression and classification. In regression models estimate continuous values whereas classification models approximate a mapping function from input variables to identify discrete output

variables, which can be labels or categories. Since generator status is binary in nature, therefore we predict whether the generator is ON/OFF. This implies that the outputs of ML model belong to a binary category. Hence, classification algorithms are studied rather than regression. For classification, several standard algorithms exist, namely decision tree classification, random forest classification and K-nearest neighbor classification. Even though these are well-established models but are still prone to errors. Since ML models are not 100% accurate, relying on these standard algorithms does not provide flexibility to adapt to the task at hand. For these reasons, logistic regression, neural networks and spatio-temporal models are proposed. This is because all the proposed models have a sigmoid output layer which restricts the output between 0 and 1. In other terms, it inherently results in probabilistic outputs which can be leveraged for post-processing the ML predictions with a decision boundary to selectively use ML predictions of high accuracy.

1.10. Industrial Feasibility

The work developed in this thesis mainly focuses on the day-ahead operations of power systems. In day-ahead operations, the unit-commitment problem is mainly utilized not only to clear the market but also to operate the system and ensure reliability. In USA, which is a competitive/deregulated market, unbiased entities such as independent system operators and transmission system operators oversee this process to clear the market. However, it can be noted that unit commitment is performed both

in vertically-integrated/regulated market and competitive/deregulated markets. Therefore, the proposed work can be adopted in any business scenario since unit commitment is a fundamental element to provide economical solutions.

1.11. Organization of the thesis

The rest of this dissertation is structured as follows. Chapter 2 presents the background of system flexibility technologies such as network reconfiguration and demand response, and ways to integrate such tools in SCUC for day-ahead operations. The results outline benefits in reduced total cost, alleviating contingency-based congestion, and line overloading.

Chapter 3 expands on the idea to use technologies present in the prior chapter to facilitate renewable energy sources through a multi-scenario stochastic approach. Results present the ability to reduce curtailment of free RES output and provide an efficient use of energy storage devices along with reduction is carbon emissions.

Chapter 4 addresses the complexity of SCUC when implemented in tandem with network reconfiguration in particular as a corrective action. Corrective network reconfiguration solutions are present in the industry but albeit through operator experience. Hence, including explicit network reconfiguration constraints in SCUC as an economic tool increases the complexity several fold. A purely optimization solution through Benders Decomposition aided by heuristic methods are discussed and the

results show that the proposed technique can be a scalable solution for large power system networks.

Chapter 5 deals with a machine learning approach for power system day-ahead operations. Several machine learning architectures are developed to learn from historical commitment and dispatch schedules to facilitate model reduction of SCUC, which can be utilized in any state-of-the-art heuristic, decomposition, and/or regular industrial approaches with ease. Results demonstrate considerable reduction of problem size resulting in increased computational efficiency with minimal loss in solution quality.

Finally, Chapter 6 concludes the report by summarizing the results and addressing the future scope of work.

2. SYSTEM FLEXIBILITY THROUGH CORRECTIVE ACTIONS

There are existing corrective actions and remedial schemes are utilized to address congesting relief, and to increase system reliability. However, such actions are only implemented through operator experience or study-based pre-determined actions. Though such actions address the immediate needs of system reliability, voltage maintenance and congestion-relief they are not considered in effective day-ahead operations. Mainly, the consideration of such tools in day-ahead operations through UC can add substantial relaxation to the constraints thereby increasing feasibility region of the problem. Therefore, a relaxed problem may provide a lower cost solution which is never considered in current practices.

Independent system operators (ISOs) collect bids from generators and utilities each day and solve the day-ahead security-constrained unit-commitment (SCUC) to provide the optimal commitment of day-ahead schedules for generators to meet the predicted load for each hour of the day. A reliable grid is maintained through adherence to system security constraints. The security criteria include, but not limited to, line thermal limits, generator physical limits, reserve requirements and ramping constraints. The grid must also operate reliably in case of emergencies such as transmission line outage or generator loss and an N-1 reliable system stresses the importance of modelling such post-contingency situations. Traditionally, the reliability of the grid is

taken care by committing extra generators to ensure ramping and reserve requirements. However, transmission congestion in the network would result in buying power from expensive generating units thereby increasing the cost of operations. Typically, voltage profiles and transfer capability of the network are maintained by transmission congestion management schemes in the case of a congested network. Currently, there are no support for operators such as decision support tools to implement network reconfiguration and the current ISO model does not include switching of transmission lines during short-term operations since transmission assets are treated as a static network. This greatly reduces the potential of an efficient implementation of the flexibility offered by excess transmission capacity. Not only that, though demand response is significantly prevalent to modify consumption patterns, the benefits of such actions in the event of a contingency as a corrective action is absent. In this chapter, we discuss two potential corrective actions that can be utilize existing system flexibility namely corrective network reconfiguration (CNR) and corrective demand response (CDR).

2.1. Literature Review

2.1.1. CNR

Presently, transmission operators follow the procedure for relieving network congestion based on experience rather than sound systematic methods especially during contingencies. The importance of NR is seen through several industrial examples based

on historical or simulated control schemes. PJM details ad-hoc NR and control procedures in [15]–[16], whereas, ISO New England presents protocols for removing internal transmission lines in [17] to support system reliability. PJM used one such method as a corrective response to damage caused during Superstorm Sandy. During the storm, PJM lost 82 bulk electric facilities and the system demand was low which led to overvoltage issues in high voltage line. Several 500 kV transmission lines were opened by PJM as part of NR implementation to mitigate the overvoltage [18].

Since, transmission assets are treated as static networks, the use of a dynamic network configuration of power system elements can help ISOs to relieve network congestion, maintain the system security, and reduce operation costs. The reliable operation of system network at optimal cost is of prime concern. Therefore, congestion in transmission network can be addressed through NR and the research in [19] and [20] points to cost-saving as a result. However, the use of transmission as a controllable asset today is limited and left to the operator to decide and relieve the network congestion in emergency situations.

NR can be of both preventive action and corrective action. However, concerns that NR causes a big network disturbance, stability issues and circuit breaker degradation makes corrective network reconfiguration (CNR) more attractive as it is only implemented after a contingency has occurred. Apart from system reliability, NR can provide significant cost-saving benefits and network congestion alleviation by rerouting the network flows. NR can be used as a preventive or corrective action. It is

16

also seen from prior research that frequent use of NR can cause large system disturbances and significant circuit breaker degradation. Therefore, it is more practical to use NR as a corrective mechanism for post-contingency scenarios as a non-invasive approach. This can be a viable option to mitigate or eliminate the transmission flow violations during contingent scenarios.

CNR first introduced in [21] is attractive for the transmission line overload reduction and realizing market surplus benefits [21]–[23]. The cost-saving benefits CNR due to the increased feasible set of solutions for the SCUC problem and a co-optimized CNR method leads to significant cost saving and network congestion alleviation [24]. In addition, CNR offers increased network flexibility as shown in [25] where it was implemented on an industry case using an in-house industry software. Therefore, mainly NR as a corrective action shows practical and promising results.

2.1.2.   CDR

With the advent of smart grid technologies, we have brought about intelligent energy management systems to operate the grid optimally and reliably. Traditionally, grid was operated in a top-down framework where the flexibility requirement of the power system is met with committing additional generators to meet the demand and the reliability requirement of the network. But the technology to sense and control signals with two-way communications has brought increased participation from

demand side in energy markets [37]. The system operators can also determine and send signals to not only redispatch generators but also adjust controllable loads.

Utilities now offer several price-based or incentive-based programs for altering demand patterns through demand side management (DSM) that reduces the cost of the electricity the customer pays [38]. DSM not only lowers cost but also enhances reliability and provides self-healing capabilities for the power grid through demand response (DR) [39]. In particular, demand response through direct load control (DLC) enables grid operators to send signals to reduce non-critical loads directly. However, most DLC actions are implemented as part of the distribution network by utilities to shift non-critical loads from peak hours experiencing high demands to non-peak hours [38].

In day-ahead scheduling, system operators use SCUC to obtain the optimal commitment status and dispatch signals for generators to meet forecasted bulk hourly loads [40]. As per Federal Energy Regulatory Commission (FERC), the SCUC solution requires to be N-1 reliable where the system is capable of handling frequent line or generator outages individually [41].

Here, system operators often utilize preventive and corrective control actions to maintain system reliability [40], [42]–[43]. Mostly, DR through controllable loads are considered as a preventive action. DR benefits the system by moving non-critical deferrable loads from peak hours to non-peak hours which increases the system flexibility and demand side market participation [37]–[38]. Though there are

emergency DR plans that several system operators implement, they are solely based on supply and demand balance for frequency regulation and typically this is factored in the SCED process where operators dispatch the participating DR resources [44].

Mostly, ISOs compensate DLC by locational marginal prices (LMP) when utilized in real-time operations and fixed-price based schemes contracted in long-term capacity markets to shift demand [45]–[49]. By studying the ISO reports for outage statistics for the network with about 350 dispatchable generators and 9,000 miles of high voltage transmission lines, it reported that a low number of cases, 833, for the unplanned outages related to line in 2019 and unplanned outages generator are very rare [50]–[51]. Here, the untapped potential of DLC considering system flexibility or capacity release is not completely considered in short-term operations. Mostly, DR through dispatchable DLC are used for economic reasons and reliability reasons in base-case; it is only used for reliability purpose in post-contingency scenario.

Most utilization of DLC is preventive in nature as seen in [52]–[53]. In [54], the DR actions were automated to respond to real-time dispatch schedule to provide additional reserves as an ancillary service to the grid. The DLC algorithms consider economic benefits in [55] where optimal control schedules are determined by nodal aggregators by optimizing the load profile. Many preventive DR actions also consider the reliability of power system but with limited contingencies being considered as seen in [56]. However, for economic benefits of DR actions, they need to be implemented in operational optimization problem such as SCUC or security-constrained economic

dispatch (SCED) and only [40],[55], and [57] include the power network constraints. Here, all the research address DR as a preventive action only, which may substantially affect customer comfort level and are susceptible to cyber security in real-time operations [58].

Currently, the use of corrective demand response (CDR) in response to contingency is never considered in the SCUC process. Similar to network reconfigurations as a corrective action [24], [43] and [60] CDR can also increase the solution quality by reducing costs when co-optimized with SCUC. But CDR can also provide additional system flexibility by shedding some non-critical load under contingency and allowing the committed units to ramp-up or ramp-down to meet the system requirements in post-contingency scenarios rather than committing additional units. Note that under CDR schemes, non-critical load shedding will occur only when the associated contingency actually occurs, which is a low probably event.

Though there exists load shedding, especially during low supply scenarios due to congestion-induced or fault-induced events, this is however implemented for reliability and not for economic benefits in [42]. In [61], DR is considered as a corrective action in post-fault condition to release network capacity but not for economic benefits. Similarly, in [62], a few DLC operations are considered in a post-contingency scenario to obtain additional system flexibility to enhance system reliability under an emergency but with limited economic considerations. In [61]–[62], the operational and network constraints are not completely considered or are only

focused on distribution networks. Therefore, the studies on benefits of utilizing DLC in day-ahead operations at the transmission level for post-contingency actions are limited.

2.2.   *N*-1 Security Constrained Unit Commitment (SCUC)

In day-ahead scenario, once the generation and demand bids are obtained, the unit commitment is run to obtain an economical viable solution along with the day-ahead generator commitment and dispatch schedule. To ensure that the commitment and dispatch solution practical the physical constraints governing the generators and networks modelled. Additionally, security constraints are added for *N*-1 reliability which implies that the system should be capable of handling events such as line or generator outage. The resulting problem is a mixed-integer linear program where the operational cost of generators is minimized subject to the underlying constraints. It can be noted that the SCUC is used in both competitive market and regulated system. Therefore, the algorithms proposed in the current chapter and later chapters can be implemented in either business environment. Section 2.2.1 details the mathematical model of a simple *N*-1 SCUC. Both CNR and CDR can be introduced into the SCUC model which is discussed in Section 2.3 and Section 2.4, respectively.

2.2.1. Mathematical Model

N-1 SCUC is a MILP problem represented by (2.1)–(2.22) where the goal is to optimize and reduce operational cost, (2.1),

$$Min \sum_g \sum_t \left(c_g P_{g,t} + c_g^{NL} u_{g,t} + c_g^{SU} v_{g,t}\right), \tag{2.1}$$

subject to base-case generation constraints (2.2)–(2.12),

$$P_g^{min} u_{g,t} \leq P_{g,t}, \forall g, t, \tag{2.2}$$

$$P_{g,t} + r_{g,t} \leq P_g^{max} u_{g,t}, \forall g, t, \tag{2.3}$$

$$0 \leq r_{g,t} \leq R_g^{10} u_{g,t}, \forall g, t, \tag{2.4}$$

$$\sum_{q \in G} r_{q,t} \geq P_{g,t} + r_{g,t}, \forall g, t, \tag{2.5}$$

$$P_{g,t} - P_{g,t-1} \leq R_g^{hr} u_{g,t-1} + R_g^{SU} v_{g,t}, \forall g, t, \tag{2.6}$$

$$P_{g,t-1} - P_{g,t} \leq R_g^{hr} u_{g,t} + R_g^{SD} \left(v_{g,t} - u_{g,t} + u_{g.t-1}\right), \forall g, t, \tag{2.7}$$

$$\sum_{q=t-UT_g+1}^{t} v_{g,q} \leq u_{g,t}, \forall g, t \geq UT_g, \tag{2.8}$$

$$\sum_{q=t+1}^{t+DT_g} v_{g,q} \leq 1 - u_{g,t}, \forall g, t \leq T - DT_g, \tag{2.9}$$

$$v_{g,t} \geq u_{g,t} - u_{g,t-1}, \forall g, t, \tag{2.10}$$

$$0 \leq v_{g,t} \leq 1, \forall g, t, \tag{2.11}$$

$$u_{g,t} \in \{0,1\}, \forall g, t, \tag{2.12}$$

base-case power flow constraints (2.13)–(2.15),

$$P_{k,t} - b_k\left(\theta_{n,t} - \theta_{m,t}\right) = 0, \forall k, t, \tag{2.13}$$

$$-P_k^{max} \leq P_{k,t} \leq P_k^{max}, \forall k, t, \tag{2.14}$$

$$\sum_{g \in g(n)} P_{g,t} + \sum_{k \in \delta^+(n)} P_{k,t} - \sum_{k \in \delta^-(n)} P_{k,t} = d_{n,t}, \forall n, t, \tag{2.15}$$

post-contingency 10-minute ramping restrictions on generators (2.16)–(2.19),

$$P_{g,t} - P_{g,c,t} \leq R_g^{10} u_{g,t}, \forall g, c \in C, t, \tag{2.16}$$

$$P_{g,c,t} - P_{g,t} \leq R_g^{10} u_{g,t}, \forall g, c \in C, t, \qquad (2.17)$$

$$P_g^{min} u_{g,t} \leq P_{g,c,t}, \forall g, c \in C, t, \qquad (2.18)$$

$$P_{g,c,t} \leq P_g^{max} u_{g,t}, \forall g, c \in C, t, \qquad (2.19)$$

and post-contingency non-radial transmission element power flow model (2.20)–(2.22),

$$P_{k,c,t} - b_k(\theta_{n,c,t} - \theta_{m,c,t}) = 0, \forall k, c \in C, t, \qquad (2.20)$$

$$-P_k^{emax} \leq P_{k,c,t} \leq P_k^{emax}, \forall k, c \in C, t, \qquad (2.21)$$

$$\sum_{g \in g(n)} P_{g,c,t} + \sum_{k \in \delta^+(n)} P_{k,c,t} - \sum_{k \in \delta^-(n)} P_{k,c,t} = d_{n,t}, \forall n, c \in C, t. \qquad (2.22)$$

Here, (2.2) and (2.3) represents the generator output min-max limits, (2.4) and (2.5) are the reserve requirements, (2.6) and (2.7) are the hourly ramping consideration, (2.8) and (2.9) are the min-up and min-down time of generators. (2.10) and (2.11) shows the start-up variable definition. The generator commitment indication variable are bound by binary integrality constraints as shown in (2.12). The base-case physical power flow constraints represented by (2.13) which models the power flow with DC line flow equations, (2.14) which depicts the long-term line thermal limits and (2.15) which represents nodal balance.

The mixed integer program is a co-optimization of base-case and post-contingency scenarios. The post-contingency generator constraints are modelled for the base-case solution through (2.16)–(2.17) which takes consideration of the 10-minute generator ramping constraints, and (2.18)–(2.19), the post-contingency generator

output min-max limits when line c is lost. Post-contingency scenarios of line flows are modelled for all non-radial lines when a transmission element outage occurs in (2.20). Equation (2.21) shows the emergency line flow limits and (2.22) is the post-contingency nodal balance.

2.3.   Integration of CNR

The concept of CNR is described pictorially in Fig. 2.1. Fig. 2.1 (a) represents the pre-contingency state with no line flow violations. Fig. 2.1 (b) shows the post-contingency state of the system. The contingency, line 3 outage, causes the injection at bus 2 to flow through the external path and line 2. However, bulk of the flow goes through line 2, which results in an overload of line 4. Traditionally, this scenario is countered by ramping the local generators to eliminate the line overload. However, this increases the operation cost as expensive generation redispatch are required. An alternative corrective action is to open line 2 which will reroute the entire injection at bus 1 and bus 2 through the external network to serve the load at bus 3 and bus 4 as represented in Fig. 2.1 (c). This action results in the elimination of line flow violations without additional cost.
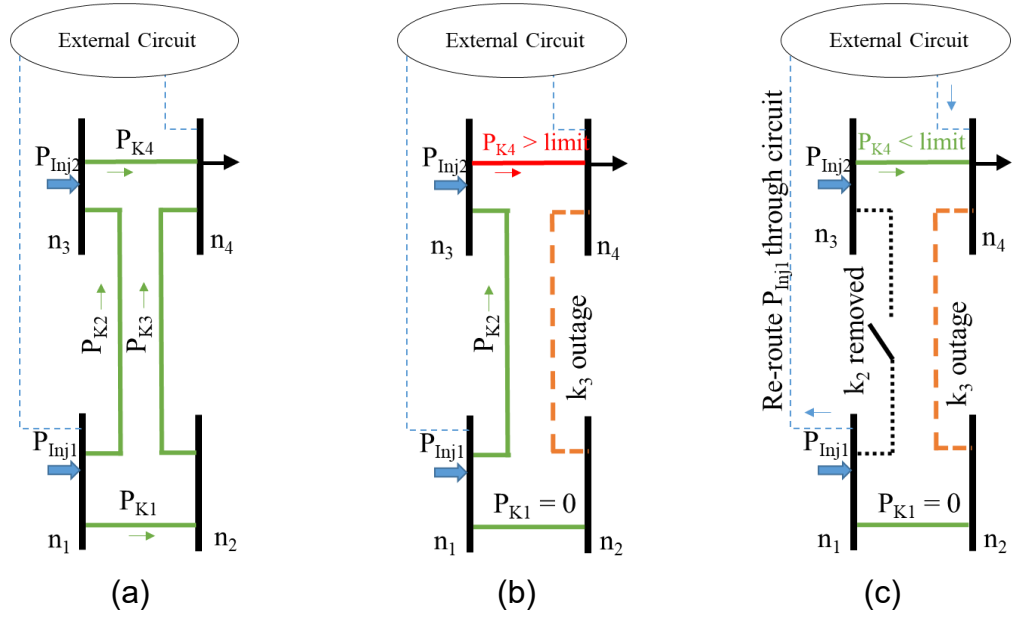
Fig. 2.1 Corrective action example: (a) Pre-contingency, (b) Post-contingency and (c) Post-switching - CNR action.

2.3.1. Modelling *N*-1 SCUC with CNR

The extensive formulation of SCUC is modelled though (2.1)–(2.22). However, the post-contingency transmission constraints in (2.19)–(2.20) are modified to offer flexibility by CNR in (2.22)–(2.26),

$$P_{k,c,t} - b_k\left(\theta_{n,c,t} - \theta_{m,c,t}\right) + \left(1 - z_{c,t}^k\right)M \geq 0, \forall k, c \in C, t, \tag{2.23}$$

$$P_{k,c,t} - b_k\left(\theta_{n,c,t} - \theta_{m,c,t}\right) - \left(1 - z_{c,t}^k\right)M \leq 0, \forall k, c \in C, t, \tag{2.24}$$

$$-P_k^{emax} z_{c,t}^k \leq P_{k,c,t} \leq z_{c,t}^k P_k^{emax}, \forall k, c \in C, t, \tag{2.25}$$

and

$$\sum_k (1 - z_{c,t}^k) \leq Z_{max}, \forall k, c \in C, t, \ Z_{max} \in \{0,1,2..\}, \tag{2.26}$$

where, the CNR action is represented by the binary decision variable, $z_{c,t}^k$, introduced in equations (2.23)–(2.25). This represents the status of switchable transmission element k under contingency c in time period t (When the value is 1, the line is in service and when value 0 the line is switched off/ not is service). M, is often represented as 'big M' which is a large real value. It ensures that equation (2.23) and (2.24) are linear in nature. The decision variable for switching decides the optimal network configurations for each contingency to relieve the post-contingency congestion in the system. Since NR can cause large system disturbance, restriction on number of transmission elements open is represented in (2.26).

Hence, the extensive formulation N-1 SCUC-CNR is modelled by together by (2.1)–(2.19) and (2.22)–(2.26). The co-optimization leads to several conclusions about the benefits of utilization of CNR in day-ahead operations which are detailed in sub-section 2.3.3.

For this study, contingency set, C, considers transmission contingencies since transmission contingencies are more likely to occur as compared to generator contingencies. However, generator contingencies can also be included to the set without modification to the model.

2.3.2. Testcase Description

The IEEE 24-bus network developed by power experts [63] was used for testing in this paper. However, a modified data for the same network was utilized. Fig. 2.2

26

represents this modified network which contains 24 buses, 33 generators, and 38 branches. The total generation capacity is 3,393 MW and the types of generator available with operational cost, min and max outputs are presented in Table 2.1. The goal of the proposed SCUC model is to find out cost-saving in congested networks. The system peak load is 2,265 MW with a maximum nodal load of 210 MW and a minimum nodal load of 0.

Table 2.1. Generator data in IEEE-24 Bus

No. of Gen	Min	Max	$/MWh
4	2.4	12	94.74
4	15.8	20	163.02
4	15.2	76	19.64
6	0	50	0
3	25	100	75.64
4	54.25	155	15.46
3	68.95	197	74.75
1	140	350	15.89
2	100	400	5.46
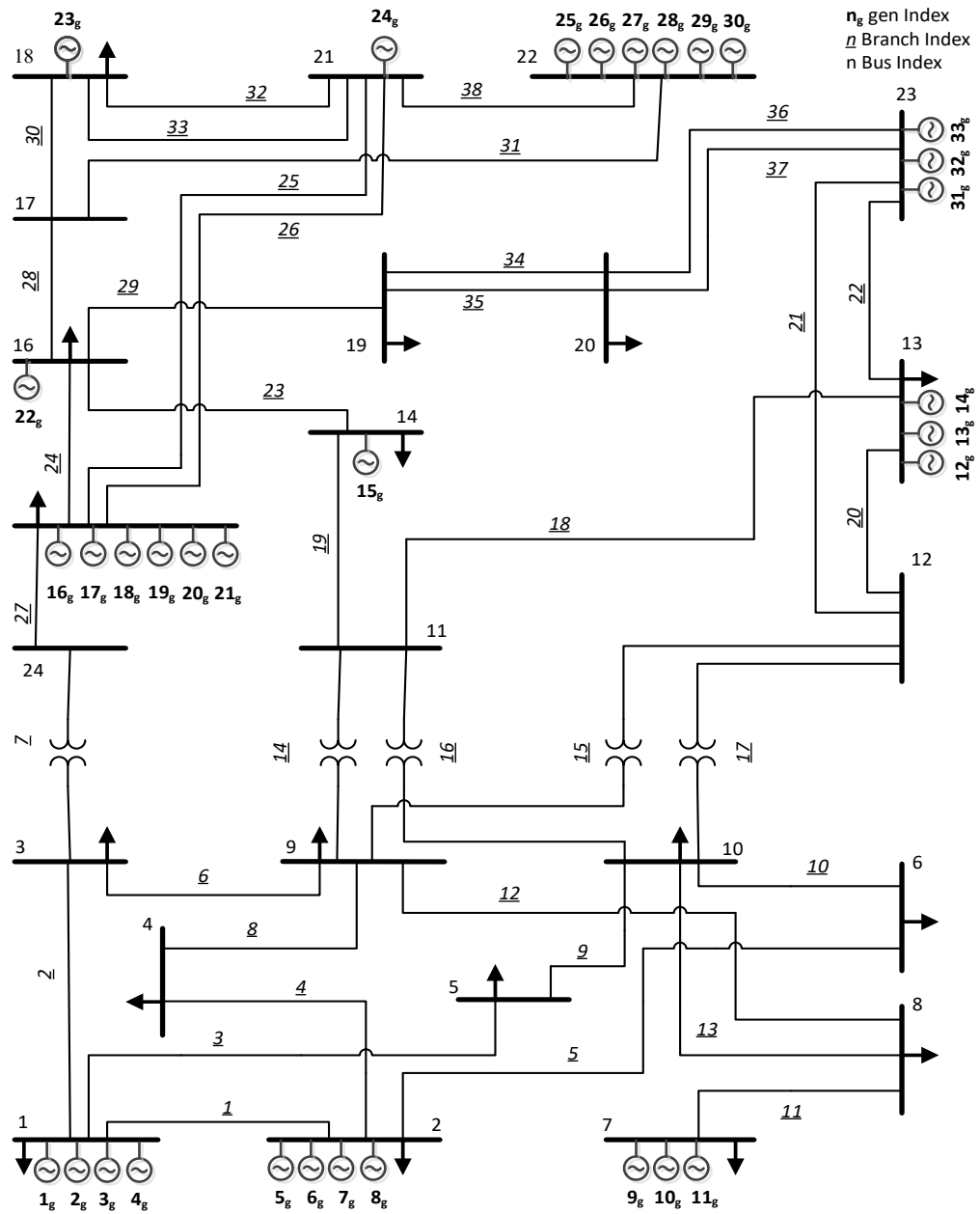
Fig. 2.2 IEEE 24-bus System – one area of IEEE RTS-96 system.

2.3.3. Results

The *N*-1 SCUC and *N*-1 SCUC-CNR are modelled in two different scenarios. Scenario I is when regular emergency rating and Scenario II is when infinite emergency rating is used for transmission elements in the network respectively. In Scenario I, the operational cost of $932,911 for N-1 SCUC and $923,995 for N-1 SCUC-CNR was obtained. This information is tabulated in Table 2.2. Scenario II operational cost shows the operational cost of the system when there are no congestion in the system in post-contingency scenario. This implies that post-contingency congestion is significantly reduced with the use of CNR. It can be further verified from the dual values of the active post-contingency emergency thermal limits constraints; the use of CNR leads lower dual values which is tightly correlated to the congestion cost.

The post-contingency congestion cost (*CC*) is defined as the difference in total operational cost in Scenario I ($TC_{Scenario\ I}$) and total operational cost in Scenario II ($TC_{Scenario\ II}$). It can be inferred that in N-1 SCUC, the post contingency congestion cost is $11,099. Whereas in N-1 SCUC-CNR, the post-contingency congestion cost is $2,183. For the test scenario, implementing CNR results in reduction of congestion cost by 80.33%. Transmission networks are built with redundancy and by including the CNR the flexibility in the network is utilized which reduces the congestion in the network.

Table 2.2. Operational Cost in N-1 SCUC

	N-1 SCUC		N-1 SCUC-CNR	
	Scenario I	Scenario II	Scenario I	Scenario II
Cost ($)	932,911	921,812	923,995	921,812
CC ($)	11,099	N/A	2,183	N/A

Table 2.3 shows that implementing CNR required less frequent generator start-ups in the 24-hour period as NR provides the opportunities for committed generators to ramp-up and meet post-contingency demand. In total, there were 26 generators start-ups in the 24-hour period while using N-1 SCUC whereas only 20 generators start-ups in N-1 SCUC-CNR. In both cases 19 generators were started in the first hour. Implementing CNR required only one additional generator start-up as it enabled the existing generators to ramp up without transmission violations to meet the demand.

Table 2.3. Generator Start-up

Time Period	ON Generators in N-1 SCUC	ON Generators N-1 SCUC-CNR
t=1	3,4,7,8,9,11,21–33	3,4,7,8,11,13,21–33
t = 9	14	9
t = 21	16,17,20	N/A
t=23	1,5,6	N/A

The solution of switching transmission lines for each contingent line was studied for a 24-hour period. We can understand the reconfiguration ideology using a

demand of 2,076 MW for period 8 and a demand of 2,265 MW for period 9. In period 9, after the load profile change, it was noted that line 10 and line 23 are susceptible to post-contingency congestion. The scenario leading to congestion is tabulated in 2.4. Line 10 connects from bus 6 to bus 10 with a long-term thermal rating of 157.5 MW and an emergency rating of 180 MW and line 23 connects from bus 14 to bus 16 with a long-term thermal rating of 315 MW and an emergency rating of 393.75 MW. During congestion of line 10 and 23 in period 9, we noticed that the scenarios leading to post-contingency congestion were reduced. CNR was beneficial to produce a maximum line overload reduction of 4% and 24% in lines 10 and 23 respectively. In the best case, 24% reduction of line overload brings the line flow below the long-term thermal limit which reduces significant stress on transmission lines. In N-1 SCUC-CNR, only 1 contingent scenario led to congestion in both lines respectively.

The number of transmission elements opened as part of CNR played a role in reducing the congestion cost. Fig. 2.3 shows that the congestion cost reduced to $0 from $11,099 when more transmission elements were allowed to be opened if required. The difference in congestion cost when one transmission element is allowed to be opened in CNR versus multiple transmission elements is $2,183.

Table 2.4. Post-contingency Congestion Scenario for Period 9

Post-contingency congested line (line number [from-bus – to-bus])	Post-contingency line outage (line number [from-bus – to-bus])	
	N-1 SCUC without CTS	N-1 SCUC with CTS
10 [6–10]	1 [1–2],2 [1–3],7 [3–24],8 [4–9],9 [5–10],27 [5–24]	2 [1–3]
23 [14–16]	7 [3–24], 18 [11–13],21 [12–13],22 [13–23],27 [5–24]	7 [3–24]
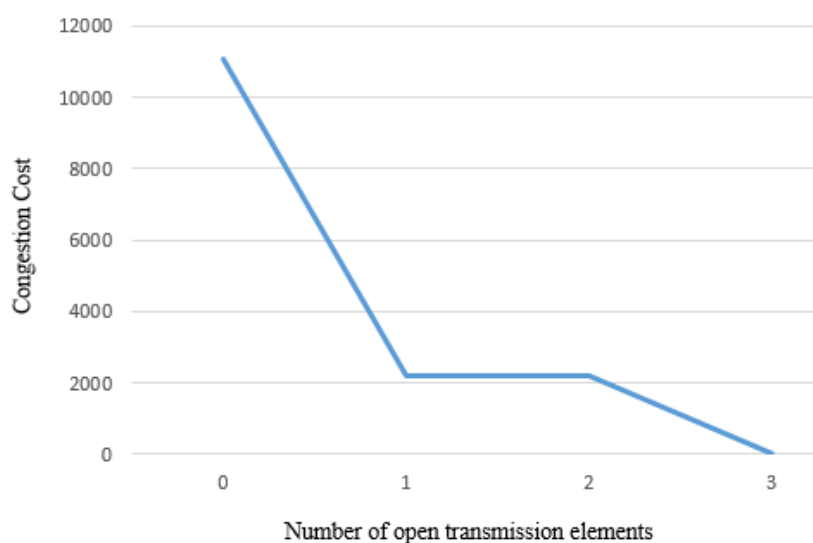
Fig. 2.3 Number of open transmission elements vs congestion cost.

2.4.   Integration of CDR

Similar to CNR, CDR can also be integrated to SCUC. Since, CDR is modification of load profile with respect to a contingency the nodal variable, $CDR_{n,c,t}$,

is introduced in the post-contingency nodal-balance constraint as shown in (2.28). However, only non-critical loads can be modified or controlled effectively without affecting user comfort. Hence, (2.29) is added to control the effect of demand response when a contingency occurs. The contingency nodal variable, $CDR_{n,c,t}$ is controlled by introducing a penalty term in the objective cost. Therefore, the objective (2.1) is replaced by (2.27) and (2.22) is replaced with (2.28)–(2.29),

$$Min \ \textstyle\sum_g \sum_t \left(c_g P_{g,t} + c_g^{NL} u_{g,t} + c_g^{SU} v_{g,t} \right) + \sum_{n,c,t} (\pi_c * \tag{2.27}$$

$$c_n^{Ctg} * CDR_{n,c,t}),$$

$$\textstyle\sum_{g \in g(n)} P_{g,c,t} + \sum_{k \in \delta^+(n)} P_{k,c,t} - \sum_{k \in \delta^-(n)} P_{k,c,t} = d_{n,t} - CDR_{n,c,t}, \tag{2.28}$$

and

$$CDR_{n,c,t} \le 0.3 * d_{n,t}. \tag{2.29}$$

2.4.1. *N*-1 SCUC with CDR

The extensive formulation *N*-1 SCUC-CDR is modelled by together by (2.2)–(2.21) and (2.28)–(2.29). The flexibility offered by CDR is modelled in (2.28)–(2.29). Since generator contingencies are very rare compared to line contingencies, different models are formulated for both SCUC and SCUC-CDR. Mainly, T-SCUC and TG-SCUC models the SCUC with only transmission contingencies and with both transmission and generator constraints, respectively. Whereas the proposed models for SCUC with corrective actions using DLC for post-contingency constraints are namely, T-SCUC-CDR and TG-SCUC-CDR, with transmission contingencies only and both

transmission and generator contingencies, respectively. Here, T-SCUC and TG-SCUC are defined by (2.2)–(2.22) and (2.28). T-SCUC-CDR and TG-SCUC-CDR are modelled through (2.2)–(2.21) and (2.28)–(2.29). The difference in T and TG models are captured through input set of contingencies, C, where $C \in K_c$ for transmission contingencies only and $C \in G_c \cup K_c$ when both transmission and generator contingencies are modelled. Based on the above constraints, the proposed models are consolidated in Table 2.5.

Table 2.5. Proposed Model Constraints

Model	T-SCUC	TG-SCUC	T-SCUC-CDR	TG-SCUC-CDR
Objective	(2.28)	(2.28)	(2.28)	(2.28)
Constraints	(2.2)–(2.22)	(2.2)–(2.22)	(2.2)–(2.21) and (2.28)–(2.29)	(2.2)–(2.21) and (2.28)–(2.29)
C	K_c	$G_c \cup K_c$	K_c	$G_c \cup K_c$

2.4.2. Total economic benefits of CDR

From Table 2.6, the difference in overall cost of T-SCUC-CDR and TG-SCUC-CDR against the T-SCUC and TG-SCUC demonstrates a cost saving of $9,825 and $14,996, respectively when CDR is introduced. This is due to the flexibility offered by CDR actions which provides a more economical commitment status and fewer generator start-ups to handle the same demand. Also, the more constrained problem which considers both line and generator contingencies, TG-SCUC and TG-SCUC-

CDR, results in a higher cost saving than the respective models, T-SCUC and T-SCUC-CDR, that only consider transmission outages. However, it can be noted that generator outages are very infrequent compared to line outages.

The proposed model considering only transmission contingencies, T-SCUC-CDR, results in a total curtailment of 25.5 MW over 24 hours as CDR action which is same in the case of TG-SCUC-CDR. It can be noted that the cumulative CDR action for line outages is only 0.01% of the peak system load and it brings about significant total operational cost reduction. It was also observed that key system line, line 7 or line 27, outage required 8.4 MW CDR action at bus 14; and line 8 outage resulted with 2.18 MW CDR action at bus 6 at various time periods. Therefore, only few critical outages required CDR to satisfy system requirements. TG-SCUC-CDR, the total amount of CDR action is much higher, 370 MW over 24 hours for generator outages and 25.5 MW over 24 hours for line outages. Similar to CDR due to line outages, only a few large generator outages, generator 23 and generator 24, utilize CDR to maintain system reliability.

Both TG-SCUC-CDR and T-SCUC-CDR models benefit by significantly faster solve time when compared to TG-SCUC and T-SCUC, respectively. In particular, TG-SCUC-CDR is 20% faster than TG-SCUC and T-SCUC-CDR is 48% faster than T-SCUC. This is because, the introduction of CDR results in a relaxed problem with increased feasible set of solutions.

Table 2.6. Operational Cost and Post-contingency Demand curtailed

	TG-SCUC	TG-SCUC-CDR	T-SCUC	T-SCUC-CDR
Cost ($)	685,670	670,674	677,851	668,026
MIPGAP	0.0095	0.0045	0.0085	0.0015
Solve time (s)	237	191	111	57
$\sum_{n,c \in K_c,t} CDR_{n,c,t}$	NA	25.46	NA	25.46
$\sum_{n,c \in G_c,t} CDR_{n,c,t}$	NA	369.81	NA	NA

2.4.3. CDR penalty cost sensitivity

Since the CDR actions result in curtailment of non-critical loads, a penalty cost for such actions are introduced in the objective cost in (2.27). Moreover, the occurrences of either transmission or generator outages are low which is modelled by π_c. The product of the probability, π_c, and cost of CDR, c_n^{Ctg}, represents the penalty cost in the system. The system was studied with varying cost of CDR from 0 \$/MWh to 40,000 \$/MWh. This is represented in two graphical forms, a low penalty cost sensitivity to CDR actions, Fig. 2.4 and a high penalty cost sensitivity to CDR actions, Fig. 2.5. The system shows inverse relations, that is the cumulative amount CDR actions decreases as cost of CDR increases.

In the low penalty cost sensitivity, at 0 $/MWh, there is no control to limit CDR actions and hence it results in cumulative curtailment of 328,925 MW for line outages and 341,379 MW for generator outages (not represented in the scale of graph). At 1 $/MWh, we notice significant reduction to the CDR action with 25.46 MW for line outages and 369.8 MW for generator outages. It was noted that at low cost of CDR, the CDR actions due to generator outages are more sensitive whereas due to line outages are constant. Here, the total cost of the system changed marginally to increasing penalty cost with the anomaly at 1 $/MWh can be explained by the associated higher relative gap in solution.
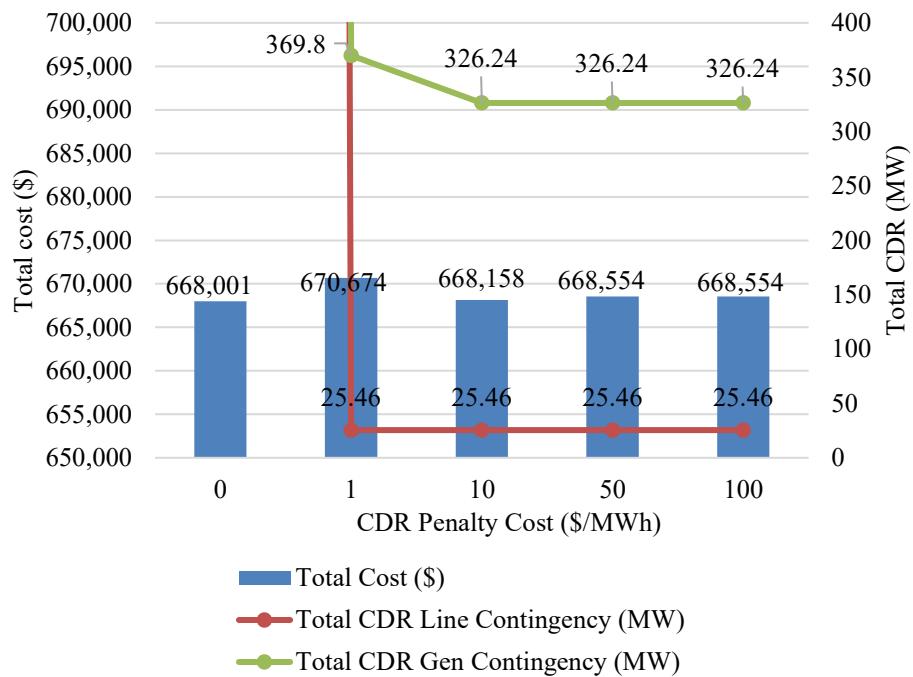
Fig. 2.4 Low penalty cost sensitivity study for TG-SCUC-CDR.
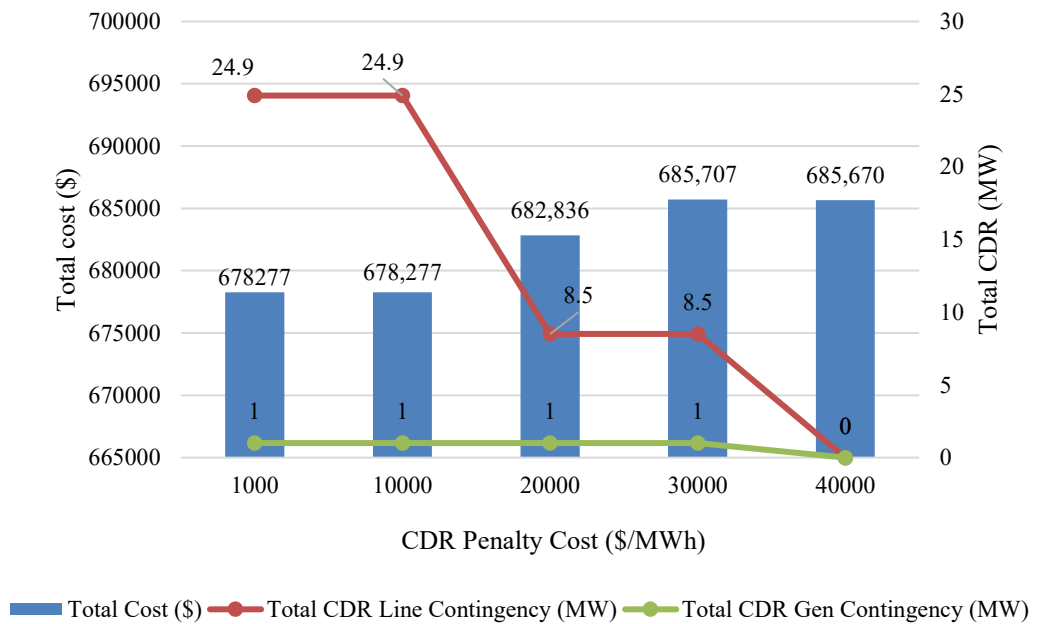
Fig. 2.5 High penalty cost sensitivity study for TG-SCUC-CDR.

A high penalty cost sensitivity study was conducted to identify when the total CDR actions result 0 MW. Here, it was noted that only at very high cost of CDR, $40,000, the system does not implement CDR for both line outages and generator outages. Therefore, the total cost of the system for TG-SCUC-CDR is same as the TG-SCUC. Also, it was noted that at high cost of CDR, the CDR actions due to generator outages and line outages are very sensitive. The cumulative CDR actions due to line outages dropped steeply from 25.46 MW to 8.5 MW at a penalty cost of $540 whereas due to generator outages dropped steeply at a penalty cost of $30 from 326.24 MW to 1 MW.

2.4.4. System Flexibility

Five scenarios were considered: two low-load scenarios (80%, 90%), a base-load scenario (100%) and two high-load scenarios (110%, 120%). The load profile was varied using a percentage multiplied to the nodal load. Fig. 3.3 shows the total cost for various methods under different load profiles and respective cumulative CDR actions for generator and line outages.
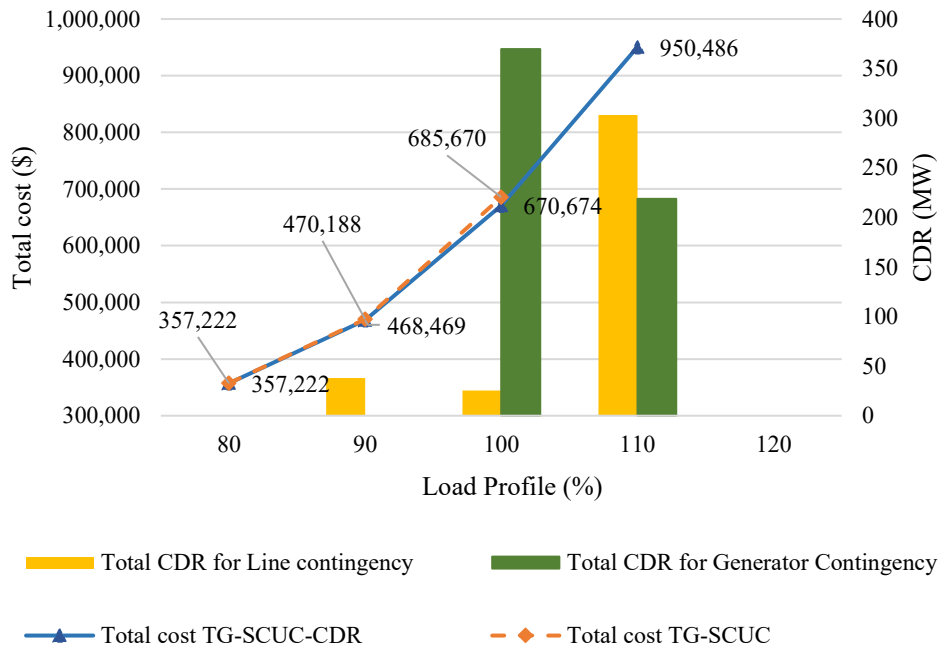
Fig. 2.6 Total system cost and cumulative DR shifted for different scenarios.

CDR is never implemented for the very low-load scenario (80%) since the base-case network loading level is low and post-contingency networks are not congested. This implies both TG-SCUC and TG-SCUC-CDR obtain the same total cost. At very high load scenario, 120%, TG-SCUC and TG-SCUC-CDR are infeasible.

39

As the system is loaded, CDR actions are observed in load scenarios of 90%-110% along with economic benefits of total cost reduction by cheaper generator dispatch schedule. Here, at 90% load scenario only line outages resulted in CDR actions whereas CDR actions in base-load (100%) and high-load scenarios (110%) are resulted from both line and generator outages. At base-load scenario (100%), the cumulative CDR actions due to line outages are lower compared to cumulative CDR actions due to generator outages.

However, at high-load scenario (110%), TG-SCUC is infeasible whereas TG-SCUC-CDR provides a feasible solution by utilizing the flexibility in the system associated with CDR. This implies that utilizing CDR is beneficial in serving higher critical loads compared to traditional SCUC which does not implement any corrective actions.

2.4.5. Market Analysis

Table 2.7 shows the market results for base-load profile (100%) which compare the load payment, generator revenue and average nodal LMP for various scheduling models when CDR is utilized (T-SCUC-CDR, TG-SCUC-CDR) and when CDR is not utilized (T-SCUC, TG-SCUC). Overall, it is observed that with CDR the average nodal LMP, load payment and generator revenue are higher, which is counter-intuitive since TG-SCUC-CDR or T-SCUC-CDR results in a lower total operation cost solution. Also,

the difference in average nodal LMP is more evident when both line and generator outages are considered compared to only line outages.

The higher LMP in TG-SCUC-CDR compared to TG-SCUC can be explained using the generator commitment solution in Table 2.8. Since the market results are calculated with LMP, it is expected to have higher load payment and generator revenue due to higher average nodal LMP. However, the commitment solution, 14 for TG-SCUC and 6 for TG-SCUC-CDR after period 1, favors long-term reliability of generators through infrequent generator start-ups with flexibility obtained through CDR. Here, all units are OFF before period 1; and in period 1, both TG-SCUC and TG-SCUC-CDR commit 18 units. However, there are more uncommitted units which are always OFF in TG-SCUC-CDR compared to TG-SCUC. Traditionally, the flexibility in the system is obtained by committing extra units as seen in TG-SCUC where a total of 474 committed generator-hours over 24 hours was noticed whereas in TG-SCUC-CDR, it was bettered efficiently to 460 committed generator-hours over 24 hours.

The nodal LMP is higher in the case of TG-SCUC-CDR due to: (i) fewer generators are committed (ii) marginal units are more expensive (iii) the cheaper generators (always ON) capacity are completely utilized in the base-case dispatch solution. There are also more expensive units that are in 'always OFF' condition in TG-SCUC-CDR, which points to reduced generator start-ups.

Table 2.7. Market Results for IEEE-24 Bus System

	TG-SCUC	TG-SCUC-CDR	T-SCUC	T-SCUC-CDR
Load payment($)	1,289,650	1,698,060	1,070,370	1,071,270
Gen revenue ($)	707,594	1,073,830	1,683,830	1,695,420
Avg LMP ($)	23.7	31.74	31.51	31.67

Table 2.8. Generator Commitment Status

	TG-SCUC	TG-SCUC-CDR
Always ON	3,7,8,21–33	4,7–8,21–33
Always OFF	12–15	1–2, 5–6,15–16,19–20
Marginal Units	1–6,9–11,16–20	3,9–11,17–18
Total start-ups $t > 1$	14	6
Total start-ups $t = 1$	18	18
Total commitment	474	460

2.5.   Summary

The use of demand response as a corrective action to system contingencies was proposed as TG-SCUC-CDR model and studied. Mainly, TG-SCUC-CDR and T-SCUC-CDR results in lower operational costs by reducing generator start-ups and

fewer generators committed for the same load profile compared to TG-SCUC and T-SCUC, respectively. In particular, the sensitivity of such CDR actions which provide significant economic benefits were studied with respect to penalty cost and load profile variation. The results indicate that given a high demand profile, SCUC is infeasible whereas SCUC-CDR is feasible as the system uses the available system flexibility. Also, the sensitivity to penalty cost shows that CDR actions with even small amounts such as 2 MW can result in substantial economic benefits. It was also noted that the CDR actions due to generator outages are more sensitive to variation in penalty costs.

The market analysis resulted in counter-intuitive results as the average nodal LMP were higher for TG-SCUC-CDR and T-SCUC-CDR compared to TG-SCUC and T-SCUC, respectively. However, this was explained by the additional units committed and the capacity of cheaper generators were not completely exhausted at the cost of expensive units running at no-load or low capacities in the case of TG-SCUC and T-SCUC

The best scenario is represented by infinite transmission capacity in the post-contingency scenario, which serves as a benchmark to measure the performance of the proposed CTS in SCUC. It is observed that CTS can alleviate the network congestion in post-contingency scenarios by rerouting power through the network. The implementation of CTS also led to fewer generator start-ups. This is evident from the results that only 1 generator start-up is required when CTS is used as compared to 7

without CTS after period 1. Overall, this results in reduced operational cost, congestion cost and higher transmission capability in the case of a congested network.

Studying the line flows in contingent scenarios, we note that line overload was reduced with CTS in most contingent scenarios. The use of CTS can lead to the removal of post-contingency transmission congestions if more transmission elements are allowed to open in each contingent scenarios which will result in $0 in congestion cost. However, there are concerns with TS as it can cause a large disturbance to the system. The additional cost due to the restriction of allowing one transmission element to be open in CTS is a tradeoff between system reliability and cost saving. The congestion cost, $2,183, is only 0.2% of the total operation cost and it can be attributed as a reliability cost to avoid system disturbance.

3. SYSTEM FLEXIBILITY CONSIDERING RENEWABLE ENERGY SYSTEMS

The electric power generated needs to be transferred and utilized concurrently since it is expensive to store bulk power. This requires state of the art approaches that optimize the scheduling before-hand to ensure reliable power supply, save cost and avoid resource wastage. This stresses on the development of smarter algorithms to effectively utilize the flexibility in the power system which includes the network. Not only that, the importance on climate change and global warming in recent years has increased the investments in renewable sources of energy. The Paris climate deal set ambitious goals to reduce the carbon emissions by 2030 to limit the rise in global temperature [64]. Such directives place an emphasis on renewable energy sources (RES) as opposed to conventional fossil fuel plants. Typically, an increase in wind and solar generation is seen as favorable. However, the intermittent nature of RES due to weather brings additional challenges to the efficient and reliable grid operations [65]. To address the integrations of RES, flexibility of the system can be utilized through preventive or corrective actions. Not only that, in addition to such actions, there is increase in energy storage system which also offers additional system flexibility.

3.1. Literature Review

3.1.1. RES through Network Reconfiguration

During high penetration of RES, a flexible power system facilitates the integration of intermittent RES. This entails the usage of storage devices, flexible transmission and flexible demand. Moreover, the requirement of favorable location and land implies RES are placed in remote locations. Therefore, even with the introduction of large-scale storage devices, the high penetration of RES results in curtailment due to network congestion. As a result, local generating sources utilizing fossil fuels are more utilized at the cost of RES curtailment.

An effective smart grid and new technologies such as energy storage or flexible AC transmission System (FACTS) are required to utilize RES concurrently without spilling free RES and to maintain lower operational costs. Due to such variations, the grid network is also built with redundancy to handle increasing future demand and maintain system reliability. This adds flexibility in the transmission network that is not fully considered as one static network cannot be always optimal.

Traditionally, the flexibility is provided by committing extra generators to handle emergencies and the transmission element in the network is treated as a static asset barring scheduled maintenance outages [19]. Hence, the transmission flexibility of the grid is less utilized in congestion management via network reconfiguration (NR) [19]. Currently, ISOs do not implement a dynamic network in day-ahead or real-time

operations. To relieve network congestion and reduce RES curtailment, it requires transmission expansion planning to increase the transfer capability [25]. Another option, as state earlier is to redirect the power flow on the lines. This can be implemented through modifying the network reconfiguration (NR) [19], [20], [66] or line parameters using FACTS devices [67]. However, flexibility through expansion planning, energy sources and FACTS devices require expensive investment and maintenance. Therefore, the usage of NR is attractive to utilize the power produced by economical generators and RES to meet the demand concurrently as it does not require any investment.

The impact of NR on high penetrative wind models were studied in [25],[25]–[28]. [29] provides a real-time implementation of enhancing optimal power flow by incorporating CNR in economic dispatch to facilitate integration of RES in the grid. However, the effect of SCUC with CNR on high penetrative RES network and RES curtailment studies has not been performed. Due to the high variability of RES, it requires solution which is satisfied in multiple scenarios. Therefore, a stochastic implementation through a known probability distribution of multiple scenarios is considered for a feasible solution as seen in [30]–[33]. In [34], optimal NR is implemented through a bi-level stochastic implementation to solve large scale networks. However, this paper does not consider the use of reconfiguration as a corrective action and post-contingency constraints were not modelled.

3.1.2. RES with Energy Storage System and NR

Due to the increase in investments in renewable energy sources (RES) to reduce carbon emissions, which in turn requires sophisticated technologies and smarter algorithms to utilize the intermittent free resource efficiently. Since RES is fed to the grid, it is also paramount to maintain the grid reliability. However, since RES is installed in remote weather-favorable locations, the transmission congestion can cause spillage of free resource [68]. Other viable technologies for reducing RES curtailments is through FACTS to reduce network congestion [35] and the use of energy storage [36]. Energy storage systems (ESS) has garnered significant attention as a solution to store excess RES output [69]. But, ESS can also be less utilized during transmission congestion when it is not located near RES.

To address the above issues, the system flexibility can be utilized to avoid transmission congestion [19],[25] and store excess power for future use [71]. However, the network is still predominantly treated as static assets and transmission congestions management through network reconfiguration is often overlooked. Since network reconfiguration (NR) is a cheap and quick action it can lead to significant economic benefits through smarter algorithms.

Presently, NR is overlooked in system scheduling or operations. The increase in complexity in introducing NR in day-ahead operations through N-1 security-constrained unit commitment (SCUC) is a major reason. Thus, operators perform such actions based on experience. Since NR is a quick action it can implemented in the base-

case as a preventive NR (PNR) [20],[26] and [72] and post-contingency-scenario as a corrective NR (CNR) [24] and [73] with economic benefits and congestion management. [74] and [75] show various approaches with promising results in computational performance while addressing PNR and/or CNR.

CNR in real-time is implemented through heuristic methods in [43],[59]–[60] and by incorporating RES enhancing optimal power flow in [29],[67]. In day-ahead operations, it is incorporated post-contingency constraints in [74],[76]. However, [75] does not consider RES or ESS and [76] does not consider ESS. RES is facilitated with preventive resource scheduling in [31] and PNR in [27], [32] and [34]. In [34], PNR is implemented through a bi-level stochastic implementation to solve large scale networks. But, [27], [32] and [34] do not consider ESS. High penetration RES introduces huge variability in the system and therefore a multi-scenario stochastic approach which provides a common commitment is required while maintaining reliability [27], [31]–[32], [34] and [76]. In [75], both PNR and CNR are considered along with energy storage but this model does not include RES or address their unpredictability.

Therefore, the effect of N-1 SCUC with PNR and CNR on high penetrative RES network with ESS for RES curtailment studies has not been studied. In this paper, we propose a model which considers a N-1 Stochastic-SCUC (SSCUC) solution integrating a multi-scenario RES such as wind and solar supported by ESS while considering PNR and CNR to achieve significant system flexibility.

3.2.   *N*-1 SSCUC for Renewable Integration

The intermittent nature of renewable sources such as wind and solar leads to uncertainty. To facilitate renewable energy sources (RES) the solutions of *N*-1 SCUC problem must be feasible for multiple scenarios. Hence, stochastic implementation of the *N*-1 SCUC problem is proposed and discussed in the following subsections. As stated in the literary review, RES are located in remote favorable destination without adequate transmission capacity. As a result, if lines are congested, RES faces congestion-induced curtailment. The goal of introducing NR and/or ESS in the model is to leverage network flexibility to reduce RES curtailments. In Section 3.2.1 we introduce the mathematical model of *N*-1 SSCUC while in Section 3.2.2 the NR and CNR constraints are explained and in Section 0, the constraints to model Energy storage are described.

3.2.1. *N*-1 SSCUC Model

Section 2.2.1 models the SCUC whereas the integration of RES brings about uncertainty to the model. Hence, the dimensionality of the *N*-1 SCUC model is increased by the introduction of scenario *s* which ensures the commitment solutions is valid for multi-scenario approach.

The utilization of free RES output is directly related to reducing the cost and hence the curtailments are lower in base-case. However, SSCUC leads to high post-contingency RES curtailment as it is not considered in the objective. Therefore, if the

study is focused on reducing or eliminating RES curtailments, a penalty cost, c_w^{pen}, was added for post-contingency curtailment as shown in (3.1),

$$\text{Minimize } \sum_{g,t}\left(c_g^{NL}u_{g,t} + c_g^{SU}v_{g,t} + \right.$$

$$\left. \sum_s\left(\pi_s c_g P_{g,t,s}\right)\right) + \sum_{w,c,t,s}\left(\pi_s c_w^{pen}(P_w^{max} - P_{w,c,t,s})\right), \tag{3.1}$$

however, if the study is focused on finding the benefits of NR/CNR and ESS then the penalty cost, $c_w^{pen} = 0$, is utilized.

The base-case generation constraints, (3.2)–(3.13), consist of the min-max limits of generator output, reserve limits, generator ramping requirements, minimum up-down time, generator start-up, commitment constraints bounded by integrality, and finally the maximum RES generation constraints,

$$P_g^{min}u_{g,t} \le P_{g,t,s}, \forall g, t, s, \tag{3.2}$$

$$P_{g,t,s} + r_{g,t,s} \le P_g^{max}u_{g,t}, \forall g, t, s, \tag{3.3}$$

$$0 \le r_{g,t,s} \le R_g^{10}u_{g,t}, \forall g, t, s, \tag{3.4}$$

$$\sum_{q \in G} r_{q,t,s} \ge P_{g,t,s} + r_{g,t,s}, \forall g, t, s, \tag{3.5}$$

$$P_{g,t,s} - P_{g,t-1,s} \le R_g^{hr}u_{g,t-1} + R_g^{SU}v_{g,t}, \forall g, t, s, \tag{3.6}$$

$$P_{g,t-1,s} - P_{g,t,s} \le R_g^{hr}u_{g,t} + R_g^{SD}(v_{g,t} - u_{g,t} + u_{g,t-1}), \forall g, t, s, \tag{3.7}$$

$$\sum_{q=t-UT_g+1}^{t} v_{g,q} \le u_{g,t}, \forall g, t \ge UT_g, \tag{3.8}$$

$$\sum_{q=t+1}^{t+DT_g} v_{g,q} \le 1 - u_{g,t}, \forall g, t \le T - DT_g, \tag{3.9}$$

$$v_{g,t} \ge u_{g,t} - u_{g,t-1}, \forall g, t, \tag{3.10}$$

$$v_{g,t} \in \{0,1\}, \forall g, t, \tag{3.11}$$

$$u_{g,t} \in \{0,1\}, \forall g, t, \tag{3.12}$$

and

$$0 \leq P_{w,t,s} \leq P_{w,s}^{max}, \forall w, t, s. \tag{3.13}$$

The base-case transmission constraints, (3.14)–(3.16), consist of DC power flow equation, the min-max line long-term thermal limits, and the nodal power balance equations with renewable generation injection,

$$\sum_{g \in g(n)} P_{g,t,s} + \sum_{k \in \delta^+(n)} P_{k,t,s} - \sum_{k \in \delta^-(n)} P_{k,t,s} = d_{n,t} -$$
$$\sum_{w \in w(n)} P_{w,t,s}, \forall n, t, s, \tag{3.14}$$

$$P_{k,t,s} - b_k\left(\theta_{n,t,s} - \theta_{m,t,s}\right) = 0, \forall k, t, s, \tag{3.15}$$

and

$$-P_k^{max} \leq P_{k,t,s} \leq P_k^{max}, \forall k, t, s. \tag{3.16}$$

The post-contingency case generator constraints, (3.17)–(3.21), models the generator 10-minute ramp up-down and min-max limits and renewable generation limit after the outage of line c,

$$P_{g,t,s} - P_{g,c,t,s} \leq R_g^{10} u_{g,t}, \forall g, c \in C, t, s, \tag{3.17}$$

$$P_{g,c,t,s} - P_{g,t,s} \leq R_g^{10} u_{g,t}, \forall g, c \in C, t, s, \tag{3.18}$$

$$P_g^{min} u_{g,t} \leq P_{g,c,t,s}, \forall g, c \in C, t, s, \tag{3.19}$$

$$P_{g,c,t,s} \leq P_g^{max} u_{g,t}, \forall g, c \in C, t, s, \tag{3.20}$$

and

$$0 \leq P_{w,c,t,s} \leq P_{w,s}^{max}, \forall w, t, s. \tag{3.21}$$

In the post-contingency case, transmission constraints are (3.23)–(3.24) and the nodal balance is maintained under a line outage through (3.22),

$$\sum_{g \in g(n)} P_{g,c,t,s} + \sum_{k \in \delta^+(n)} P_{k,c,t,s} - \sum_{k \in \delta^-(n)} P_{k,c,t,s} = d_{n,t} - \tag{3.22}$$

$$\sum_{w \in w(n)} P_{w,c,t,s}, \forall n, c \in C, t, s,$$

$$P_{k,c,t,s} - b_k \left(\theta_{n,c,t,s} - \theta_{m,c,t,s} \right) = 0, \forall k, c \in C, t, s, \tag{3.23}$$

and

$$-P_k^{emax} \leq P_{k,c,t,s} \leq P_k^{emax}, \forall k, c \in C, t, s. \tag{3.24}$$

3.2.2. NR and CNR modelling

Branch power flow equations and limits without NR is modelled in (3.14)–(3.15),whereas without CNR is modelled in (3.23)–(3.24). NR or CNR modelling requires the binary decision variables, $z_{k,t,s}^{PNR}$ and $z_{k,c,t,s}^{CNR}$, respectively. The decision variable is incorporated in (3.27) for PNR and (3.31) for CNR. Here, a value of 0 represents line is disconnected from the system and the value of 1 indicates line is available. Also, since network topology changes can cause a big disturbance in the system, (3.28) for PNR and (3.32) for CNR, is added to limit to at-most one topology change per instance. Linearity in the power flow equation of (3.14) and (3.23) are

53

implemented by introducing the 'big-M' method. Therefore, for PNR, (3.14) is replaced by (3.25)–(3.26) and for CNR, (3.23) is replaced by (3.29)–(3.30).

To summarize PNR is implemented in the base-case and is modelled with,

$$P_{k,t,s} - b_k(\theta_{n,t,s} - \theta_{m,t,s}) + (1 - z_{k,t,s}^{PNR})M \geq 0, \forall k, t, s, \tag{3.25}$$

$$P_{k,t,s} - b_k(\theta_{n,t,s} - \theta_{m,t,s}) - (1 - z_{k,t,s}^{PNR})M \leq 0, \forall k, t, s, \tag{3.26}$$

$$-z_{k,t,s}^{PNR} P_k^{max} \leq P_{k,t,s} \leq z_{k,t,s}^{PNR} P_k^{max}, \forall k, t, s, \tag{3.27}$$

and

$$\sum_k (1 - z_{k,t,s}^{PNR}) \leq 1, \forall k, t, s. \tag{3.28}$$

CNR is implemented in post-contingency and is modelled with,

$$P_{k,c,t,s} - b_k(\theta_{n,c,t,s} - \theta_{m,c,t,s}) + (1 - z_{k,c,,t,s}^{CNR})M \geq 0, \forall k, c, t, s, \tag{3.29}$$

$$P_{k,c,t,s} - b_k(\theta_{n,c,t,s} - \theta_{m,c,t,s}) - (1 - z_{k,c,t,s}^{CNR})M \leq 0, \forall k, c, t, s, \tag{3.30}$$

$$-P_k^{emax} z_{k,c,t,s}^{CNR} \leq P_{k,c,t,s} \leq z_{k,c,t,s}^{CNR} P_k^{emax}, \forall k, c, t, s, \tag{3.31}$$

and

$$\sum_k (1 - z_{k,c,t,s}^{CNR}) \leq 1, \forall k, c, t, s. \tag{3.32}$$

3.2.3. Energy storage system modelling

ESS can be modelled by characteristic equations of charging and discharging of the battery for base-case in (3.33)–(3.39) and post-contingency case in (3.41)–(3.47). These constraints of the batteries can be introduced in SSCUC by replacing both (3.16) and (3.22) by (3.40) and (3.48), respectively.

For the base-case, BESS constraints can be modelled with,

$$b_{e,t,s}^{cha} + b_{e,t,s}^{dis} \leq 1, \forall e, t, s, \tag{3.33}$$

$$0 \leq P_{e,t,s}^{cha} \leq Pmax_e^{cha} b_{e,t,s}^{cha}, \forall e, t, s, \tag{3.34}$$

$$-Rmax_e^{cha} \leq \left(P_{e,t,s}^{cha} - P_{e,t-1,s}^{cha}\right)\Delta T \leq Rmax_e^{cha}, \forall e, t, s, \tag{3.35}$$

$$0 \leq P_{e,t,s}^{dis} \leq Pmax_e^{dis} b_{e,t,s}^{dis}, \forall e, t, s, \tag{3.36}$$

$$-Rmax_e^{dis} \leq (P_{e,t,s}^{dis} - P_{e,t-1,s}^{dis})\Delta T \leq Rmax_e^{dis}, \forall e, t, s, \tag{3.37}$$

$$SOC_e^{min} ESS_e^{max} \leq E_{e,t,s} \leq SOC_e^{max} ESS_e^{max}, \forall e, t, s, \tag{3.38}$$

$$E_{e,t,s} = E_{e,t-1,s} + \left(\eta_e^{cha} P_{e,t,s}^{cha} - \frac{P_{e,t,s}^{dis}}{\eta_e^{dis}}\right), \forall e, t, s, \tag{3.39}$$

and

$$\sum_{g\in g(n)} P_{g,t,s} + \sum_{k\in\delta^+(n)} P_{k,t,s} - \sum_{k\in\delta^-(n)} P_{k,t,s} = d_{n,t} - \sum_{w\in w(n)} P_{w,t,s} + \tag{3.40}$$

$$\sum_{e\in e(n)}\left(P_{e,t,s}^{cha} - P_{e,t,s}^{dis}\right), \forall n, t, s.$$

Since BESS are also used in the post-contingency scenario, constraints are required to ensure the operation as,

$$0 \leq P_{e,c,t,s}^{cha} \leq Pmax_e^{cha} b_{e,t,s}^{cha}, \forall e, c, t, s, \tag{3.41}$$

$$-Rmax_e^{cha} \leq \left(P_{e,c,t,s}^{cha} - P_{e,t,s}^{cha}\right)\Delta T \leq Rmax_e^{cha}, \forall e, c, t, s, \tag{3.42}$$

$$0 \leq P_{e,c,t,s}^{dis} \leq Pmax_e^{dis} b_{e,t,s}^{dis}, \forall e, c, t, s, \tag{3.43}$$

$$-Rmax_e^{dis} \leq \left(P_{e,c,t,s}^{dis} - P_{e,t,s}^{dis}\right)\Delta T \leq Rmax_e^{dis}, \forall e, c, t, s, \tag{3.44}$$

$$SOC_e^{min} ESS_e^{max} \leq E_{e,c,t,s} \leq SOC_e^{max} ESS_e^{max}, \forall e, t, s, \tag{3.45}$$

$$E_{e,c,t,s} = E_{e,t,s} + \left(\eta_e^{cha} P_{e,c,t,s}^{cha} - \frac{P_{e,c,t,s}^{dis}}{\eta_e^{dis}} \right), \forall e, c, t, s, \qquad (3.46)$$

$$0 \leq P_{e,c,t,s}^{cha} \leq Pmax_e^{cha} b_{e,t,s}^{cha}, \forall e, c, t, s, \qquad (3.47)$$

and

$$\sum_{g \in g(n)} P_{g,c,t,s} + \sum_{k \in \delta^+(n)} P_{k,c,t,s} - \sum_{k \in \delta^-(n)} P_{k,c,t,s} = d_{n,t} - \qquad (3.48)$$

$$\sum_{w \in w(n)} P_{w,c,t,s} + \sum_{e \in e(n)} \left(P_{e,c,t,s}^{cha} - P_{e,c,t,s}^{dis} \right), \forall n, c, t, s.$$

3.2.4. Proposed models

Several proposed models were introduced in this chapter as mentioned in Table 3.1. The benchmark model is SSCUC which includes RES. The proposed SSCUC-CNR includes RES but does not include ESS. The proposed models SSCUC-P introduce RES,ESS, and PNR, whereas SSCUC-C includes RES,ESS, and CNR. The proposed model SSCUC-PC includes both PNR and CNR in addition to RES and ESS.

Table 3.1. Proposed Models

Model	Technologies added	Base-Case Constraints	N-1 Constraints
SSCUC	RES	(3.2)–(3.16)	(3.17)–(3.24)
SSCUC-CNR	RES, CNR	(3.2)–(3.16)	(3.17)–(3.22),(3.29)–(3.32)
SSCUC-P	RES, ESS, PNR	(3.2)–(3.13), (3.25)–(3.28), (3.33)– (3.40)	(3.17)–(3.21), (3.23)–(3.24), (3.41)–(3.48)
SSCUC-C	RES, ESS, CNR	(3.2)–(3.13), (3.15)–(3.16), (3.33)–(3.40)	(3.17)–(3.21),(3.29)–(3.32), (3.41)–(3.48)
SSCUC-PC	RES, ESS, PNR, CNR	(3.2)–(3.13), (3.25)–(3.28), (3.33)– (3.40)	(3.17)–(3.21),(3.29)–(3.32), (3.41)–(3.48)

3.3. Test case modification for ESS and RES

For this chapter, two different test systems were created by modifying the IEEE 24-Bus system utilized in sub-section 2.3.2 as described below.

3.3.1. Testcase I: Modification for Scenario-based RES curtailment studies

The IEEE 24-Bus system utilized in sub-section 2.3.2 contains 24 buses, 33 generators and 38 branches. However, the system was modified to include three wind farms located at bus 12, bus 16 and bus 22 to study the effect of network constraints on RES curtailment. Five different scenarios are considered for wind generation; and the base total system renewable generation over 24 hours for each scenario are represented in Fig. 3.1.
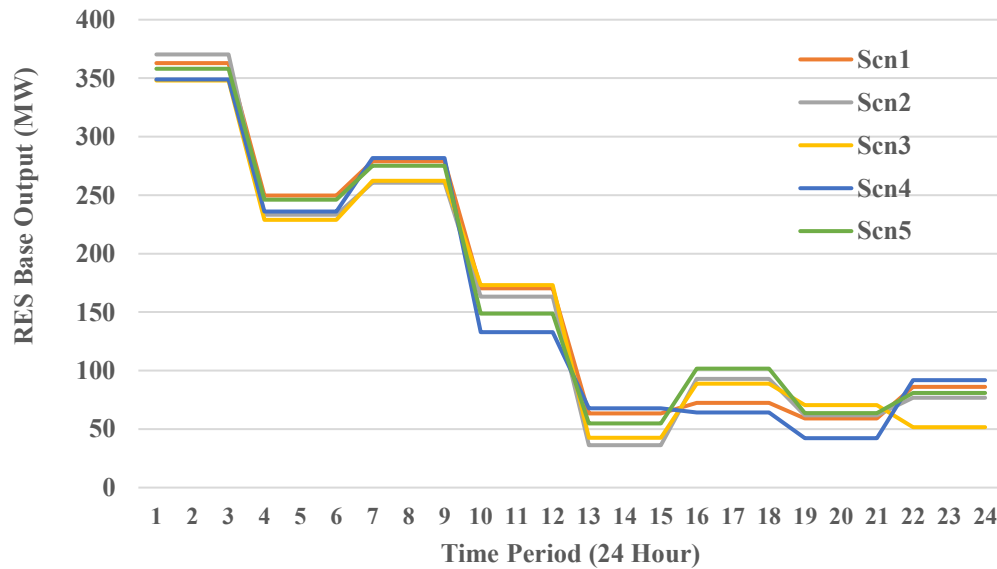
Fig. 3.1 The base total RES output for each scenario.

The system-wide RES output for various penetration level is represented in Fig. 3.2. The base total RES output was modified to obtain five cases considered for the study and can be classified using the peak load period penetration as ~15%, ~30%, ~50%, ~60 and ~80%. Apart from the wind generation, the total generation capacity

58

from traditional units is 3,393 MW and the system peak load is 2,270 MW. The wind output was assumed to be constant for each three-hour-period due to the computational complexity of CNR for this study.
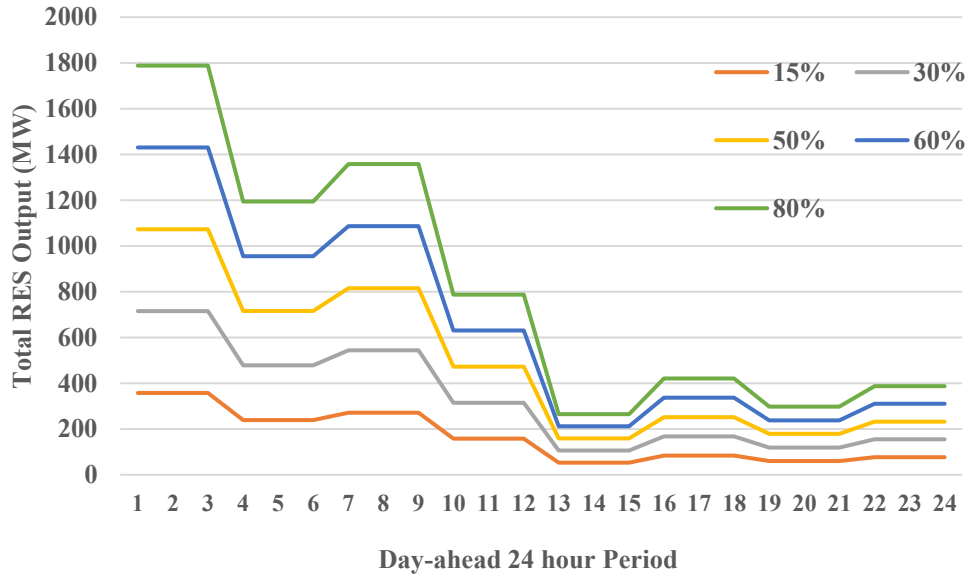
Fig. 3.2 System-wide RES generation for various penetration levels.

3.3.2. Testcase II: Scenario-based RES NR and ESS benefits studies

The IEEE 24-Bus system utilized in sub-section 2.3.2 contains 24 buses, 33 generators and 38 branches were modified. Modifications introduced in the system are the addition of multi-scenario RES at bus 16, and bus 21 while ESS were installed at bus 14 and bus 23. The total available traditional generation capacity is 3,393 MW and the system peak load is 2,270 MW.

The ESS parameters are present in Table 3.2. Four scenarios were considered for the RES with an average system penetration of 48% is considered with equal

probability distribution and is presented in Fig. 3.3. The RES output is assumed to be

constant for four-hour-blocks.

Table 3.2. ESS Data

Parameter	Value
Max Charging/Discharging capacity (MW)	220
Max rate of charging/discharging (MW/h)	100
SOC min/max	20%/90%
Charging/discharging efficiency	0.9
Max Energy (MWh)	250
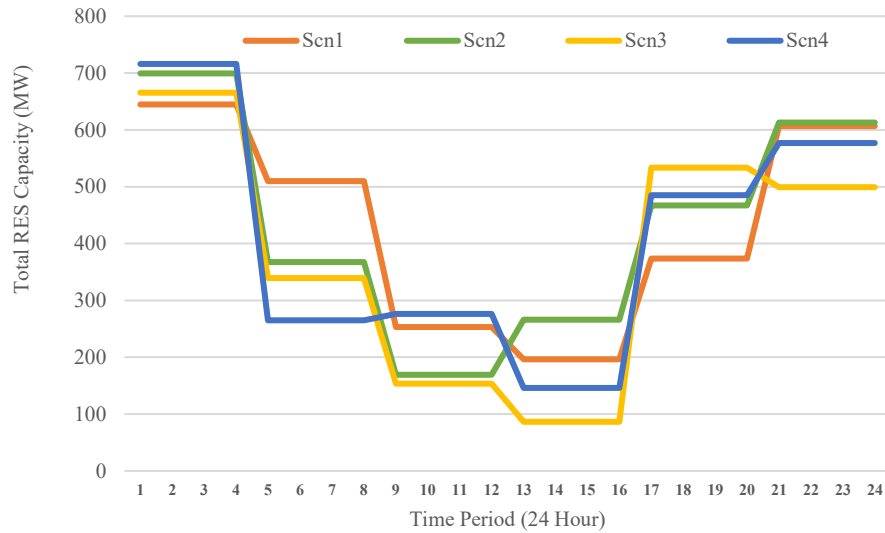
Fig. 3.3. The total RES capacity for each scenario.

3.4.   Results and Analysis: Benefits of RES curtailment with CNR

The benefits of CNR in reducing RES curtailments by increasing system flexibility. In this section, Testcase I highlighted in sub-section 3.3.1 is utilized to obtain the results. The following sub-sections analyze the results in detail.

3.4.1. Rationale for Penalty Costs

Initially, the system with peak penetration of 30% was studied under two cases, complete wind output usage (CWOU) that uses up all available wind power and variable wind output usage (VWOU) that allows the system to curtail some wind power for both models with and without CNR. Table 3.3 and Table 3.4, shows the total costs, the base-case curtailments (BCC) and the expected post-contingency curtailments (PCC) for day-ahead SSCUC and SSCUC-CNR respectively. The BCC is aggregated over all periods, $\forall t$ and RES units, $\forall w$. Similarly, the PCC is aggregated over all periods, $\forall t$, and RES units, $\forall w$, and then averaged over all contingencies, $\forall c$. Since, this is a multi-scenario stochastic implementation, as shown in (3.49) and (3.50), the probability of scenarios is utilized to obtain BCC and PCC,

$$BCC = (\textstyle\sum_{w,t,s}(\pi_s(P_w^{max} - P_{w,t,s})), \tag{3.49}$$

and

$$PCC = (\textstyle\sum_{w,c,t,s}(\pi_s(P_w^{max} - P_{w,c,t,s}))/n_c, \tag{3.50}$$

respectively.

From the initial assessment, SSCUC-CNR offers lower total costs. But from VWOU, both SSCUC and SSCUC-CNR are susceptible to heavy renewable curtailment since there is no cost associated with PCC in the objective when minimizing operational costs. It is also seen that the total cost for CWOU and VWOU is the same for the respective implementations. Therefore, introducing a penalty cost to limit PCC eliminates the curtailment in post-contingency cases without increasing total cost. Further studies in this section leverage the penalty for PCC.

Table 3.3. Penalty Cost Studies for N-1 SSCUC

	No PCC penalty		With PCC Penalty
	CWOU	VWOU	
Total cost ($)	201,769	201,769	201,769
BCC (MW)	NA	0	0
PCC (MW)	NA	9.14	0

Table 3.4. Penalty Cost Studies for N-1 SSCUC-CNR

	No PCC penalty		With PCC Penalty
	CWOU	VWOU	
Total cost ($)	177,170	177,170	177,170
BCC (MW)	NA	0	0
PCC (MW)	NA	80.90	0

3.4.2. Penetration Sensitivity Studies

The renewable energy penetration-based sensitivity studies are performed, and the associated results are presented in Fig. 3.4 and Fig. 3.5. As shown in Fig. 3.4, the general trend observed is that (i) the total cost reduces as more free renewable power was utilized and (ii) SSCUC-CNR always offered lower cost solutions compared to SSCUC. This demonstrates that CNR alleviates network congestion and reduce congestion-induced cost by increasing the transmission flexibility.

As shown in Fig. 3.5, the network utilizes all available renewable power in low penetration levels. However, RES curtailments are observed for both base case and contingency cases when RES penetration level is above 30%; it is also observed that CNR actions alleviate the post-contingency congestions for high penetration levels, 50%-80%. However, under very-high penetration of 80%, CNR alone is not beneficial as both PCC and BCC are higher with SSCUC-CNR against traditional SSCUC. This can be characterized by the cost saving offered through congestion alleviation that provides a much lower cost (even if it includes the penalty for curtailment). Therefore, increasing the penalty costs for 80% RES penetration resulted in a reduction of PCC from 323 MW to 153 MW and a reduction of BCC from 1047 MW to 655 MW for SSCUC-CNR. However, there are no changes for SSCUC; instead, the total cost increases marginally because of higher penalty. Hence, a combination of dynamic penalty factor along with CNR may be more beneficial.
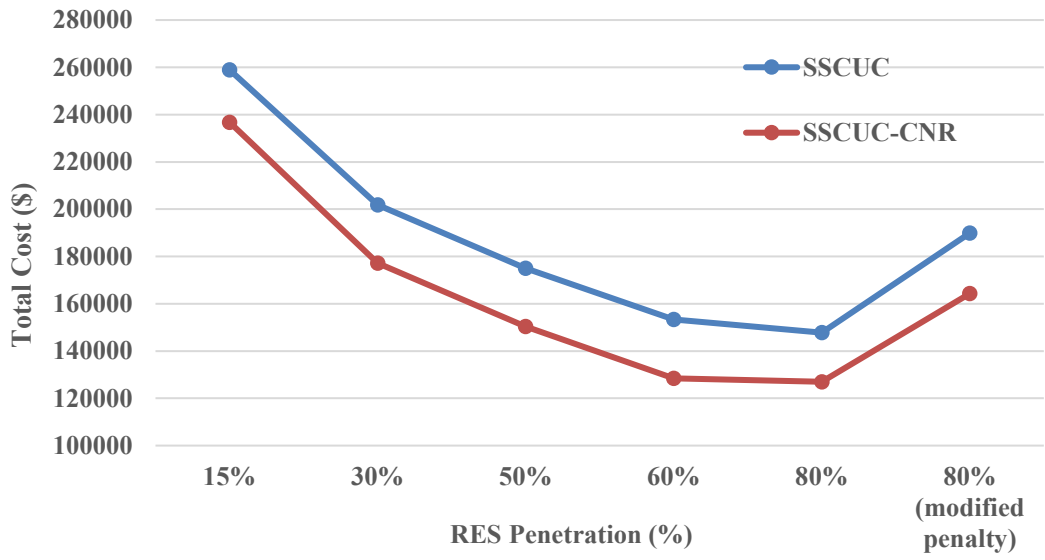
Fig. 3.4 Total Cost in $ under various penetration levels.
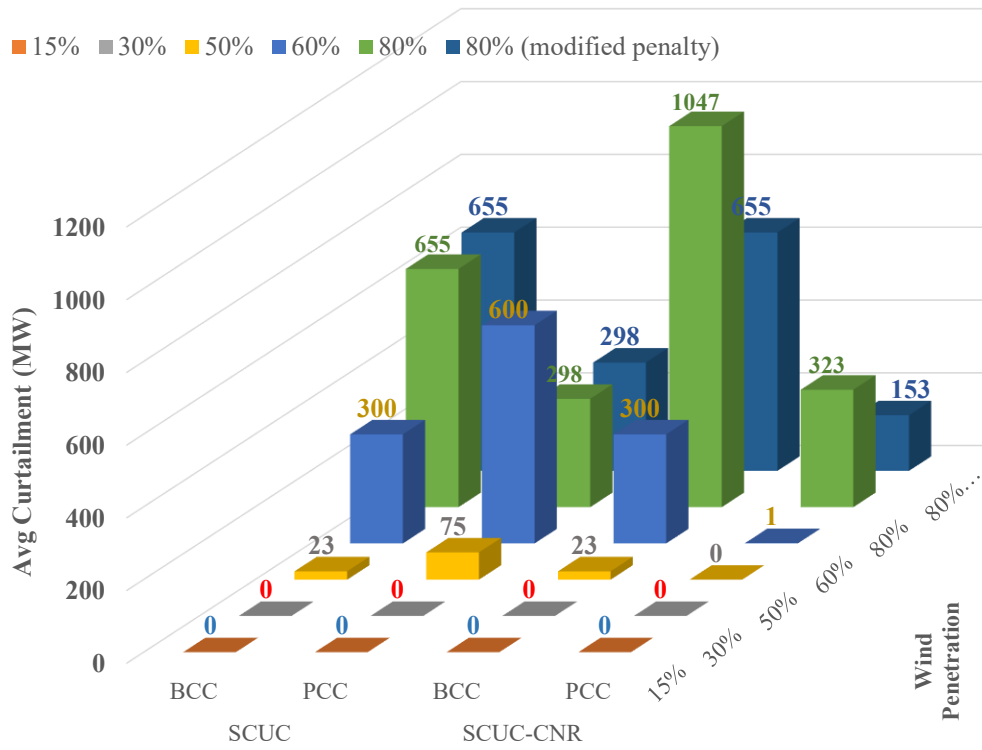
Fig. 3.5 RES curtailment under various penetration levels.

3.4.3. CNR Actions

The peak RES penetration of 80% shows high PCC in periods 1–3 and 7–9 due to the load profile, intermittent nature of RES and network congestion. However, periods 1–3 shows the most reconfiguration action taken. In total there were 64 line outage cases across 5 scenarios, 38 lines in periods 1–3 that required CNR action. Since only one line is removed as an action, a pattern to note here is that line 5 [bus 2 – bus 6], line 16 [bus 10 – bus 11], and line 30 [bus 17 – bus 18] were common choices to remove from the network.

On closer observation, firstly, these lines are closer to where RES are located in the network. Secondly, the bottleneck lines are typically line 10 [bus 6 – bus 10] and line 23 [bus 14 – bus 16]. The above CNR actions help relieve the congested lines which in turn reduces RES curtailments.

3.4.4. Carbon Emission Studies

One of the key aspects of integrating renewables in the system is the reduction of emissions. The emission data for the generators are used to highlight the reduced emissions. The base-case generation outputs were used to calculate the total net heat and emission of each generator for the test system. When averaged over multiple scenarios, it is seen from Fig. 3.6 that SSCUC-CNR leads to significantly lower carbon emissions at high penetration, 60%-80%, of RES. In comparison, SSCUC shows an increase in emissions at high penetration of RES due to higher curtailments. This

implies more traditional generators are used to meet the demand thereby increasing carbon emissions.
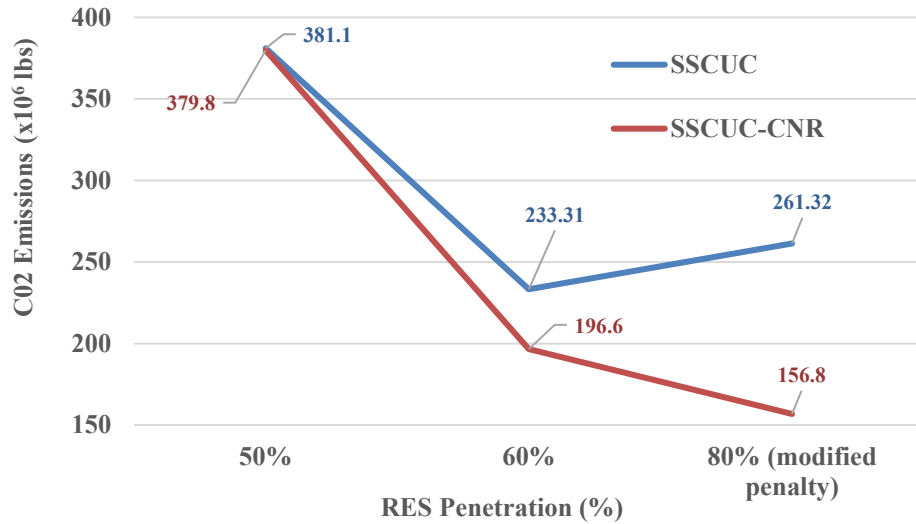
Fig. 3.6 System carbon emission under various penetration levels.

3.5.   Results and Analysis: Benefits of ESS and NR

The benefits of PNR and/or CNR with the aide of ESS in facilitating RES integrations is considered. In this section, Testcase II highlighted in sub-section 3.3.2 is utilized to obtain the results. The following sub-sections analyze the results in detail.

3.5.1. Total Cost Studies (ESS)

Table 3.5 presents the results for proposed models for total expected cost in $, solve time in seconds and average RES curtailed per scenario in MW. The benchmark results for SSCUC present that the total expected cost (averaged over four scenarios) is $161,340 and it leads to an average RES curtailment over four scenarios of 208 MW.

The transmission flexibility through PNR and/or CNR results in significant economic benefits over SSCUC. Mainly, SSCUC-P and SSCUC-C implement only PNR and only CNR, respectively, results in alleviation of congestion cost of $6,505 and $2,940 over SSCUC. This implies that PNR, implemented in base-case, can provide more flexibility benefits to the system than CNR, implemented in post-contingency case. The combination of PNR and CNR leads to further saving in SSCUC-PC since this provides additional transmission flexibility in both base-case and post-contingency case at $13,109 over SSCUC due to the increase in total feasibility region. The RES curtailment is the highest in SSCUC due to the similar reason and is bettered in models which implement PNR and/or CNR. A decrease in curtailment of free RES output of 139.75 MW and 35.75 MW is noticed per scenario for SSCUC-P and SSCUC-C. Again, SSCUC-PC provides the maximum decrease in curtailment of free RES output of about 162.5 MW per scenario.

The computation complexity of the problem increases due to the binary variables introduced by PNR or CNR with CNR resulting in higher computational burden than PNR. This is evident from SSCUC-PC, though leads to the best solution, the solver results in timeout solution with higher MIPGAP of 0.02.

Table 3.5. Cost Studies for SSCUC

MIPGAP=0.01	SSCUC	SSCUC-P	SSCUC-C	SSCUC-PC
Total Cost ($)	161,340	154,835	158,400	148,231
Solve time (s)	82.09	260.36	561.67	2500 (Timeout)
Avg. RES Curtailed (MW)	208	68.25	172.25	45.5

3.5.2. ESS Benefits

In this section, we study the ESS usage in the proposed models. From Fig. 3.7, we notice a similar pattern that alleviation of congestion enables SSCUC-PC to utilize the ESS systems charge more in low demand (periods 1–8) than other models and whereas only SSCUC-C provides higher discharge capability than SSCUC-PC in peak demand (periods 9-17). This is because SSCUC-PC significantly reduces RES curtailment which directly implies more RES power is utilized by the system and hence this excess power in the initial periods is stored for future use.

SSCUC-P shows the flattest trend which implies that the battery goes through smaller cycles. Therefore, PNR enables the ESS by decreasing the depth of discharge in batteries in the long run. This in turn can lead to long term benefits for ESS longevity before replacement.
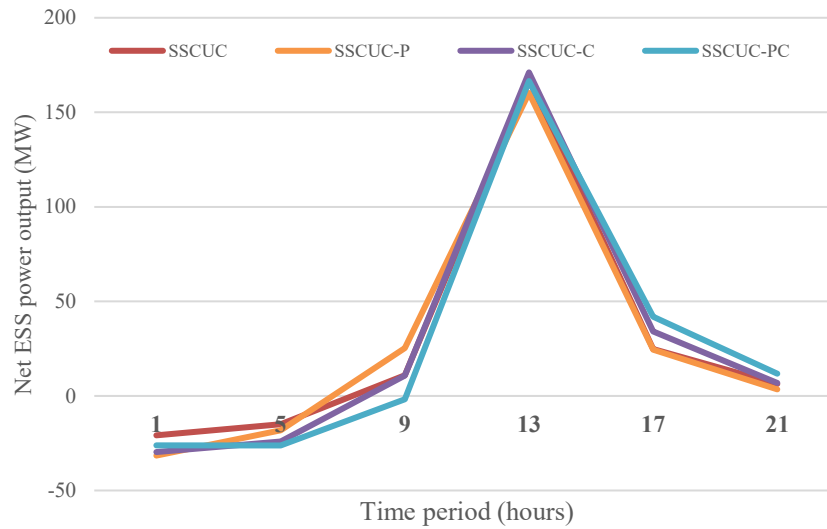
Fig. 3.7. Total Cost in $ under various penetration levels.

3.5.3. Preventive and Corrective Action Strategy with ESS

One of the key aspects of CNR is that not all contingencies lead to system congestion. Predominantly, line 31 [bus 17 – bus 22] and line 38 [bus 21– bus 22] are viable candidates for CNR. In both PNR and CNR, the reconfiguration action is preferred in high voltage side of the system. This is because the bottleneck line is line 23 [bus 14 – bus 16].

PNR is considered more favorable since it is implemented in over 98% of time period in each scenario. Since the network is a mesh network, there are redundancies in the network and a single topology is not optimal for serving the demand. For PNR, reconfiguring line 14 [bus 9 – bus 11] and line 19 [bus 11 – bus 14] which links the high voltage and low voltage side yields the best topology to serve the demand.

It is evident that only a few key reconfiguration actions are critical in addressing transmission flexibility. CNR action are closer to generation buses which enable committed cheaper generators to ramp up or ESS to discharge during low RES penetration period. Whereas PNR actions identify the optimal network topology to serve the load is ideally performed on key lines closer to the low voltage side or loads of the network.

3.6. Summary

The increase in RES in the network is key to addressing climate change issues. Due to the intermittent nature of RES, smart grids are required to facilitate the integration of RES. To avoid undesired congestion-induced curtailment of free energy, a flexible network is required. The day-ahead operational procedure still uses a static network which impedes further deployment of renewables in the grid.

It was observed that SSCUC-CNR provides more transfer capability of the network thereby avoiding congestion-induced and contingency-induced RES curtailment in high-penetration of RES. Along with reduction of curtailment, SSCUC-CNR also lowers the cost of operation, and reduces green-house gas emissions. Numerical simulations also showed that SSCUC-CNR is also beneficial in moderate-penetration of RES by committing efficient green (less emission) generators which reduces the overall carbon emissions in a day-ahead schedule.

To address the imbalances, other technologies like ESS are required to store electrical energy. However, network congestion can still lead to RES curtailment and inefficient use of ESS. A smarter grid is required which utilizes a dynamic network to alleviate transmission congestion in both pre-contingency cases through PNR and post-contingency cases through CNR to integrate the above resources.

The cost studies demonstrate remarkable cost saving by reducing network congestion and utilizing additional free RES output by utilizing existing flexibility in transmission network. The ESS studies reveal that SSCUC-PC and SSCUC-C enable ESS to produce more power during peak periods whereas SSCUC-P ensure the longevity of storage devices by reducing the depth of discharge in each cycle in day-ahead operations.

4. SCALABILITY OF CORRECTIVE NETWORK RECONFIGURATION

4.1. Literature Review

Network flexibility can be introduced in both real-time and day-ahead operations in the bulk power system. Due to the complexity, it can be noted from [78]–[80], NR is implemented by various heuristic methods to obtain quick results. [81] utilizes three concurrent NR actions to improve performance. In real-time scenarios, [43] presents a framework for integrating CNR with real-time contingency analysis and [59]–[60] proposed an enhanced energy management system with inclusion of a CNR module that can seamlessly and practically connect with real-time contingency analysis and security-constrained economic dispatch.

In day-ahead scenario, the security-constrained unit commitment (SCUC) is run to obtain an economical viable solution along with the day-ahead generator commitment and dispatch schedule. Since SCUC is used in both regulated and deregulated environments, the algorithm developed in the paper can be implemented in either business environment.

One main reason for not including NR/CNR is the increase in complexity of the N-1 SCUC model as it introduces additional binary variables to the mixed integer linear programming (MILP) problem. Here, decomposing the SCUC by iterative multi-stage approaches or using heuristic techniques is beneficial for algorithm performance. [82]

recognize NR benefits with a small subset of reconfigurable assets. [83] proposes a co-optimized method which enhances N-1 security by considering both a preventive optimal NR scheduling and a CNR rescheduling that tolerate short-term overloads in post-contingency scenarios. [84]–[85] detail a two-stage SCUC with NR that can be solved iteratively for large-scale power systems. [86] proposes an iterative fast SCUC method to compute for each hour and provide the resulting solution as a starting point for the original SCUC. Typically decomposing the SCUC is implemented using Bender's decomposition algorithm (BDA) or column and constraint generation algorithms (CCGA).

BDA can effectively reduce the complexity of SCUC by decomposing it as a master problem and associated sub-problems. [77] solves a stochastic-SCUC problem which implements NR to mitigate wind uncertainty and considers an AC optimal power flow through linearized network losses by utilizing BDA to reduce the problem complexity. [87] implements a multi-stage discrete approach through BDA acceleration techniques to include emerging technologies in SCUC. However, [77], [86] and [87] does not consider NR/CNR. In [88], a sequential extensive approach to implement CNR in N-1-1 SCUC is considered, which is not scalable.

Several authors have indicated slow convergence and sought heuristics to speed up BDA. In [89], a mixed-integer non-linear problem of long-term planning of distributed generation and reconfiguration of distribution system was solved by using BDA and accelerated by considering both feasibility and optimality cuts. In [90],

ordered sets, pre-solve and warm-start techniques were used for short-term hydropower maintenance scheduling. However, [89]–[90] do not perform any day-ahead market operations. In [91], a security-constrained optimal power flow was solved using heuristics and parallel solving of sub-problems using BDA. In [92], the concept of strong cuts using sensitivity factors were introduced to reduce iterations for solving SCUC. However, NR/CNR was never considered in [89]–[92].

CCGA, like BDA, also helps in reducing the problem complexity in SCUC. It is seen from [75], that energy and reserves are co-optimized while considering CNR and pre-contingency NR (PNR). A multi-level nested CCGA is used in [75]. Though this method addresses several extensions and considers umbrella contingencies, only one worst-case critical contingency per iteration is addressed to provide convergence for an exact solution and not compromise solve time. Therefore, the solution obtained from this method does not provide reconfiguration or re-dispatch solution for all contingencies. If more contingencies are required to be addressed, then the method proposed in [75] requires further iterations which may lead to substantial increase in solve time.

4.2. Overview of Benders Decomposition Algorithm (BDA)

The BDA method can be used to solve large-scale optimization problems that are computationally difficult due to the large number of constraints and variables. BDA partitions the problem into multiple smaller problems to solve it iteratively, which can

be more efficient than optimizing the original a single large problem. In this paper, the BDA decomposes SCUC, a large MILP problem, as a Master-slave formulation where the master problem is a MILP problem, and the slave problems are linear programming (LP) problems. The optimal solution of the master problem, a relaxed problem, may produce an infeasible solution for the slave problem. The slave problem verifies the master problem solution and if infeasible, then dual variables of the equations are used to provide feasibility cuts that are sent back to the master problem as constraints to refocus problem on a reliable feasible region. Fig. 4.1 represents the simplistic flow of BDA.
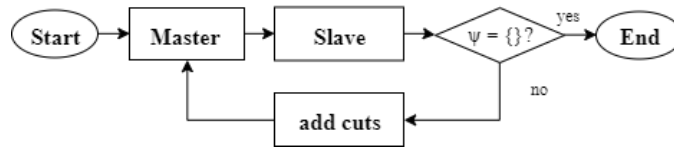
Fig. 4.1 Procedural flowchart for BDA approach.

4.3. Decomposition of *N*-1 SCUC and *N*-1 SCUC CNR

The mathematical model presented in sub-section 2.3.1 depicts the extensive formulation of *N*-1 SCUC which co-optimizes both the base-case constraints (2.2)–(2.15) and post-contingency constraints (2.16)–(2.22). However, this MILP formulation has increased complexity. As stated in the above section, a large MILP problem can be decomposed as master-slave problem and solved iteratively. While decomposing, the objective (2.1), and base-case constraints (2.2)–(2.15) and cut equation (4.1) forms the Master UC (MUC) problem which is a MILP problem. The

resulting MUC problem is same for both *N*-1 SCUC and *N*-1 SCUC-CNR. The cut-equation described in (4.1) is formed from sub-problems,

$$\sum_{g\in G}(P_g^{min}u_{g,t}^{fix}(\alpha_{g,c,t}^+ - \alpha_{g,c,t}^-) + (R_g^{10}u_{g,t}^{fix} - P_{g,t}^{fix})\beta_{g,c,t}^+ +$$

$$(R_g^{10}u_{g,t}^{fix} + P_{g,t}^{fix})\beta_{g,c,t}^-) + \sum_{k\in K}(P_k^{emax}(F_{k,c,t}^+ + F_{k,c,t}^-) + \qquad (4.1)$$

$$0(S_{k,c,t})) + \sum_{n\in N}d_{n,t}\lambda_{n,c,t} \leq 0, \forall\psi,$$

where, $\alpha_{g,c,t}^+, \alpha_{g,c,t}^-, \beta_{g,c,t}^+, \beta_{g,c,t}^+, F_{k,c,t}^+, F_{k,c,t}^-, S_{k,c,t}$ and $\lambda_{n,c,t}$ are dual variables of constraints present in the PCFC sub-problem discussed in the following section.

Once the MUC problem is solved the commitment and dispatch solution is checked for feasibility in the post-contingency constraints (2.16)–(2.22) for each period, *t* and contingency, *c* to maintain the slave problem as a LP. The process of checking feasibility in each individual case is known as post-contingency feasibility check (PCFC) and is represented in the following section. If the MUC solution is not feasible in PCFC sub-problem for (*c,t*) a cut is generated which comprises of the dual-variables of each equation of the PCFC sub-problem. The aggregated cuts of all non-feasible sub-problem of PCFC is added as a single constraint at the end of each iteration to the MUC problem. This process is followed until all sub-problems are feasible for the MUC solution.

In order to propose CNR action the network-reconfigured PCFC (NR-PCFC) is derived from (2.16)–(2.19) and (2.21)–(2.26). Here, the important thing to note is the presence of reconfiguration variable, $z_{c,t}^k$, makes the constraints a MILP. To make sure

that NR-PCFC is an LP problem, the reconfiguration are implemented one at a time and then checked for feasibility of the MUC solution. NR-PCFC is only implemented if the PCFC is infeasible. The PCFC and NR-PCFC are discussed in detail in the following section.

Two accelerators were identified to make the typical-decomposition approach solve faster: ranked closest branches to contingency element (CBCE) list [43], and critical subproblem identification. Firstly, it was observed that only a subset of the contingency sub-problems are critical, and an accelerator was developed to identify critical sub-problems to reduce computational burden. This accelerator can be implemented for both SCUC and SCUC-CNR and is represented in sub-section 4.3.3 as critical sub-problem screener (CSPS). Secondly, the CNR actions can be implemented through the CBCE list, a ranked priority list of 20 closest branches to each contingent element in the network to obtain quick feasible results for CNR. The CBCE list is only used in NR-PCFC sub-problems and therefore, it is only used in the proposed methods implementing SCUC-CNR for large networks.

4.3.1. PCFC Model

The PCFC sub-problems derived from prior equations (2.16)–(2.22) are modelled with a slack variable, s_1 and is represented through (4.2)–(4.11). The goal of post-contingency feasibility check is to check system feasibility for each contingency in set Ω^{cri} by conducting economic dispatch without CNR action. This is done by

77

minimizing the slack variable, s_1, which indicates the feasibility of the sub-problem. If s_1 is exactly zero, then the problem is feasible; otherwise, it is infeasible,

$$Minimize\ s_1. \tag{4.2}$$

The objective is subject to post-contingency generation modeling for a given contingency c in time-period t in set Ω^{cri} is modelled with,

$$-P_{g,c,t} + s_1\left(R_g^{10}u_{g,t}^{MUC} - P_{g,t}^{MUC}\right) \leq R_g^{10}u_{g,t}^{MUC} - \tag{4.3}$$
$$(\beta_{g,c,t}^-),$$
$$P_{g,t}^{MUC}, \forall g$$

$$P_{g,c,t} + s_1\left(R_g^{10}u_{g,t}^{MUC} + P_{g,t}^{MUC}\right) \leq R_g^{10}u_{g,t}^{MUC} + \tag{4.4}$$
$$(\beta_{g,c,t}^+),$$
$$P_{g,t}^{MUC}, \forall g$$

$$P_g^{min}u_{g,t}^{MUC} \leq P_{g,c,t} + s_1\left(P_g^{min}u_{g,t}^{MUC}\right), \forall g \qquad \left(\alpha_{g,c,t}^-\right), \tag{4.5}$$

and

$$P_{g,c,t} + s_1\left(P_g^{max}u_{g,t}^{MUC}\right) \leq P_g^{max}u_{g,t}^{MUC}, \forall g \qquad \left(\alpha_{g,c,t}^+\right). \tag{4.6}$$

Along with generation modelling, the post-contingency modeling of power flow for non-radial lines for a given contingency c in time-period t in set Ω^{cri} is modelled with,

$$P_{k,c,t} - b_k\left(\theta_{n,c,t} - \theta_{m,c,t}\right) = 0, \forall k \in \frac{K}{\{c\}} \qquad (S_{k,c,t}), \tag{4.7}$$

$$P_{c,c,t} = 0, \tag{4.8}$$

$$-P_k^{emax} \leq P_{k,c,t} - s_1(P_k^{emax}), \forall k \qquad (F_{k,c,t}^-), \tag{4.9}$$

78

$$P_{k,c,t} + s_1(P_k^{emax}) \leq P_k^{emax}, \forall k \qquad (F_{k,c,t}^+), \qquad (4.10)$$

and

$$\sum_{g \in g(n)} P_{g,c,t} + \sum_{k \in \delta^+(n)} P_{k,c,t} - \sum_{k \in \delta^-(n)} P_{k,c,t} + \qquad (4.11)$$
$$(\lambda_{n,c,t}),$$
$$s_1(d_{n,t}) = d_{n,t}, \forall n$$

where, $\alpha_{g,c,t}^+, \alpha_{g,c,t}^-, \beta_{g,c,t}^+, \beta_{g,c,t}^+, F_{k,c,t}^+, F_{k,c,t}^-, S_{k,c,t}$ and $\lambda_{n,c,t}$ are dual variables of respective constraints.

The post-contingency equations are modelled through the post-contingency generation constraints of (4.3)–(4.6), transmission limit constraints of (4.7)–(4.8) and nodal power balance constraint of (4.11). (4.3)–(4.4) is the 10-minute ramp up/down limit, (4.5)–(4.6) models the minimum and maximum limit of the generator. (4.7) represents the DC line-flow calculation and the contingent transmission element lost is represented by (4.8). (4.9)–(4.10) enforce the emergency rating of the transmission element. Finally, (4.11) represents that the nodal power balance in the post-contingency case. If PCFC fails feasibility, the respective sub-problem c,t will be recorded to set Ω_1^{inf} along with respective cut in the cut-set, ψ. Fig. 4.2 depicts the flow of PCFC.
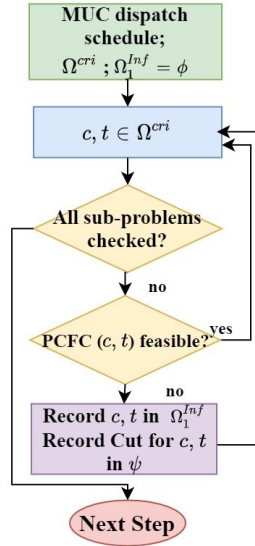
Fig. 4.2 Procedural flowchart for PCFC.

4.3.2. NR-PCFC Model

The goal of network-reconfigured post-contingency feasibility check is to check system feasibility with CNR for the set Ω_1^{inf}. (4.12)–(4.22) models NR-PCFC that is similar to PCFC except for (4.17) and (4.19). The feasibility is checked by switching one non-radial transmission element at a time from the network. The line to be switched is chosen from closest branches to contingency element (CBCE) list or complete enumeration (CE) of non-radial lines [43]. For each scenario (with line j removed from the network), NR-PCFC minimizes the slack variable, s_2, which represents the feasibility of the problem. If s_2 is 0, then the specific scenario for the respective sub-problem is feasible and for all other values of s_2, it is infeasible. If the sub-problem is feasible for one such scenario, then the sub-problem c,t is feasible

through CNR and is removed from the cut-set, ψ , obtained from PCFC. Record the line selected from the CBCE/CE list that facilitates CNR. If no switching scenario leads to a feasible solution for sub-problem c,t, then the infeasible sub-problem will be recorded in set Ω_2^{inf}. Fig. 4.3 depicts the flow of NR-PCFC and the NR-PCFC objective is described by,

$$Minimize \ s_2. \tag{4.12}$$

The objective is subject to post-contingency generation modeling for a given contingency c in time-period t in set Ω_1^{inf} and is modelled with,

$$-P_{g,c,t} + s_2\left(R_g^{10} u_{g,t}^{MUC} - P_{g,t}^{MUC}\right) \leq R_g^{10} u_{g,t}^{MUC} - P_{g,t}^{MUC}, \forall g, \tag{4.13}$$

$$P_{g,c,t} + s_2\left(R_g^{10} u_{g,t}^{MUC} + P_{g,t}^{MUC}\right) \leq R_g^{10} u_{g,t}^{MUC} + P_{g,t}^{MUC}, \forall g, \tag{4.14}$$

$$P_g^{min} u_{g,t}^{MUC} \leq P_{g,c,t} + s_2\left(P_g^{min} u_{g,t}^{MUC}\right), \forall g, \tag{4.15}$$

and

$$P_{g,c,t} + s_2\left(P_g^{max} u_{g,t}^{MUC}\right) \leq P_g^{max} u_{g,t}^{MUC}, \forall g. \tag{4.16}$$

Along with generation model, the post-contingency modeling of power flow for non-radial lines for a given contingency c in time-period t in set Ω_1^{inf} and line j from CBCE/CE is considered in,

$$P_{k,c,t} - b_k\left(\theta_{n,c,t} - \theta_{m,c,t}\right) = 0, \forall k \in \frac{K}{\{c,j\}}, \tag{4.17}$$

$$P_{c,c,t} = 0, \tag{4.18}$$

81

$$P_{j,c,t} = 0, \tag{4.19}$$

$$-P_k^{emax} \leq P_{k,c,t} - s_2(P_k^{emax}), \forall k, \tag{4.20}$$

$$P_{k,c,t} + s_2(P_k^{emax}) \leq P_k^{emax}, \forall k, \tag{4.21}$$

and

$$\sum_{g\in g(n)} P_{g,c,t} + \sum_{k\in\delta^+(n)} P_{k,c,t} - \sum_{k\in\delta^-(n)} P_{k,c,t} + s_2(d_{n,t}) = d_{n,t}, \forall n. \tag{4.22}$$
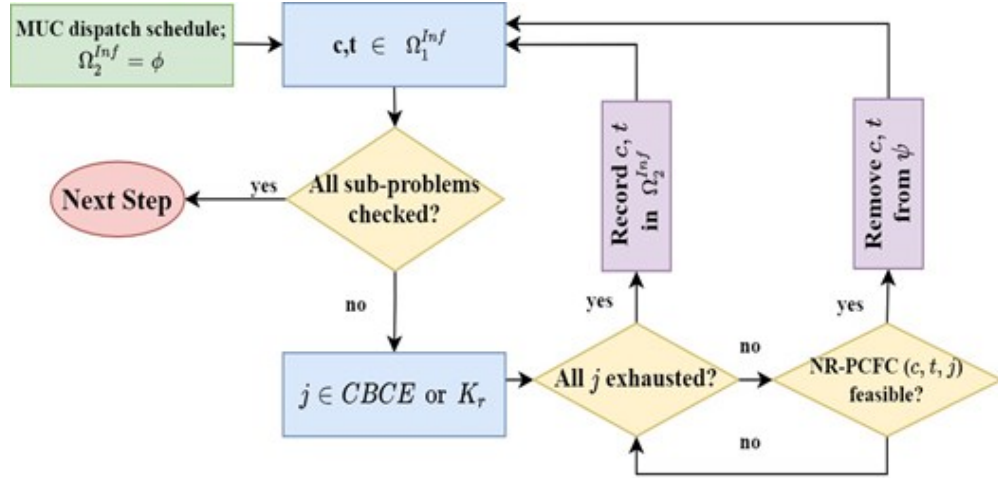
Fig. 4.3 Procedural flowchart for NR-PCFC.

4.3.3. Critical Sub-Problem Screener (CSPS) Model

The purpose of the critical sub-problem screener (CSPS) is to screen out non-critical sub-problems before PCFC and NR-PCFC. Post-contingent line flows critical set, Ω^{cri}, are obtained through the predetermined line outage distribution factor (LODF) of the network, (4.23),

$$P_{k,c,t} = P_{k,t}^{MUC} + LODF_{k,c}(P_{c,t}^{MUC}), \forall k \tag{4.23}$$

The contingent line flows are then compared against the emergency line limit for violations. The non-critical sub-problems determined by CSPS are removed from the set Ω^{cri} leaving only critical problems. Fig. 4.4 depicts the flow of CSPS.
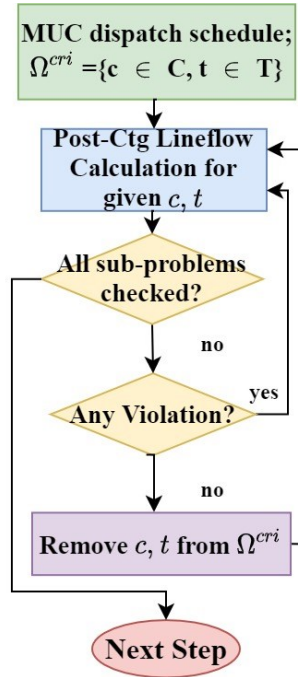
Fig. 4.4 Procedural flowchart for CSPS.

4.4. Iterative Decomposition Approaches

This chapter compares the extensive formulations against decomposition approaches of SCUC and SCUC-CNR and details the benefits of decomposed approaches. The extensive formulations were discussed in Chapter 2. The decomposition approaches to SCUC and SCUC-CNR are explained in the following sub-sections. This paper proposes two decomposed approaches for SCUC namely: a typical-decomposition approach to SCUC (T-SCUC) and an accelerated-

decomposition approach to SCUC (A-SCUC). Along with the above proposed methods, this paper also proposes two decomposed approaches for SCUC-CNR which perform network reconfiguration as a corrective action namely: typical-decomposition approach to SCUC-CNR (T-SCUC-CNR) and accelerated-decomposition approach to SCUC-CNR (A-SCUC-CNR). The proposed approaches are explained through the decomposed-features of master and sub-problems explained in sub-sections 4.3.1–4.3.3.

4.4.1. Typical-Decomposition Approach

The proposed typical-decomposition approach by using MUC and PCFC only for SCUC whereas SCUC-CNR also utilizes NR-PCFC. The MUC problem is initially solved to obtain the generator commitment and base-case output. The feasibility of each sub-problem in set Ω^{cri} is checked by post-contingency generation redispatch implemented by PCFC. For the typical-decomposition approach, the set Ω^{cri} holds the complete list of all sub-problems and the set Ω_1^{inf} is an empty set at the beginning of each iteration. When the feasibility of a sub-problem is not achieved, it is recorded in the set Ω_1^{inf}.

For SCUC, once all sub-problems are examined, an iteration is completed. The infeasible sub-problem are recorded in set Ω_1^{inf} at the end of each iteration. The problem is converged when set Ω_1^{inf} is empty at the end of an iteration.

For SCUC-CNR, the set Ω_1^{inf} is passed on to NR-PCFC and feasibility of each sub-problem is examined with CNR. If the sub-problem is infeasible then it is recorded in set Ω_2^{inf}. Once all sub-problems in set Ω_1^{inf} are checked, an iteration is completed.

The respective cuts for infeasible sub-problems in set Ω_1^{inf} for SCUC and infeasible sub-problems in set Ω_2^{inf} are formed using the dual value of (4.2)–(4.11) and added as (4.1), respectively, after each iteration.

4.4.2. Accelerated-Decomposition Approach

Accelerated-decomposition approach uses MUC, CSPS and PCFC only for SCUC whereas SCUC-CNR also utilizes NR-PCFC. The flow of this approach is similar to typical-decomposition approach, but it is substantially sped through the CSPS, an accelerator to reduce the computational burden by identifying critical sub-problems. The MUC problem is initially solved to obtain the generator commitment and base-case output. With the MUC schedule, the critical sub-problems are identified and recorded in set Ω^{cri} by using CSPS. Only the critical sub-problems, rather than all sub-problems, are then checked by post-contingency generation redispatch through PCFC.

4.4.3. Proposed Methods

Fig. 4.5 represents the flow of the proposed typical decomposition approach and proposed accelerated-decomposition approach to SCUC/SCUC-CNR and the

pseudo-code is represented in Algorithm 4.1 where (i) A-SCUC-CNR is implemented using lines 1–35; (ii) T-SCUC-CNR is implemented through lines 1–5 and 12–35; (iii) T-SCUC is implemented by lines 1–5, 13–14, 24, and 26–35; and (iv) A-SCUC is implemented through lines 1–15 and 23–35.
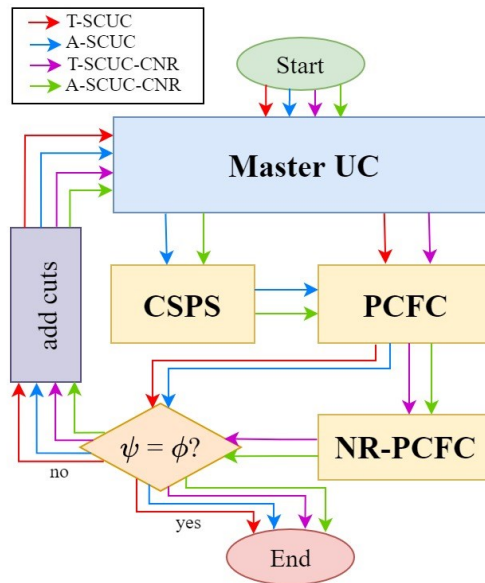
Fig. 4.5. Flowchart of typical-decomposition approach to SCUC.

Algorithm 4.1 Accelerated-decomposition approach to SCUC-CNR

1: Solve MUC and obtain the commitment and dispatch
2: **repeat**
3:      cut = ∅;
4:      **for** all $t \in T$ **do**
5:          **for** all $c \in C$ **do**
6:              solve CSPS(c,t)
7:              **for** all $k \in K$ **do**
8:                  **if** $P_{k,c,t}$ violation **then**
9:                      record (c,t) in set Ω^{cri}
10:                 **end if**
11:             **end for**
12:             **for** all (c,t) $\in \Omega^{cri}$ **do**
13:                 solve PCFC(c,t)
14:                 **if** PCFC(c,t) is infeasible **then**
15:                     Flag = false
16:                     **for** line $j \in$ CBCE **do**
17:                         Remove line j from topology
18:          solve NR-PCFC(j,c,t)
19:                         **if** NR-PCFC(j,c,t) feasible **then**
20:                             Flag = true; **break**
21:                         **end if**
22:                     **end for**
23:                     **if** Flag = false **then**
24:                         {cut} = {cut} + {cut of PCFC(c,t)}
25:                     **end if**
26:                 **end if**
27:             **end for**
28:         **end for**
29:     **end for**
30:     **if** {cut} != ∅ **then**
31:         add cut to MUC; solve updated MUC
32:     **else**
33:         problem converged; report results; **break**
34:     **end if**
35: **until** converged

4.5.   Testcase Summary

The proposed methods, T-SCUC/A-SCUC and T-SCUC-CNR/A-SCUC-CNR were validated against the extensive formulation detailed in SCUC and SCUC-CNR, respectively, on the IEEE 24-bus system with 33 generators and 38 branches [63]. The network includes a total generation capacity of 3,393 MW and the system peak load is 2,265 MW. Furthermore, the IEEE 73-bus system and the Polish system were utilized to show the effectiveness and scalability of T/A-SCUC-CNR. Table 4.1 summarizes the test systems.

The IEEE 73-bus system consists of 99 generators and 117 branches [63]. The total generation capacity is 10,215 MW and the system peak load is 8,550 MW. The Polish system, modified to include default min-up/min-down times and ramp-up/ramp-down limits, is used for demonstrating the scalability of the algorithm. It is the largest system used for this work and it consists of 2,383 buses, 327 generators and 2,895 branches [93]. The total generation capacity is 30,053 MW serving a system peak load of 21,538 MW. Two cases of the Polish system, covering a single-hour period and a 24-hour period respectively, are considered. The single-hour period case is effective to compare performance against smaller systems whereas scalability is shown through the 24-hour period case. To demonstrate CNR, only non-radial transmission line contingencies are considered in the N-1 SCUC formulation since contingency of radial lines will lead to islanding and system separation; this is consistent with industrial

practice. Similarly, CNR actions, at most one action per contingency, considers only non-radial lines as possible reconfiguration actions for the same reason.

In addition, the IEEE 118-bus system with 54 generators and 186 branches, [93], was also considered to draw comparison with state-of-the-art methods to show the efficacy of proposed methods. However, the IEEE 118-bus system lacks the generator data and thermal limits and thus it was modified to include such information.

Table 4.1. Test System Summary

System	Pgen (GW)	Pload (GW)	# bus	#gen	# branch	# radial branch
IEEE 24	~3.4	~2.1	24	33	38	1
IEEE 73	~10.2	~8.6	73	99	117	2
IEEE 118	~5.8	~3.1	118	54	186	7
Polish	~30.1	~21.5	2,383	327	2,895	644

4.6.   Results and Analysis

The mathematical model is implemented using AMPL and solved using Gurobi. The models were run on a computer with Intel® Xeon(R) W-2195 CPU @ 2.30GHz; the CPU contains 24.75 MB of cache and 128 GB of RAM. The proposed methods were initially validated, following which sensitivity analysis, scalability and market impact are discussed.

4.6.1. Algorithm Validation

Since the proposed methodologies are all iterative in nature, an accuracy validation was performed to test the robustness against non-iterative extensive formulations. A MIPGAP of 0.00 was utilized on the congested network of IEEE 24-bus system for 24-hour period and the SCUC results are tabulated in Table 4.2 and SCUC-CNR results are tabulated in Table 4.3. It was observed from Table II that the results for SCUC, T-SCUC and A-SCUC are the same. Similarly, the solutions obtained from SCUC-CNR, T-SCUC-CNR and A-SCUC-CNR are the same.

The results presented in Table 4.2 and Table 4.3 prove that the proposed typical-decomposition and accelerated-decomposition methods are significantly faster for the same solution than extensive formulations of SCUC and SCUC-CNR respectively. It is intuitive that incorporating CNR will lead to additional computational complexity, which is demonstrated by the observation that the computing time of SCUC-CNR is longer than SCUC. However, it is the other way for the proposed approaches: the computational time for solving T/A-SCUC-CNR is much less than that for T/A-SCUC. The reason is that the addition of NR-PCFC sub-problem in addition to PCFC in T/A-SCUC-CNR leads to increased feasibility region of the sub-problems and reduced number of cuts and iterations.

Table 4.2. SCUC Accuracy on IEEE 24-Bus System

MIPGAP=0.00	SCUC	T-SCUC	A-SCUC
Total cost ($)	963,893	963,893	963,893
Solve time (s)	6,013	2,440	1,351

Table 4.3. SCUC-CNR Accuracy on IEEE 24-Bus System

MIPGAP=0.00	SCUC-CNR	T-SCUC-CNR	A-SCUC-CNR
Total cost ($)	928,794	928,794	928,794
Solve time (s)	9,625	47	9

4.6.2. AC Feasibility for CNR Solutions

Since the proposed methodologies are for a DC solution which is utilized in the industry for unit commitment, an AC feasibility check was performed to validate the CNR benefits. An example from the post-contingent sub-problems is presented in this subsection. Fig. 4.6 and Fig. 4.7 shows the MW flow as a percentage of line loading of lines close to the contingent line 27 in both DC solution and AC solution for IEEE 24-bus system, respectively. It was also noted that line 23, connecting the high-voltage and low-voltage regions, is the main bottleneck line in the IEEE 24-bus system in most of the critical contingencies. The CNR solution provided is line 37 as a congestion relief option in post-contingency phase. It can be observed from the line loading level for DC and AC solution that the benefits offered by CNR solution is not lost in an AC setting.

As stated earlier, the CNR action is only performed when there is a line congestion or overload after a contingency. From Fig. 4.6, we notice that the DC solution resulted in line overload in a post-contingency case for line 23 which is at 109%. The CNR action of switching line 37 resulted in flow redistribution in the network which relieves the line violation and brings the flow on line 23 to 100%.

An AC feasibility check for the above DC solution was verified and Fig. 4.7 represents the line loading in an AC setting. Here, line 23 is violated with a post-contingent flow of 108% after the contingency of line 27. Similarly, the CNR action of line 37 alleviates the violation on line 23 and results in a line-loading of 99.4%. This implies a similar decrease of ~9% is achieved with CNR action in both DC and AC setting for the violated line 23. The benefit of CNR is not lost in an AC solution as shown in Table 4.4. Moreover, the results showed that the MW flow on the lines were similar for most lines in both the AC and DC solutions. Therefore, the DC approximation holds well even when CNR is implemented.

Table 4.4. Line Loading of Line 23 In IEEE 24-Bus System

Solution	Post-contingency	Post-reconfiguration
DC	109 %	100 %
AC	108 %	99.4 %
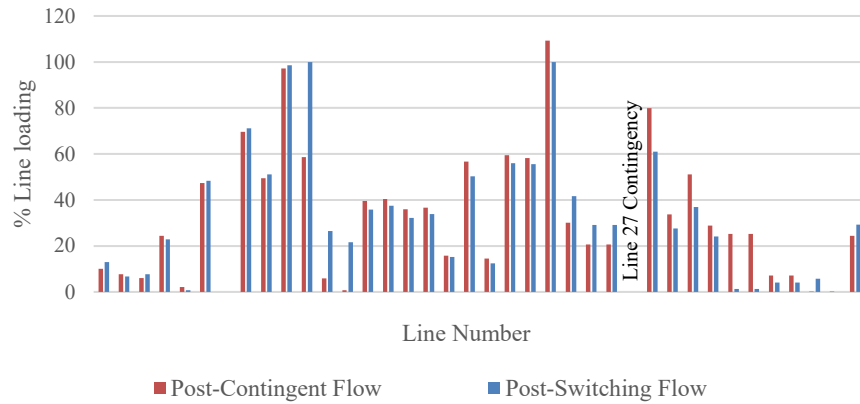
Fig. 4.6. Line loading for DC solution in IEEE 24-bus system.
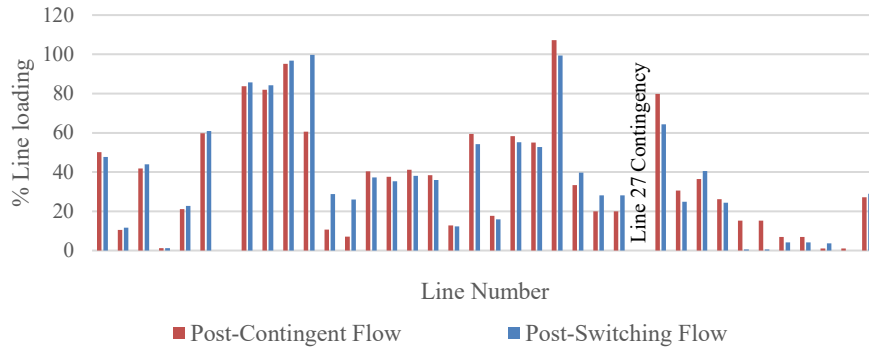
Fig. 4.7. Line loading for AC solution (MW only) in IEEE 24-bus system.

4.6.3. MIPGAP Sensitivity Analysis

The MUC MIPGAP, μ, affects the performance of all the methods. Specifically, increasing the μ increases the total cost. The change in cost (ΔCost) in total cost is calculated with (4.24),

$$\Delta Cost_\mu = \frac{Cost_\mu - Cost_{\mu=0}}{Cost_{\mu=0}}, \qquad (4.24)$$

and is shown in Fig. 4.8. The solve-time decreases significantly as shown in Fig. 4.9 with respect to μ.

Based on the sensitivity analysis, μ=0.01 provides reasonable maximum cost change of ~0.4% in a short time. However, the performance of the proposed methodologies implementing CNR fares well under tighter tolerances if higher accuracy is required. For the rest of the paper, μ=0.01 is used.
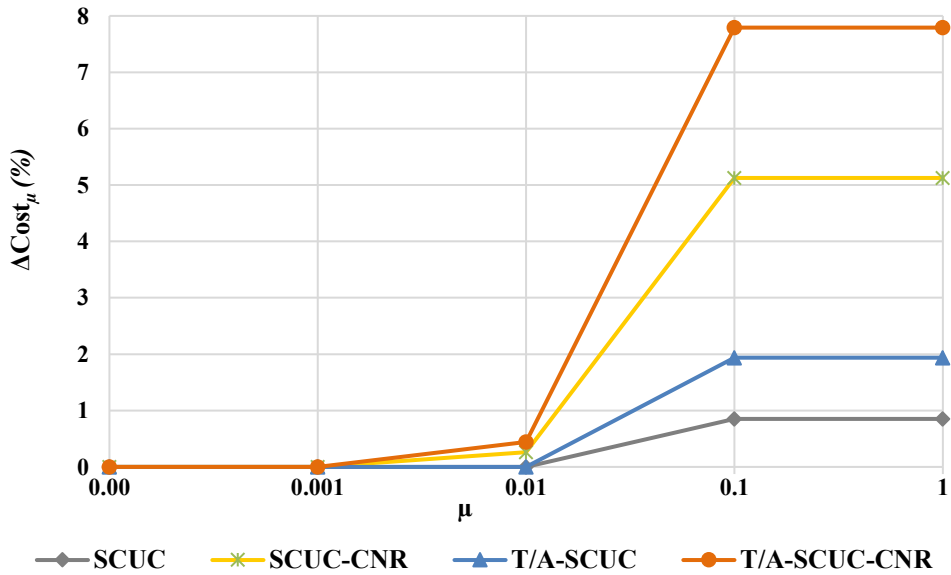
Fig. 4.8 Change in cost (ΔCost) versus MIPGAP μ on IEEE 24-Bus System.
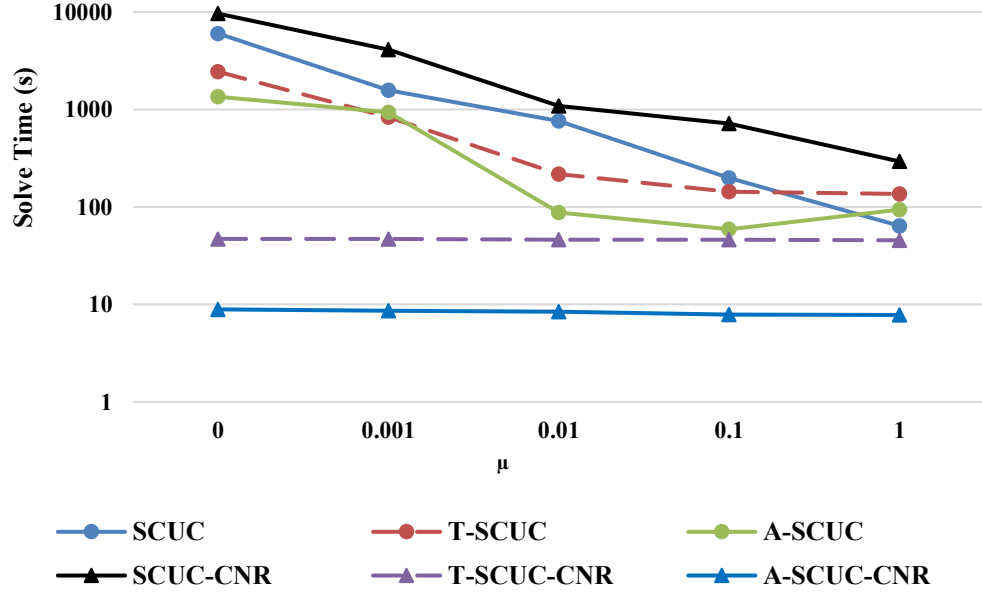
Fig. 4.9 Solve time versus MIPGAP μ on IEEE 24-Bus System.

4.6.4. Load Sensitivity Analysis

Four scenarios were considered: two low-load/uncongested scenarios (80%, 90%), a base-load scenario (100%) and a high-load scenario (110%). The load profile was varied using a percentage multiplied to the nodal load. Table 4.5 shows the total cost for various methods under different load profiles.

In the low-load scenarios (80%, 90%), it is evident that CNR is never implemented as there are no post-contingency line flow violations. CNR actions are observed in base-load and high-load scenarios (100%, 110%) where the network reconfiguration is utilized to relieve system congestion. This allows cheaper generators to produce more power, resulting in a reduced total operational cost. Interestingly, without CNR, the demand cannot be met due to network congestion. The difference in

95

total cost for load profile 90% and 100% in *N*-1 SCUC and *N*-1 SCUC-CNR can be attributed to non-zero MIPGAP.

Table 4.5. Load Sensitivity Analysis on IEEE 24-Bus System

Load Profile (%)	Total operational cost ($)			
	N-1 SCUC	*N*-1 SCUC-CNR	BDA *N*-1 SCUC	EBDA *N*-1 SCUC-CNR
80	467,883	467,883	467,883	467,883
90	624,398	623,458	624,398	623,459
100	963,893	931,224	963,893	932,919
110	Infeasible	1,424,140	Infeasible	1,424,140

4.6.5. Scalability Studies

One of the key research gaps is the lack of an effective algorithm for solving SCUC-CNR that is scalable for large-scale power systems and solvable in realistic time. Table 4.6 and Table 4.7 tabulate the performance of SCUC and SCUC-CNR on IEEE 73-bus system respectively. Table 4.6 points that the extensive formulation of SCUC, requires a good starting point to solve in 7,743 seconds. One approach to have a good starting solution is to utilize the commitment and dispatch results obtained from the relaxed MUC problem. However, without a starting solution, even SCUC proves to be infeasible in 100,000 seconds. A default starting solution can also be utilized where all generators are committed, which results in feasibility within 1% optimality gap in about 30,000 seconds that is still impractical. In the execution of the proposed

decomposition approaches, a starting point solution is not considered and yet a feasible solution can be achieved faster. Based on Table 4.7, the starting point has a significant influence on a large optimization problem, and it can be considered for T/A-SCUC and T/A-SCUC-CNR. Since the proposed decomposition approaches are iterative in nature, the best starting point can be obtained from the MUC solution from previous iteration. This may lead to further reduction in computational time. Also, the sub-problems are sequentially solved, and a parallel solving can speed up the algorithm.

Table 4.6. Scalability Of SCUC to IEEE 73-Bus System

MIPGAP=0.01	SCUC	T-SCUC	A-SCUC
Total cost ($)	3,224,980	3,223,760	3,223,760
Solve time (s)	7,743	1,273	367
Feasibility	Feasible	Feasible	Feasible
Starting point	Yes	No	No

Table 4.7 shows that SCUC-CNR lacks scalability as it times out without a feasible solution for the IEEE 73-bus system when solved for 100,000 seconds with a good starting solution. Table 4.8 describes the complexity of the unit-commitment problem with respect to size of equalities, inequalities, binary variables and, continuous variables problem for IEEE-73 bus system. It is evident that a SCUC problem without N-1 constraints has 13,707 variables, and 24,792 constraints. Once N-1 constraints are included, the variables and constraints are significantly increased for the SCUC

problem to 799,515and 1,555,824, respectively. Additionally, if CNR is included in this problem, then the variables and constraints increase exponentially to 1,121,747 and 2,517,160, respectively. Since the problem complexity increases exponentially with the addition reliability and new technologies, the SCUC-CNR is not scalable to obtain a feasible solution in a practical time. However, with decomposition and acceleration, this issue with complexity can be addressed with the proposed T/A-SCUC-CNR.

Table 4.7. Scalability SCUC-CNR to IEEE 73-Bus System

MIPGAP=0.01	SCUC-CNR	T-SCUC-CNR	A-SCUC-CNR
Total cost ($)	NA	3,218,980	3,218,980
Solve time (s)	100,000	392	168
Feasibility	Timeout	Feasible	Feasible
Starting point	Yes	No	No

Table 4.8. Problem Complexity for IEEE 73-Bus System

Model Element	SCUC	SCUC	SCUC-CNR
N-1 constraints	No	Yes	Yes
Binary Variables	4,539	4,539	326,771
Continuous Variables	9,168	794,976	794,976
Equality Constraints	4,560	525,432	205,272
Inequality Constraints	20,232	1,030,392	2,311,888

T/A-SCUC and T/A-SCUC-CNR are scalable to large networks such as the Polish system. Fig. 4.10 plots the solve time with respect to the size of the network. T/A-SCUC and T/A-SCUC-CNR are iterative in nature and Fig. 4.11 plots the number of iterations to solve the problem with respect to the size of the network. Due to the size of the Polish system, the 1-hour Polish case is utilized in Fig. 4.10 and Fig. 4.11 rather than the 24-hour Polish case to compare the performance with smaller systems. Here, it is noted that T/A-SCUC that do not perform CNR require more iterations to converge. The transmission flexibility obtained through implementing CNR in T/A-SCUC-CNR is evident from fewer iterations required to converge to a feasible solution with desired accuracy. This also means that the MUC problem that is more computationally intensive compared to sub-problems is solved fewer times, which saves a substantial amount of computational time. In addition, the number of cuts generated from infeasible post-contingency sub-problems for T/A-SCUC-CNR are also less than T/A-SCUC. In other words, the number of constraints added to the MUC problem for each iteration for T/A-SCUC-CNR is less than T/A-SCUC, which may lead to a less complex MUC problem and require less time to solve the MUC for each iteration for T/A-SCUC-CNR. The total number of cuts added to MUC for those decomposition methods is presented in Table 4.9.

Table 4.9. Sub-Problem and Cut Details

	IEEE 24-Bus		IEEE 73-Bus		Polish 1-Hr	
	T/A-SCUC	T/A-SCUC-CNR	T/A-SCUC	T/A-SCUC-CNR	T/A-SCUC	T/A-SCUC-CNR
# cuts	198	42	65	17	76	14
α	NA	16	NA	20	NA	57

α in this table denotes number of sub-problems that were infeasible for post-contingency constraints without CNR but were feasible with CNR.
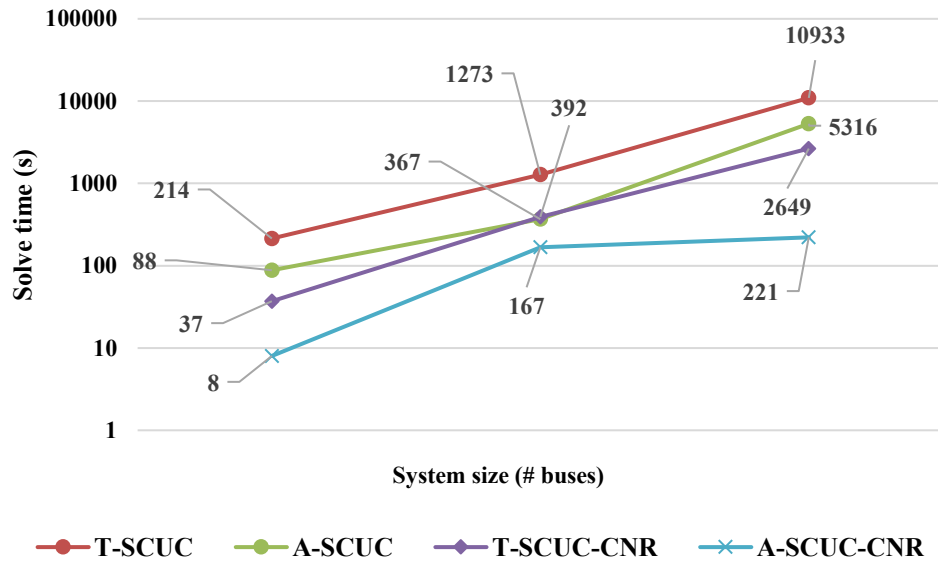
Fig. 4.10 Solving time versus system size.
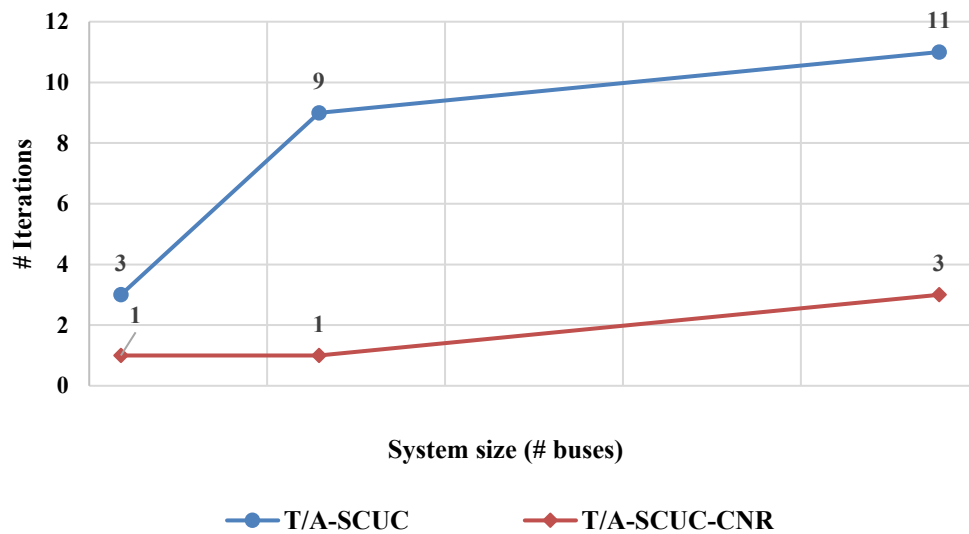
Fig. 4.11 Number of iterations versus size of the network.

Table 4.10 details the results of the Polish system when it is scaled to solve for 24-hour period. A-SCUC-CNR utilizes accelerators such as the CSPS and closest branches to contingency element (CBCE), a list of 20 closest lines to the contingent line. However, it was noted that over 96% of the 637 CNR actions, a top 10 choice from the CBCE list yields the solution. Therefore, the choice of 20 closest elements is a conservative approach. The inclusion of accelerators in A-SCUC-CNR decreases the solve time by 90% as compared to T-SCUC-CNR while the solution quality is retained. It is also evident that due to fewer iterations, T-SCUC-CNR is over 40% faster than A-SCUC-CNR.

The comparison between A-SCUC and T/A-SCUC-CNR shows that there are 1,499 sub-problems resulting in cuts being added as constraints to the MUC problem for A-SCUC, as opposed to 192 cuts required for T/A-SCUC-CNR. Therefore, the

MUC problem in A-SCUC is more constrained and takes longer to solve when compared to the MUC problem in T/A-SCUC-CNR. Not only that, the flexibility offered by CNR is evident by the following fact: out of 829 sub-problems that failed PCFC, 637 sub-problems are feasible with CNR through NR-PCFC, which implies about 77% of contingencies that failed feasibility in post-contingency check becomes feasible when CNR actions were implemented. Moreover, T/A-SCUC-CNR converge faster and require only 2 iterations against A-SCUC that requires 14 iterations. This implies the complex MUC problem is solved fewer times with T/A-SCUC-CNR leading to significant reduction in computational time.

The consideration of network reconfiguration for post-contingencies to alleviate network congestion in the large-scale Polish system for 24-hour period leads to a cost saving of $14,890. It is to be noted that the results present an exhaustive monitoring of all non-radial transmission elements: 2,250 non-radial lines for the Polish system. This leads to 54,000 sub-problems for a 24-hour period per iteration whereas only 1,761 sub-problems were swiftly deemed as critical by CSPS. Subsequently, PCFC checked those 1,761 sub-problems and identified 829 sub-problems that failed feasibility check. The NR-PCFC that verifies feasibility of these contingencies with network reconfiguration further reduced the number of cuts required to be added to 192. Therefore, 637 sub-problems satisfied feasibility of post-contingency constraints by modifying the network topology. Though those 637 sub-problems that implemented CNR actions amounts to only 1.18% of all the sub-problems considered in the first

iteration, considerable economic benefits are achieved with T/A-SCUC-CNR over A-SCUC. The solve time can be further significantly reduced if only a watch-list of key contingent lines are monitored as this will reduce the number of sub-problems drastically.

Table 4.10. Scalability To Polish System For 24-Hour Period

Parameters	A-SCUC	T-SCUC-CNR	A-SCUC-CNR
Total Cost ($)	5,350,220	5,335,330	5,335,330
€ ($)	NA	14,890 (0.28%)	14,890 (0.28%)
Time (s)	15,133.9	59,473.1	6,257.3
δ	0.04%	0.12%	0.12%
Iterations	14	2	2
# CNR	NA	637	637
# Cuts	1,499	192	192

€ denotes the cost saving for T/A-SCUC-CNR as compared to A-SCUC. δ denotes the MIPGAP of the reported solution of MUC in the last iteration.

4.6.6. Congestion Cost and Market Analysis

The contingency-induced congestion cost (CICC) is calculated as the difference in total operation cost when emergency post-contingency line limits are imposed (TC) and not imposed (TC_{NoEL}) as represented in **(4.25)**. The scenario when post-contingency emergency limits are not imposed is used as a benchmark since it is equivalent to implying that the system is not congested in the post-contingency

situations. A-SCUC and A-SCUC-CNR are considered since we are interested in calculating the amount of *CICC* reduced when CNR is implemented where,

$$CICC = TC - TC_{NoEL}. \tag{4.25}$$

From Fig. 4.12, the IEEE 24-bus system was the most congested system with a contingency-induced congestion cost of \$35,099 due to the considered load profile along with lower transmission capability. This was followed by the 73-bus system and 1-hour polish system with \$4,550 and \$4,150 respectively. The *CC* is considerably reduced in all the cases by 88%, 100% and 74% respectively. This is significant in heavily congested system as seen in the case of IEEE 24-bus system where \$30,794 is saved.
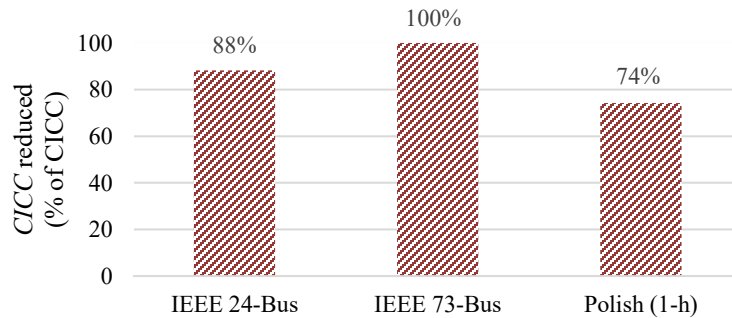
Fig. 4.12 *CICC* reduction for the IEEE 24-bus, IEEE 73-Bus and Polish systems.

The market implication of reduction in *CICC* can be seen through the impact of CNR on nodal locational marginal prices (LMP). Table 4.11 shows the average nodal LMP calculated in various systems when CNR is not used and when CNR is implemented. Overall, it is observed that with CNR, (i) the average nodal LMP is reduced and (ii) the nodal LMP curve is flattened. It can be noted that congestion relief

has a direct impact on the reduction in average nodal LMP. Similarly, it is also noted that the load payment is significantly reduced with CNR. Table 4.12 shows the total load payment for each test system with and without CNR. CNR resulted in a load payment reduction of $58,840 in the IEEE 24-bus system, $1,576,880 in the IEEE 73-bus system and $3,977 in the 1-hour Polish system, which correspond to percentage reductions of around 5.0%, 20.1% and 1.1% respectively. This makes sense since compared to the IEEE test systems, (i) the production cost of generators in the Polish system is low, (ii) the variation of system-wide generation cost in the Polish system is small, and (iii) the Polish system is loaded.

Table 4.11. Average Nodal Locational Marginal Price ($/MWh)

Test System	A-SCUC				A-SCUC-CNR			
	Mean	Min	Max	StdD	Mean	Min	Max	StdD
IEEE 24-Bus	23.39	5.46	150.6	0.86	23.23	5.46	150.6	0.84
IEEE 73-Bus	42.75	9.5	648.4	1.36	42.19	4.9	582.4	1.34
Polish (1-hour)	17.72	15.7	20.8	0.24	17.56	17.2	17.8	0.19

Table 4.12. Load Payment ($)

Test System	A-SCUC	A-SCUC-CNR
IEEE 24 Bus	1,171,220	1,112,380
IEEE 73 Bus	7,840,770	6,263,970
Polish (1-hour)	372,740	368,763

4.7.   Summary

This chapter proposes typical-decomposition and accelerated-decomposition approaches of SCUC and SCUC-CNR. The proposed decomposition approaches are generic and can be implemented to both SCUC and SCUC-CNR while outperforming the extensive formulations of SCUC and SCUC-CNR, respectively, in terms of (i) computational speed, (ii) algorithm scalability, and (iii) solution quality.

The accelerated-decomposition approach can easily link multiple accelerators to substantially reduce solution time. Specifically, CSPS, an exhaustive fast screening of sub-problems accurately identifies the critical contingent sub-problems which can lead to system overload or congestion. In addition, the A-SCUC-CNR benefits in computational speed achieved from ordered list, CBCE, for corrective actions.

The proposed A-SCUC-CNR utilizing the proposed accelerators, CSPS and CBCE, can solve a large-scale power system for 24-hour period in a reasonable time. As compared to T-SCUC-CNR, the proposed A-SCUC-CNR achieves a reduction of about 90% in the computational time without compromising solution accuracy. It can be noted that parallel solving of sub-problems was not considered in this paper and can provide additional computational time savings in future.

It was noted that implementation of CNR can achieve significant cost saving and provide feasible solutions for high critical demands where there are no feasible solutions without CNR. In addition, A-SCUC-CNR can provide high quality solutions much faster than the A-SCUC since fewer iterations are required. The load payment is

dramatically reduced with CNR. A load payment reduction of 1%–20% can be realized for various networks. Mainly, the advantage of the proposed A-SCUC-CNR is that it provides quality solutions in a reasonable short time while dramatically reducing post-contingency network constraints induced congestion cost by 75%–100% in various scenarios. As a result, the total operation cost is reduced with CNR for congested networks.

5. MACHINE LEARNING APPLICATIONS FOR SCUC

The short-term power system operation is a complex process which begins with day-ahead markets where generator schedules are identified for the least operational cost. Here, unit commitment is an optimization problem utilized to meet the supply and demand for tomorrow's need. The day-ahead market is responsible for scheduling and commit majority of the demand requirement making it a vital step in power system operations. Since the optimization problem involves the ON/OFF status of generators, it involves binary variables and constraints making the problem a mixed-integer linear program (MILP). However, MILP makes the problem harder to solve typically for larger systems. Moreover, there are several security constraints and physical constraints to adhere with to ensure reliable and low-cost solutions. Thus, the resulting MILP is a security-constrained unit commitment (SCUC) [24],[76], [94]–[95] and [96]. In the deregulated regions in the United States, SCUC is solved by independent system operators (ISOs). ISOs have strict timelines to produce results for example, California ISO closes the input bids by 10:00 am and posts the schedules by 01:00 pm whereas New York ISO collects the bids by 05:00 am and posts solution by 08:00 am. This implies that the day-ahead market is cleared, and the commitment schedules are provided in 3 hours [7]–[8]. Here, state-of-the-art algorithms are required to provide significant time saving benefits without loss in solution quality. Therefore, several heuristic or decomposition-based algorithms were proposed to obtain the solution faster

[57],[75]–[74]. However, techniques involving machine learning (ML) to enhance SCUC were seldom studied. In comparison, learning historical information can be beneficial in reducing the complexity of the SCUC. Not only that, learning-based methods can also be used in tandem with other heuristic or decomposition to obtain further improvements.

ML has two broad classes of problems namely, regression and classification. In regression models estimate continuous values whereas classification models approximate a mapping function from input variables to identify discrete output variables, which can be labels or categories. Since generator status is binary in nature, therefore we predict whether the generator is ON/OFF. This implies that the outputs of ML model belong to a binary category. Hence, this chapter focuses on classification rather than regression. For classification, several standard algorithms exist, namely decision tree classification, random forest classification and K-nearest neighbor classification. Even though these are well-established models but are still prone to errors. Since ML models are not 100% accurate, relying on these standard algorithms does not provide flexibility to adapt to the task at hand. For these reasons, logistic regression, neural networks and spatio-temporal models are proposed. This is because the proposed models have a sigmoid output layer which restricts the output between 0 and 1. In other terms, it inherently results in probabilistic outputs which can be leveraged for post-processing the ML predictions with a decision boundary to

selectively use ML predictions of high accuracy. The proposed models are discussed in detail in the subsequent sections.

5.1. Literature Review

An important factor for ML methods is the availability of good data and the right models for training to provide high quality outputs. Since the SCUC is run daily, the historical information can be leveraged to learn non-linear relationships between inputs and outputs. ML has been successfully utilized in the prediction or decision support in complex problems in various power system fields [97]–[101]. The advantage of ML is that once the model is trained the outputs can be obtained instantaneously for similar inputs. Since ML uses large amounts of data to train, it can be robust to noisy data. Therefore, combining ML techniques with traditional algorithms such as SCUC can improve the overall performance [102]–[120].

The SCUC problem consists of parameters (known fixed values), variables (continuous and binary) and constraints (equalities and inequalities). The SCUC problem can have multiple feasible solutions but the optimal commitment and dispatch schedule leads to the lowest-cost solution. ML techniques and data-driven approaches have been utilized recently in aiding or replacing the SCUC process. However, most papers predominantly focus only on replacing the MILP with ML [103]–[105] or screening redundant constraints [106]–[114]. In particular, replacing SCUC with ML techniques can definitely provide the most time-saving benefits but it can never

guarantee feasibility, and/or optimality. An infeasible solution is not a practical solution since several physical constraints can be breeched and [103]–[105] did not compare the solutions with the respective MILP solutions.

The papers proposing screening of constraints mostly focus only on removing redundant transmission constraints in SCUC. In [106], a good starting solution was achieved for SCUC by integrating data-driven approach along with variable categorizing to improve the computational performance of SCUC. In [107], historical data was utilized to screen transmission constraints that are non-binding in the SCUC to speed up the process. Similarly, [108] uses an offline ML tool to learn about outage schedules and identifies planned outages. In [109], the authors perform a feasibility study where they mention that ML techniques cannot guarantee optimality and hence can only be used for warm-start application. The same authors in [110] then use ML techniques to identify line outages under drastic weather conditions for stochastic SCUC to eliminate congested transmission constraints. In [111], the optimization is benefitted by replacing few active and inactive constraints line-flow constraints by cost-based inequality through ML. In [112], a two-step offline and online process is implemented where the offline process screens security constraints for SCUC whereas this further screened in real-time in the security-constrained economic dispatch (SCED). Similarly, [113] performs screening only for SCED which does not bring about much time-saving benefits whereas [114] creates artificial colorful images to utilize convolutional neural networks (CNN) in SCED to study the network constraints.

Though constraint screening relaxes the SCUC algorithm when aided by ML, they cannot offer a greater time-saving benefits than variable reduction by learning the commitment schedules as seen in [115]–[120]. This is because in constraint screening the feasibility region of the SCUC solutions remains unaltered and only redundant constraints or inactive constraints are eliminated. [115]–[117] tries to eliminate all binary variables in SCUC and perform SCED. This may work for smaller systems or eliminating temporal constraints (single period application) or if the dataset is invariable which is not practical. Hence, this does not guarantee feasibility of the SCUC problem. Only [118]–[120] performs a reduced-SCUC (R-SCUC) which were also tested on large practical systems and can be considered as the state-of-the-art methods. A few machine learning techniques are proposed in [119] to use historical information to improve the performance of SCUC to solve identical instances in the future. However, [119] uses support vector machine (SVM) and k-nearest neighbor (KNN) classification algorithms to learn commitment solutions for SCUC and yet are associated with drawbacks from infeasible problems. [120] utilizes an offline ML tool to categorize load profile into different categories with a pre-determined commitment schedule from history. However, [120] provides only a feasible solution and does not guarantee optimality or high solution quality. Also, the proposed methods in [118]–[120] do not address renewable generation and only works on deterministic models. Renewable energy source (RES) is addressed in [121]–[122] albeit the proposed methods only learn the varying nature of renewables to identify a most likely scenario.

5.2. SCUC formulation

The objective of the SCUC is to minimize the operational cost of generators, $F(x, y)$ in (5.1),

$$Minimize\ F(x, y), \tag{5.1}$$

which includes the production, start-up and no-load costs. In (5.1), x denotes the continuous variables of the problem such as generator dispatch points, power flows and bus phase angles; and y denotes the generator commitment status and start-up binary variables. This is performed subject to generation limits, power flow constraints and reliability requirements in (5.2)–(5.3),

$$G(x, y) \leq b, \tag{5.2}$$

and

$$H(x, y) = d. \tag{5.3}$$

The inequality constraints are modelled in (5.2) representing the minimum and maximum generation and transmission limits, the hourly generation ramp capability, and emergency 10-min reserve ramping capability while ensuring that reserves are held at the least to handle the failure of the largest generator. The equality constraints in (5.3) represent the nodal power balance and the power flow calculation. The detailed SCUC model used in this work is the formulation consisting of equations (2.1)–(2.15) and for a multi-scenario stochastic-SCUC (SSUC) can be modelled with (3.1)–(3.16).

5.3.   Data Generation

To ISO's run the SCUC daily, therefore, data related to daily load-profiles and respective cleared generator commitment and dispatch schedules are stored. This data is assumed to be the starting point for this work. To train ML models, a large amount of data is required. Hence, the SCUC model specified in Section-II is utilized to generate the data. By varying the input nodal load-profile, we can generate multiple optimal commitment and dispatch schedules for respective profiles that can be collected as historical information.

It can be noted that RES can also be modelled in this step if the system has wind/solar units. The load profile then becomes a net-load profile with multiple scenarios. RES are integrated to SCUC with a multi-scenario stochastic approach in SCUC as seen in [76],[96] and only a single resultant commitment schedule satisfies all the scenarios.

For the test systems considered in this study, the historical information is generated by modifying the nodal load profile artificially mimicking uncertainty. Since the test systems considered do not consist of the same information, a data creation step using the proposed BC-RPG method is required. To begin, a common load profile for each test system is considered with average seasonal peak information from [63]. If seasonal information are considered then average seasonal load-profile can be utilized and different ML models can be trained and stored for each season by curating the data into seasonal buckets, if needed. Once the standard profile is chosen, multiple profiles

can be generated using random variables as seen in (5.4) where the random variables, α^m and $\beta_{n,t}^m$, shift the entire system load profile up/down or the composition of the system load profile can be altered, respectively,

$$SysD_t^m = \sum_{n \in N} d_{n,t}^m = (\sum_{n \in N}(d_{n,t} + \beta_{n,t}^m d_{n,t})) * (1 + \alpha^m),$$
$$\forall m \in M, t \in T$$

(5.4)

where,

$SysD_t^m$ is the system demand in time period t for sample m.

α^m is a random variable ($\pm$ 10%) for sample m.

$\beta_{n,t}^m$ is a random variable ($\pm$ 4%) for sample m for bus n in time period t.

Since demand profiles only change marginally day-to-day, the value for α^m is considered to be $\pm$ 10%. Nodal values cannot be altered significantly as this would lose the correlation of nodal information. Therefore $\beta_{n,t}^m$ is considered to be $\pm$ 4%. The combination of both random variables provide varying load-profile curves. From Fig. 5.1, for example, curve 1 represents the initial load profile whereas curve 2 and curve 3 are generated only using only α^m, curve 4 is generated through only $\beta_{n,t}^m$, and curve 5 and curve 6 are generated using the combination of both random variables.
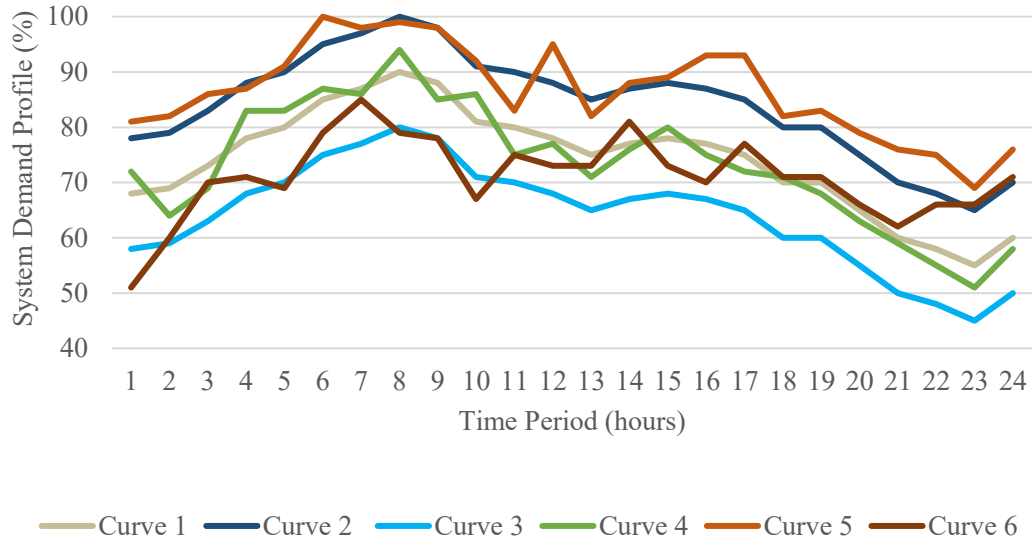
Fig. 5.1. Sample demand profile curves.

Only feasible samples of the SCUC are considered and denoted as M are created for each test system. The created M samples, once shuffled, are split into two datasets: 80% training samples denoted as M^{train} and 20% testing samples denoted as M^{test}.

5.4.   Warm-Start vs Model Reduction

A warm-start application provides a starting point for the optimization solver to begin with, which may converge faster to the optimal solution. Note that the optimal solution could be very different from the starting point. Traditionally, most of the literature uses a warm-start application citing that ML models leads to infeasible solution [101],[105]–[106]. It is true that ML cannot purely replace optimization procedures since ML outputs are not 100% accurate. Therefore, utilizing ML outputs

in completeness will result in infeasible problems. However, earlier research disregarded model reduction as a possible solution, i.e., partial usage of ML outputs.

In this paper, model reduction is proposed which fixes certain subset of variables/solutions that are determined from ML outputs with high confidence. This directly relates to reduction of variables and constraints in the MILP problem. Hence, the resultant MILP is an R-SCUC model which treats the remaining flexible generators as variables whereas the fixed generator statuses are treated like constants/parameters.

An advantage of warm-start is maintaining solution quality, i.e. the solution does not change with or without ML solution. However, the disadvantage is that time reduction is minimal in most cases. When compared against model reduction, R-SCUC results in significant time savings. Additionally, through well-defined post-procedures to utilize the ML outputs, the solution quality is maintained to a high degree in R-SCUC.

5.5. Test cases

The proposed methods were validated with the following standard test systems summarized in Table 5.1. It can be noted that a modified IEEE 24-bus system was also introduced with 2 additional renewable units with a peak capacity of 200MW each. Three scenarios with varying renewable outputs are considered in the modified IEEE 24-bus system. Simulation results are presented in the following sections.

Table 5.1. Summary Of Test Systems

System	Gen cap (MW)	#bus	# gen	# branch
IEEE 24-Bus [63]	3,393	24	33	38
Modified IEEE 24-Bus [76]	3,793	24	35	38
IEEE 73-Bus [63]	10,215	73	99	117
IEEE 118-Bus [93]	5,859	118	54	186
South Carolina (SC) [123]	12,189	500	90	597
Polish [93]	30,053	2,383	327	2,895

5.6. ML Approach

The overall supervised ML approaches are described at a fundamental level in Fig. 5.2. We focus on building a supervised ML model to predict the commitment status of each generator g in each time interval t (24-hours) for day-ahead operations. The commitment status of 1 implies the generator is ON whereas 0 represents the generator is OFF. Ideally a classification model can be utilized when the targets only belong to two classes, also known as binary classification. There are several classification models but only few models provide probabilities as an output. We also require a generative classifier that does not assume independence in pairs of input features. In this work, the input features are the respective normalized nodal demands and therefore cannot be

considered independent in real-world data. The training and test samples are produced

using data generation mentioned in section 5.3.
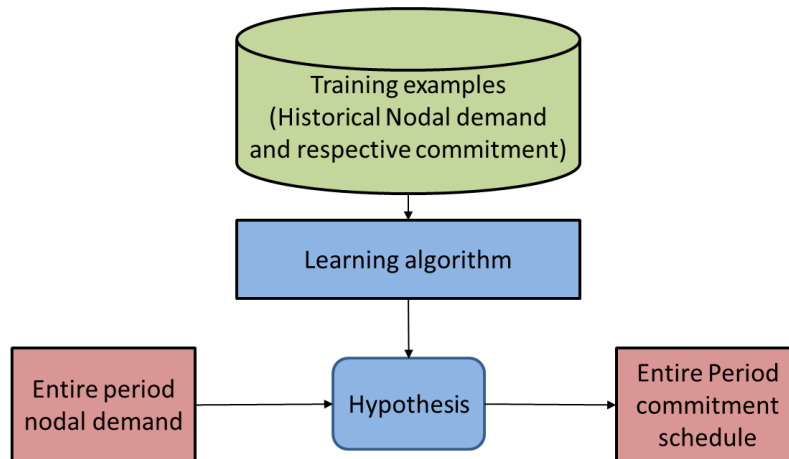
Fig. 5.2. Supervised ML approach.

The proposed method The ML step is utilized to reduce the number of variables

in the SCUC model. The traditional approach is to utilize all the information such as

constants, continuous and binary variables in an online SCUC model as shown in Fig.

5.3. However, we can train an ML algorithm to identify variables that follow a pattern,

especially binary variables by leveraging historical information. It is known that binary

variables increase the complexity in an MILP [103]–[104],[115]–[120].
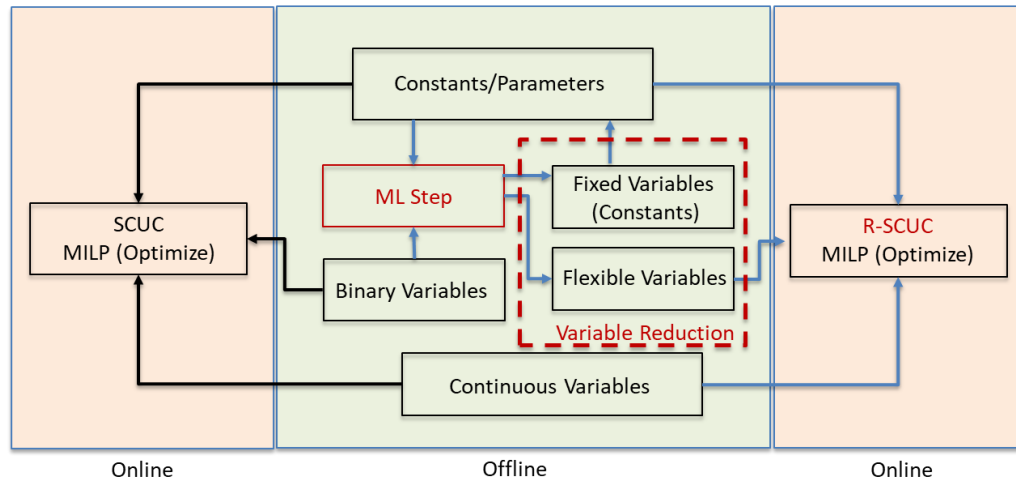
Fig. 5.3. SCUC Model Reduction.

In SCUC, the binary variables are the generator commitment schedule. The constants include forecasted load profiles, generator cost and ramping information whereas the continuous variables are generator dispatch, line flows and bus angles. By studying the historical commitment schedules with respective load profiles, the ML algorithm can identify many generator states with certainty for any given load profile. The generator states can be classified as either (i) flexible, to be determined by online optimization step, or (ii) fixed, as identified by offline ML algorithm. Therefore, the fixed generators are now constants and the resultant R-SCUC online model only determines the states of flexible generators.

It can be noted here that this approach of model reduction is agnostic to the MILP model. This implies that the proposed approach of model reduction is unaltered

and can be applied to deterministic, stochastic and/or decomposition or heuristic techniques based SCUC models

5.7. Accuracy

The proposed ML models are trained using M^{train} and tested using M^{test} through the data generation mentioned in section 5.3. The ML model accuracy can be verified using the post-processed outputs. Once the model is trained, the output probabilities, $P(u_{i,g,t}^{ML})$, are post-processed to obtain the predicted commitment schedule $u_{i,g,t}^{ML}$: 1 if $P(u_{i,g,t}^{ML}) \geq P^{th}$, and 0 if $P(u_{i,g,t}^{ML}) < P^{th}$. P^{th} is the probability threshold that varies between $0.5 \leq P^{th} \leq 0.9$. The accuracy in terms of $u_{i,g,t}^{ML}$, defined in (5.5), is calculated for both $i \in M^{train}$ and $i \in M^{test}$ using the true commitment $u_{i,g,t}$,

$$Accuracy = 1 - \frac{1}{m}\sum_{i=1}^{m}(\Sigma_{g \in G}\Sigma_{t \in T}|u_{i,g,t} - u_{i,g,t}^{ML}|), \qquad (5.5)$$

where, m represents the number of samples, G represents the set of generators and T represents the set of time periods.

5.8. Preliminary UC Model and ML Method

In this section, preliminary work was implemented using a simplified SCUC process described by (2.1)–(2.7),(2.10)–(2.15). The minimum-up and minimum down requirements of generators were assumed to be 1 hour and therefore the constraints

121

(2.8)–(2.9) were not considered. The data generation and verification steps also conform with the above model.

5.8.1. ML Model

The logistic regression (LR) model was chosen as the classifier method in this paper. Since LR is a well-established classifier method, several python packages provide a default package for outputs with input data. The LR model is implemented through scikit-learn package [124]. Scikit-learn provides a package that fits the input and outputs based on the LR algorithm using the solver liblinear. The liblinear solver uses a coordinate descent algorithm and only supports binary classification. The package is capable of handling one target or output at a time and the regularization is applied by default. This package trains the LR model with the following cost function in (5.6),

$$Cost = \frac{1}{2}w^T w - C \sum_{i=1}^{m} \log\left(\exp(-y_i(X_i^T w + c)) + 1\right), \tag{5.6}$$

where, w represents the trainable weights, y_i represents the target/output, X_i represents the input vector of sample i, and C is the penalty.

In this work, the input features are the respective normalized nodal demands. The output targets are the generator g commitment status which indicates the ON and OFF schedule in each time period t. A commitment status of 1 implies the generator g is ON whereas 0 represents the generator g is OFF. Therefore, the targets belong only to two different classes (binary classification).

The ML model accuracy can be verified using the post-processed outputs. Once the model is trained, the output probabilities, $P(u)^{ML}_{i,g,t}$, are post-processed to obtain the predicted commitment schedule $u^{ML}_{i,g,t}$: 1 if $P(u)^{ML}_{i,g,t} \geq P^{th}$, and 0 if $P(u)^{ML}_{i,g,t} < P^{th}$. P^{th} is the probability threshold that varies between $0.2 \leq P^{th} \leq 0.8$. The accuracy in terms of $u^{ML}_{i,g,t}$, defined in (5.5), is calculated for both $i \in M^{train}$ and $i \in M^{test}$ using the optimal commitment $u_{i,g,t}$ obtained by solving SCUC.

5.8.2. Benchmark Methods

To obtain the boundary conditions, the benchmark methods are utilized to compare against the proposed methods. Therefore, two benchmark methods are utilized namely, *B1* and *B2*. The SCUC model described in Section 5.8 is the benchmark model *B1* that does not utilize any ML information and is purely optimization. Whereas *B2* is an R-SCUC model only uses ML solution. This implies all the binary variables are fixed in SCUC, which is effectively converted into an economic dispatch problem. The following summarizes the benchmark methods:

- *B1*: normal SCUC that does not utilize any ML outputs $u^{ML}_{g,t}$, in which $u_{g,t}$ is solved only through MILP.

- *B2*: fix $u_{g,t} = u^{ML}_{g,t}$ and solve the reduced-SCUC (linear model in *B2*).

123

5.8.3. Proposed Methods

In this chapter, the LR model proposed in sub-section 5.8.1 is extended with two proposed post-processing procedures. Once the LR model provides the probabilities of the generator commitment status, the decision boundary is then utilized to determine values of ML identified commitment status. The proposed methods in this section identifies which among the ML solution can further be processed to provide additional insights to reduce the complexity of the SCUC. The goal to choose the right post-procedure involves the elimination of infeasible problems while also maintaining the solution quality. The following are the proposed two procedures namely, *P1* and *P2*, to utilize the ML outputs to assist in establishing an R-SCUC for each power grid load profile of the testing samples:

- *P1*: R-SCUC where fix $u_{g,t} = 1$ if $u_{g,t}^{ML} = 1$. The warm-start uses $u_{g,t} = 0$ if $u_{g,t}^{ML} = 0$.

- *P3*: R-SCUC where always ON/OFF generators are identified using $u_{g,t}^{ML}$. For each testing sample (grid profile), if a generator g is predicted to be always ON in 24-hour period then fix $u_{g,t} = 1$ for the entire 24-hour period for the corresponding generator. Similarly, if generator g is always OFF in 24-hour period, then fix $u_{g,t} = 0$ for all periods for the corresponding generator. For all other generators, use warm-start $u_{g,t} = u_{g,t}^{ML}$.

For each sample $i \in M^{test}$, the above procedures *P1–P2* are implemented and the respective R-SCUC is solved to verify the quality of the LR solution. The quality of solution and time for computation for R-SCUC are compared against *B1* and *B2* which provides the minimum and maximum time reduction possible for each test sample, respectively. The overall flow of the proposed LR assisted R-SCUC process is represented in Algorithm 5.1. Here, steps 1–5 represent data generation, steps 6–10 represent the training phase of LR, step 11–12 represent the testing phase of LR and steps 13–16 represent verification of proposed LR assisted R-SCUC procedures.

Algorithm 5.1 LR assisted SCUC process

1: **For** $i \in M$
2:     Randomize nodal demand
3:     Solve SCUC
4:     Store $d_{i,n,t}, u_{i,g,t}$, results and computing time
5: **End**
6: **Shuffle** M samples
7: **Split** M as 80% for M^{train} and 20% for M^{test}
8: **Train** LR using M^{train} for different hyperparameters
9: Calculate training accuracy.
10: **Tuning**: identify hyperparameters with best accuracy
11: **Test** using M^{test} and report test accuracy
12: Save ML predicted output probabilities for M^{test}
13: **For** $i \in M^{test}$
14:     Perform *B1–B2, P1–P2* and verify resultant SCUC for $d_{i,n,t}$
15:     Record results and computing time
16: **End**

5.8.4. Results and Analysis

The SCUC mathematical model is implemented in AMPL. The data creation and verification steps are thus conducted using AMPL and solved using Gurobi solver with MIPGAP = 0.01. The ML step is implemented in Python 3.6. The computer with Intel® Xeon(R) W-2295 CPU @ 3.00GHz, 256 GB of RAM and NVIDIA Quadro RTX 8000, 48GB GPU was utilized. The proposed methods were validated with the following standard test systems summarized in Section 5.5. Simulation results are presented in the following sub-sections. In this Section, it can be noted that the dataset was created with an assumption of 1-hour minimum-up and minimum-down time for all generators.

5.8.4.1. Decision Boundary Sensitivity Analysis

The decision boundary, P^{th}, is an important parameter that is utilized to classify generator status as ON or OFF. The outputs of LR algorithms are the probability of a generator g in time period t being ON. This does not affect warm start application since they are only used as starting values for the MILP.

However, in this paper, we focus on R-SCUC methods by directly using ML solution partially to reduce problem complexity. In the case of $B2$, benchmark method that uses complete ML solution, we notice P^{th} significantly affects results. A key observation is that lower value of Pth reduces the number of infeasible problems but affects solution quality (SQ) since more non-optimal generators are switched ON in

certain time periods. The trade-off to consider in *B2* is more feasible problems vs solution quality. For example, in the IEEE 24-Bus system, from Fig. 5.4, it can be seen that it changes from 48 (16.6%) infeasible test samples for $0.5 \leq P^{th} \leq 0.7$ to 85 (29.4%) infeasible test samples at $P^{th} = 0.8$. For $P^{th} = 0.9$, this increases to 261 (90.3%) infeasible test samples. The reason is that fewer generators are committed, and they are unable to meet the load. Ideally, $0.5 \leq P^{th} \leq 0.7$ is the threshold based on the sensitivity analysis performed on *B2*.

This provides an important conclusion that ML solutions cannot completely replace optimization even if the accuracy is high. However, *B2* presents the maximum solve time (ST) savings achieved for feasible samples and this serves as a boundary condition to gauge the proposed methods, *P1* and *P2*.
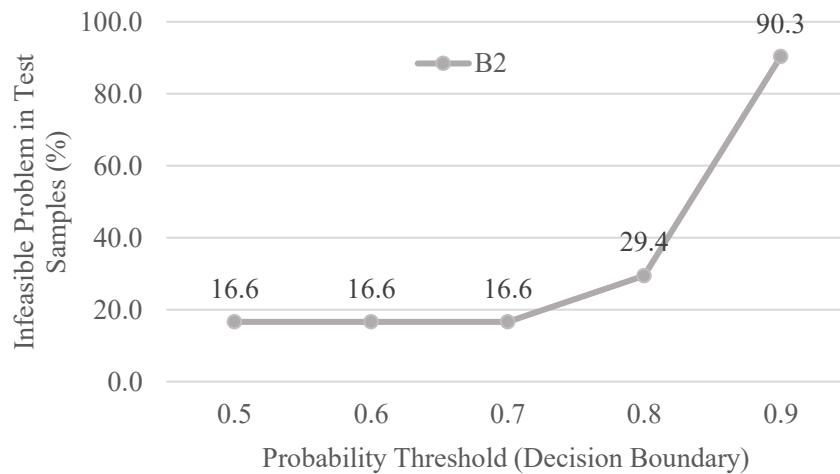
Fig. 5.4. Test sample infeasibility in IEEE 24-Bus system for *B2*.
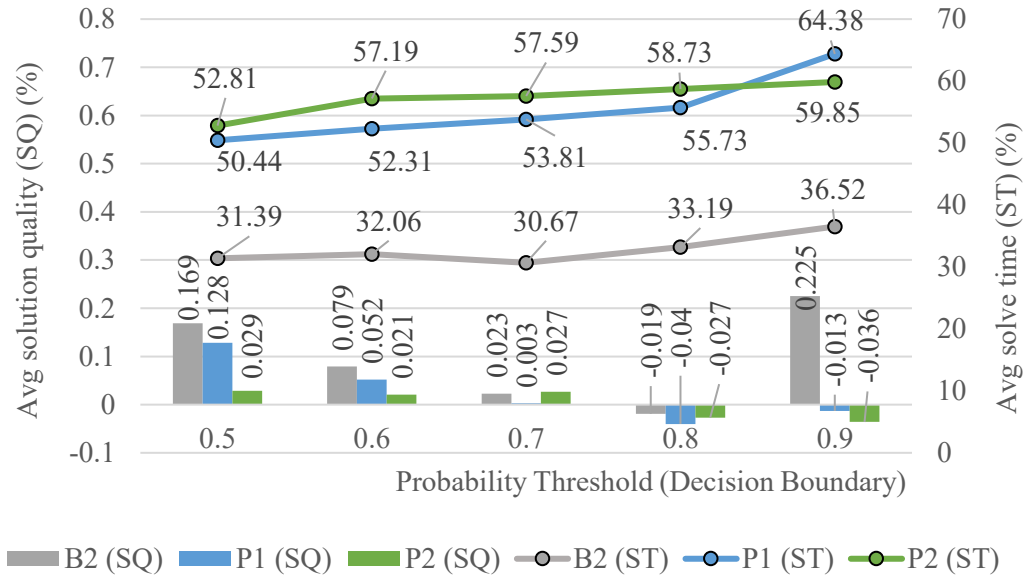
Fig. 5.5. B1-Normalized solution quality (SQ) and solve time (ST) averaged over test samples for IEEE 24-Bus system with respect to decision boundary.

On further analysis, from Fig. 5.5, we can notice two trends for *P1* and *P2*. Firstly, as P^{th} increases, the solution quality continuously improves. SQ values closer to 0 is more accurate as it represents the change in objective cost with respect to *B1*. SQ greater than 0 implies that the model provides a higher cost than *B1* and SQ less than 0 implies that the model provides lower cost than *B1*. This is because, (i) more variables are determined from optimization as opposed to ML solution and (ii) problem relaxations due to R-SCUC models are capable of achieving lower cost compared to SCUC model, *B1*. Secondly, time savings reduces as P^{th} increases. Therefore, a trade-off between solution quality and time-savings is considered to obtain the best decision boundary.

5.8.4.2. ML Training

Table 5.2 summarizes the M, M^{train}, M^{test}, accuracy, cumulative training time and decision boundary for each test system once the tuning and sensitivity analysis are completed. The LR algorithm provides high accuracy >93% for both the training and test samples for all test systems considered in this work.

The training time is the cumulative training time for all targets (each generator g in each time period t) for a particular test system. The training time is an offline step and is only implemented once for each system prior to the online step. Therefore, training time will not be considered in R-SCUC which is online. Even so, training times are reasonable even for the large systems (Polish 2383-bus system) with ~85 min to train.

Ideally, the offline training can be done with grouped seasonal profiles that are similar in characteristics, patterns and resultant commitment schedules. This can increase the robustness of the algorithm. For the purpose of highlighting the benefits of LR algorithm and post-processing techniques, a higher variation in load profile is considered in this work. Here, it can be noted that a high accuracy directly implies a higher decision boundary, P^{th}, which implies ON and OFF generators are very well distinguished.

Table 5.2. Training Summary

# Bus	Number of Samples			Accuracy (%)		Training time (min)	P^{th}
	Total	Train	Test	Train	Test		
24	1,446	1,157	289	98.97	98.96	<1	0.7
73	1,391	1,113	278	96.89	96.88	<8	0.7
118	1500	1200	300	93.61	93.53	<5	0.3
500	1499	1200	299	98.56	98.51	<17	0.6
2383	1200	960	240	95.94	95.86	<85	0.5

5.8.4.3. Verification of Proposed Method

ML Training, verification Once each system was trained, a verification process was conducted for *P1* and *P2*. This was benchmarked against the *B1* method that does not use any ML solution and against the *B2* method that only uses ML solution to determine all generator commitment status. Therefore, the SQ from *B1* method is considered as 100% since it is purely an MILP optimization. The solutions cost and solution time of the R-SCUC models *P1*, *P2* and *B2* are represented as *B1*-normalized values.

Fig. 5.6, and Fig. 5.7, presents the *B1*-normalized objective value and computing time in percent when averaged over all test samples for each test system,

respectively. From Fig. 5.6, *P2* provides comparable SQ to the *B1* method. However, *P1* leads to marginally increased costs since the ML solution may result in scheduling sub-optimal generators as ON. A key observation here is that not all samples of *B2* are feasible even though the accuracy is >93%. This is because *B2* fixes the status for all generators and only an optimal economic dispatch is then implemented. For the feasible samples, *B2* results only in marginal loss of SQ in IEEE 24-bus system (0.02%), IEEE 73-bus system (0.66%), IEEE 118-bus system (2.33%) and Polish system (2.02%) while it leads to a substantial increase of total cost on the IEEE 500-bus system. However, the SQ can be improved by *P1* and *P2* without infeasible problems. Therefore, the proposed methods, *P1* and *P2*, not only avoid infeasible problems but also maintain SQ. Among the proposed methods, *P2* offers the highest SQ similar to *B1* for all test systems.

From Fig. 5.7, though *B2* results in lower solution quality, it provides the most computational time savings ~95% in the Polish system since this eliminates all the binary variables in the problem. Therefore, the solution of *B2* serves as the maximum time-saving benchmark. *P1* and *P2* are R-SCUC models that reduce the number of variables and constraints and therefore result in considerable time-savings when compared to *B1*. Among the proposed methods, *P1* offers 50.9% time-savings and *P2* offers 38.8% time-savings on average across different test systems. *P1*, identifies more generator status (variables) to be ON, provides higher time-savings mainly because this

procedure reduces more variables. In comparison, *P2* only identifies generators that are

Always-ON or Always-OFF.
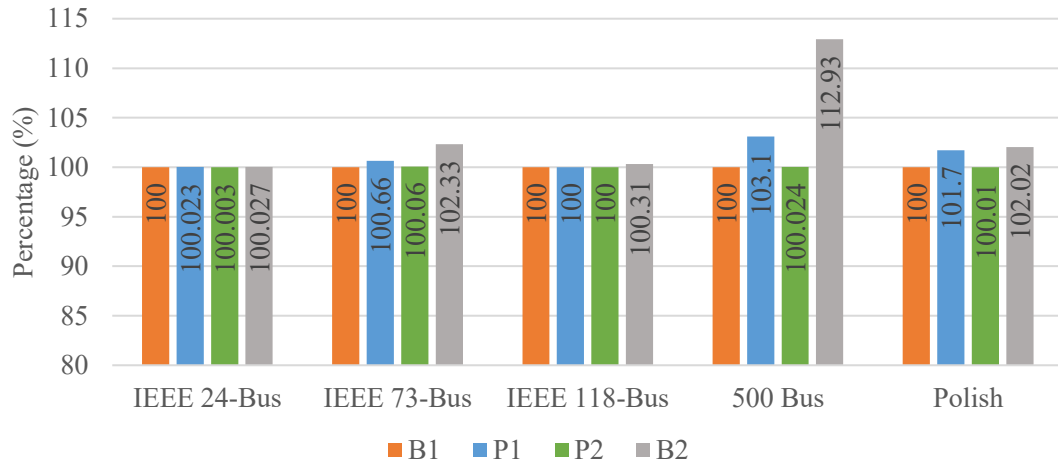
Fig. 5.6. Normalized cost in percentage averaged over test samples.
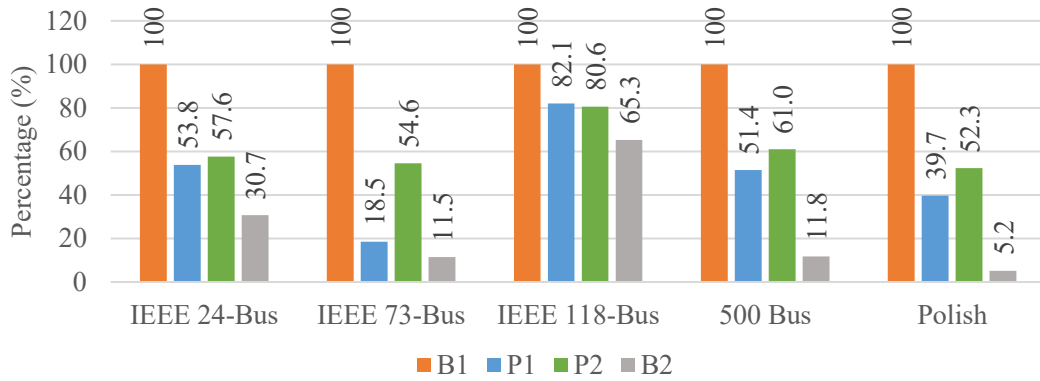
Fig. 5.7. Normalized computing time in percentage averaged over test samples.

5.8.4.4. Problem Size Reduction

B2, *P1* and *P2* use ML solutions to fix the status of generators, which results in R-SCUC models. In particular, *B2* eliminates all binary variables in the problem whereas *P1* and *P2* results in decreased variables and constraints as seen in Table 5.3. *B1* represents the pure optimization process and therefore has the full list of variables and constraints. A warm-start is not a proposed methodology in the paper. However, if a warm-start is utilized it will have the same problem size as the *B1* method since the ML solution is only used as a warm-start solution. By utilizing the ML solution, *B2*, *P1* and *P2* effectively reduces linear variables, binary variables, constraints and non-zeroes in the SCUC problem. As a result, it leads to smaller problem which results in time-savings.

Table 5.3. Average Problem Size for Polish System

Procedure	Linear Var	Binary Var	Constraints	Non-zeroes
B1	142,296	15,696	197,112	3,176,376
P1	128,856	3,700	153,296	2,924,834
P2	142,296	10,464	184,104	3,135,024
B2	125,330	0	136,168	2,027,850

5.8.4.5. Inferences

It was evident that ML cannot directly replace the optimization procedure from *B2* since this lead to infeasible problems, which is detrimental. Not only that, the solution quality also suffers in feasible problems of *B2*. The only advantage is it points that almost 95% computational time can be reduced for large systems and is hence used as a benchmark boundary. The proposed ML assisted SCUC model reduction method can relieve the computational burden of the MILP problem while maintaining solution quality. The results also point that the ML model's decision boundary selection plays a vital part in the model accuracy.

Further, once the models are trained, the proposed post-processing techniques, *P1* and *P2*, effectively utilize the ML predicted outputs without causing any SCUC infeasibility. The proposed approaches only use part of the ML solutions with high confidence to reduce the variables and constraints in SCUC. Not only that, but the solution quality was also not compromised especially in *P2*. *P1*–*P2* results in problem size reduction, which results in significant time-savings across multiple test systems. *P1* and *P2* result in time savings of 50.9% and 38.8%, respectively, on average across all the test systems while also resulting in high-quality solutions.

5.9.   Advanced Post-Processing Methods

This section extends on the preliminary idea in section 5.8 but has several improvements and innovations to supersede the prior work. Firstly, this section

addresses the a compete SCUC model by utilizing the minimum-up and minimum down requirements of generators constraints in (2.8)–(2.9) which were earlier eliminated from the SCUC model. Here, the SCUC model is defined by (2.1)–(2.15). Therefore, the data for this section is also regenerated with updated SCUC model considering minimum up and minimum down time of generators in the test systems. Secondly, several ML classifications were studied, namely, KNN, random forest (RF), fully connected neural networks (NN), logistic regression (LR), and a novel multi-target logistic regression (MTLR). Among these, the LR, MTLR and NN algorithm provided the most flexibility to post-process the ML outputs while also providing very high-quality solutions. Lastly, the proposed method in this section introduces a novel feasibility layer (FL) to correct machine learning predictions to be feasible for (2.8)–(2.9). The following contributions were explored:

- An NN model and an innovative multi-target logistic regression (MTLR) model are utilized to leverage historic demand profiles to predict generation commitment schedule as an offline step.

- Effective post-processing methods, utilizing the ML output to reduce the variables in SCUC model achieving model-reduction, are addressed while maintaining solution quality.

- A feasibility layer (FL) is proposed to ensure feasibility of ML solution in online optimization step.

- A bus-correlated randomized profile generation (BC-RPG) method is used to obtain data to train ML models.

5.9.1. Classification Models from Scikit-learn

Performance of several classification models, namely KNN, RF, NN and LR are considered initially. All the models used for comparison are obtained from Scikit package, [124]. The neighbors-based classification is a type of instance-based learning *or* non-generalizing learning. This implies a general internal model is not constructed but rather training data are stored as instances. Classification is computed from a simple majority vote of the nearest neighbors of each point. For KNN classification, the optimal choice of the value K is highly data-dependent: in general, a larger K suppresses the effects of noise, but makes the classification boundaries less distinct. KNN works by identifying the most similar examples in the training dataset and conducting a simple majority vote [125].

Another supervised learning method used for classification is the class of non-parametric decision trees where a target variable is predicted by the model by learning simple decision rules inferred from the data features. Here, a tree can be seen as a piecewise constant approximation. The RF model is a classification where an ensemble of many individual decision trees is used for prediction. Each individual tree in the random forest predicts a class output and the class with the most votes become the RF prediction [126].

LR is a well-established classifier method which works in a one vs rest classification meaning it identifies one output based on the set of training inputs [127]. LR algorithm using the solver liblinear which uses a coordinate descent algorithm and only supports binary classification. The package is capable of handling one target or output at a time and the regularization is applied by default [127]. The architecture of LR is represented in Fig. 5.8.
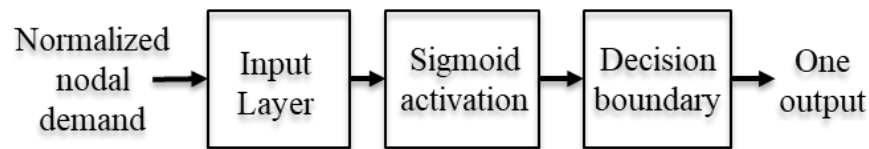
Fig. 5.8. LR architecture.

Multi-layer perceptron (MLP) is a supervised learning algorithm that learns a mapping between inputs and outputs by training on a dataset. MLP is also known as NN where a non-linear function approximator for either classification or regression is used for learning. Mainly, NN differs from LR, in that between the input and the output layer, there can be one or more non-linear layers hidden layers. The outputs from the hidden layer are processed by a sigmoid layer to provide probability estimates and followed by a classification to represent the class. It uses a cross-entropy loss function and trains via backpropagation. For classification, it minimizes the cross-entropy loss function, providing a vector of probability estimates [128]. The architecture of NN is shown in Fig. 5.9.

Normalized nodal demand → Input Layer → Hidden layer with Relu activation → Output layer Sigmoid activation → Decision boundary → Entire commitment schedule
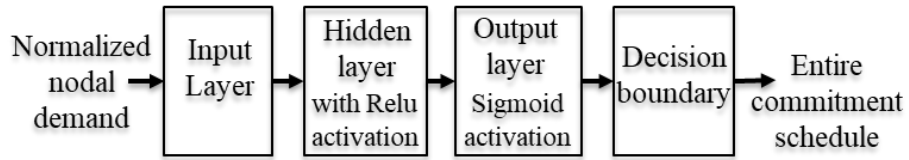
Fig. 5.9. NN architecture.

5.9.2. Multi-Target Logistic Regression

In this section, the training model/algorithm considered is an MTLR model as denoted in Fig. 5.10. This model is similar to LR as it is a regression model which predicts the value of probability of an output being 1 [129]–[130]. The difference is that MTLR uses a single set of weights, w_j, as opposed to multiple models with different weights, $w_{j,m}$, in LR.

Input features: Nodal demand vector $\forall n, t$

1, w_0
x_1, w_1
x_2, w_2
w_3
x_3
w_{n*t}
x_{n*t}

Training
error

$h_w(x)$ Σ $\sigma(h_w(x))$ σ

$\hat{y} = \sigma(h_w(x)) = P(y = 1)$
$P^{th} = 0.5$

Decision Boundary
$P(u_{g,t}) \geq P^{th} : u_{g,t} = 1$
$P(u_{g,t}) < P^{th} : u_{g,t} = 0$

where, $\sigma(t) = \frac{1}{1 - e^{-t}}$ (sigmoid function)

$u_{g,t}^{ML}$
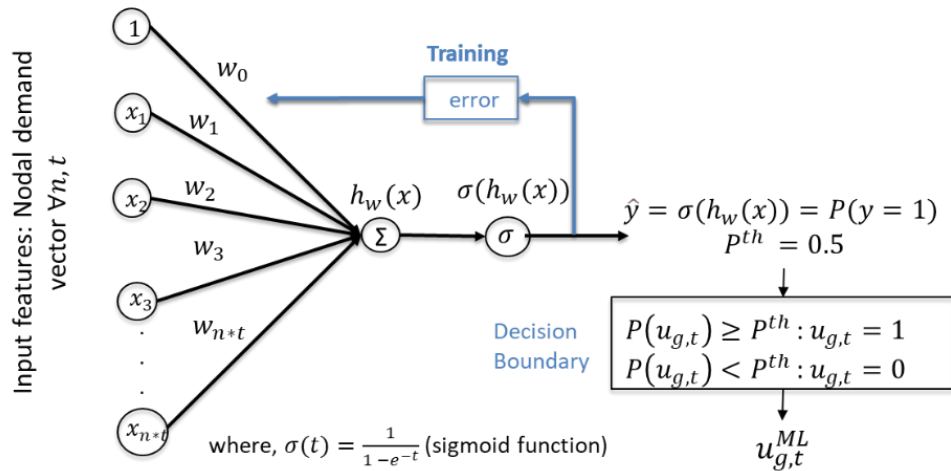
Fig. 5.10. MTLR based SCUC model reduction algorithm.

The hypothesis of LR model, (5.7), is a linear summation of normalized nodal demand and the parameters/weights, w_j,

$$h_w(x) = w_0 + \sum_{j \in N*T} w_j x_j. \tag{5.7}$$

The LR model uses a sigmoid activation layer, (5.8), which restricts the output from 0–1 which represents the probability of the output being 1, $P(y = 1)$,

$$\sigma(t) = \frac{1}{1 - e^{-t}}. \tag{5.8}$$

Finally, the output, $\hat{y}$, is obtained after the hypothesis function followed by the sigmoid activation as seen in (5.9),

$$\hat{y} = \sigma(h_w(x)) = P(y = 1). \tag{5.9}$$

To train the LR model, we need to obtain the best parameters, w_j, that fit the input and output features. This is implemented using the LR cost/loss function, (5.10),

$$J(h_w(x)) = -\frac{1}{m} \left[\sum_{i=1}^{m} (y^{(i)} \log h_w(x^{(i)}) + (1 - y^{(i)}) \log (1 - h_w(x^{(i)}))) \right]. \tag{5.10}$$

To obtain the weights, we minimize the LR cost/loss function, (5.11),

$$min_w J(h_w(x)), \tag{5.11}$$

by using a gradient descent algorithm, (5.12), for several iterations until the cost/loss values saturates for all samples in M^{train},

$$\text{Repeat} \left\{ \omega_i := \omega_i - \delta \sum_{i=1}^{m} (h_w(x^{(i)}) - y^{(i)}) x_j^{(i)} \right\}, \tag{5.12}$$

where, δ represents the learning rate of the gradient descent algorithm. The number of iterations and learning rate represents the hyper-parameters of the LR model.

The model accuracy can be verified using the post-processed outputs. Once the model is trained, the output probabilities are post-processed as $P \geq 0.5$ as 1 and $P < 0.5$ as 0 to obtain the predicted commitment schedule, $u_{i,g,t}^{ML}$. The accuracy is calculated for both $m \in M^{train}$ and $m \in M^{test}$ using (5.5).

5.9.3. Feasibility Layer

Once the ML model provides the classification results, a FL is added to avoid any erroneous commitment schedules in ML outputs, $U_{m,g,t}^{ML}$, by making minor but necessary corrections across time period $t \in T$ as defined in (5.13),

$$Min \ \Sigma_t\left(u_{g,t}^{Up} + u_{g,t}^{Dn}\right). \tag{5.13}$$

As shown in (5.14), if $U_{m,g,t}^{ML} = 1$, then it can be turned off with $u_{g,t}^{Dn} = 1$. Similarly, if $U_{m,g,t}^{ML} = 0$, then it can be turned on with $u_{g,t}^{Up} = 1$,

$$u_{m,g,t}^{MF} = U_{m,g,t}^{ML} + u_{g,t}^{Up} - u_{g,t}^{Dn} \ \forall t. \tag{5.14}$$

The FL ensures that minimum up/down time limit constraints (2.8)–(2.9) are not violated by reforming them as (5.15)–(5.16),

$$\Sigma_{p=t+1}^{t+DT_g} v_{g,p}^{MF} \leq 1 - u_{m,g,t}^{MF} \ \forall t \leq nT - DT_g, \tag{5.15}$$

and

$$\sum_{p=t-UT_g+1}^{t} v_{g,p}^{MF} \leq u_{m,g,t}^{MF} \ \forall t \geq UT_g. \tag{5.16}$$

(5.17) defines the respective start-up variable, $v_{g,t,m}^{MF}$,

$$v_{m,g,t}^{MF} \geq u_{m,g,t}^{MF} - u_{m,g,t-1}^{MF} \ \forall t. \tag{5.17}$$

Finally, (5.18) ensures that the flexible generator can either be turned on or turned off whereas (5.19) describes the variables are bound by binary integrality,

$$u_{g,t}^{Up} + u_{g,t}^{Dn} \leq 1 \ \forall t, \tag{5.18}$$

and

$$u_{g,t}^{Up}, u_{g,t}^{Dn}, v_{m,g,t}^{MF}, u_{m,g,t}^{MF} \in \{0,1\}, \forall t. \tag{5.19}$$

The FL is represented by (5.13)–(5.19) and is solved in the online phase. Therefore, it is performed for each generator g independently per sample $m \in M^{test}$ during the verification process. Here, it can be noted that Always ON/OFF as determined by ML outputs, $u_{m,g,t}^{ML}$, in each sample m can be excluded as they are already feasible for minimum up/down constraints. The solve time for FL for each generator g is aggregated and added to the respective R-SCUC solve time for each sample m.

5.9.4. Post-Process Technique

The LR, MTLR and NN models presented in Section 5.9.1 and Section 5.9.2 are extended with a post-processing technique which includes the FL described in Section 5.9.3 as seen in Fig. 5.11. Since the ML outputs of the above models are probabilities of generator being ON, a decision boundary of $P^{th} = 0.5$ is used to

141

classify ON and OFF status of generators. This implies, the generator status $u_{m,g,t}^{ML} = 1$ if $P(u_{m,g,t}^{ML}) \geq P^{th}$ or $u_{m,g,t}^{ML} = 0$ if $P(u_{m,g,t}^{ML}) < P^{th}$. Since this would lead to inaccuracies along the decision boundary which in-turn lead to infeasible solutions, the outputs are further checked for feasibility using the FL, discussed in Section 5.9.3. The following steps are used to complete the post-process technique for each training sample m:

- *Step 1*: Identify always ON/OFF generators using $u_{m,g,t}^{ML}$. If a generator g is always ON ($P(u_{m,g,t}^{ML}) \geq 0.95$) in each $t \in T$ then $fix\ u_{g,t}^{m} = 1$ for all periods for the corresponding generator. Similarly, if the generator g is always OFF ($P(u_{m,g,t}^{ML}) \leq 0.05$) in $t \in T$ then $fix\ u_{g,t}^{m} = 0$ for all periods for the corresponding generator.

- *Step 2*: for remaining generators after Step 1, run FL. If $P(u_{m,g,t}^{ML}) \geq 0.90$ or $P(u_{m,g,t}^{ML}) \leq 0.10$ and $u_{m,g,t}^{ML} = u_{m,g,t}^{MF}$ then generator g in time-period t has a fixed state, $fix\ u_{g,t}^{m} = u_{m,g,t}^{MF}$.

- *Step 3*: If generator g in time-period t is identified as a flexible generator, i.e. $0.1 < (u_{m,g,t}^{ML}) < 0.9$ or if $u_{m,g,t}^{ML} \neq u_{m,g,t}^{MF}$ then warm-start $u_{g,t}^{m}$ with $u_{m,g,t}^{MF}$.

For each sample $m \in M^{test}$, the above steps are implemented and the respective R-SCUC is solved to verify the quality of the ML solution. The overall flow of the process is represented in Algorithm 5.2.
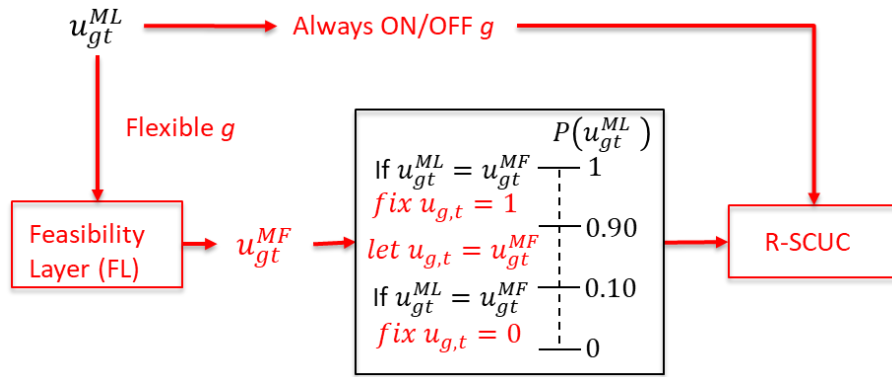
Fig. 5.11. Post-process technique with FL.

Algorithm 5.2 ML assisted R-SCUC-FL process

17: **Repeat**
18:      randomize nodal demand
19:      Solve SCUC
20:      Store $d_{n,t}^m, u_{g,t}^m$, objective and time
21: **until** $m \in M$
22: **Shuffle** M samples
23: **Split** M as 80% for M^{train} and 20% for M^{test}
24: **Train** ML using M^{train} for different hyper-parameters
25: Calculate train and test accuracy
26: **Tuning**: identify hyper-parameters with best accuracy
27: Save ML predicted output probabilities
28: **Repeat**
29:      Perform *step 1–step 3* and verify R-SCUC using $u_{g,t}^m$
30:      record objective and time
31: **until** $m \in M^{test}$

5.9.5. Results and Analysis

The mathematical model is formulated in AMPL. The data creation and verification steps are implemented using AMPL and solved using Gurobi solver. For ML step is implemented in Python 3.6. A computer with Intel® Xeon(R) W-2295 CPU

143

@ 3.00GHz, 256 GB of RAM and NVIDIA Quadro RTX 8000, 48GB GPU was utilized. In this Section, the dataset was re-created with realistic minimum-up and minimum-down time for each type of generator have been considered.

5.9.5.1. Comparison for Scikit-Learn Packages

There are several classification techniques currently available. By utilizing scikit-learn package, we were able to compare some common classification techniques, namely, KNN, RF, LR, and a fully connected three-layer neural network NN on the IEEE 24-Bus system data. The models were trained using M^{train} and tested on M^{test}. The accuracy is calculated using (5.5).

Table 5.4. Classification Model Comparison

Classification model	Training accuracy	Testing accuracy	Infeasible samples
LR	97.95%	97.55%	43.14%
NN	97.48%	97.46%	44.48%
KNN	97.48%	97.42%	41.14%
RF	97.31%	97.28%	47.16%

From Table 5.4, it can be noticed that all the classification methods fare well for commitment outputs. LR provides the highest accuracy followed by NN, KNN, and RF, respectively. To verify which model results in identifying more accurate

sequences, we implement SCED. From Algorithm 5.2 in section 5.9.4, SCED can be implemented by replacing *step1–step3* as $fix \, u_{g,t}^m = u_{m,g,t}^{ML} \, \forall \, m \, \in \, M^{test}, g \, \in G, t \in$ T. By performing SCED using ML solutions, we understand that ML models cannot accurately identify the sequences and may either result in sub-optimal solutions or infeasible solutions. Therefore, ML cannot completely replace the SCUC. However, we realized that the accuracy alone is not the best metric since KNN has lower accuracy than LR and NN but results in fewest infeasible samples in comparison. RF has the lowest accuracy, and this is also seen in the number of infeasible cases.

Table 5.5. Confusion Matrix Comparison

Classification Model	True +	True −	False +	False −
LR	50.47%	47.01%	1.25%	1.20%
NN	50.29%	47.16%	1.17%	1.38%
KNN	50.77%	46.65%	1.67%	0.91%
RF	50.23%	47.04%	1.28%	1.44%

On studying the results further, Table 5.5 summarizes the confusion matrix respective to the result in Table 5.4. A confusion matrix provides an idea on the number of true predictions and false predictions in M^{test}. For any sample $m \, \in \, M^{test}$, if the predictions are accurate and entire sequence is identified implies the optimal solution is predicted. But if the number of false negatives increases, this implies that generator

g in period *t* is identified as OFF instead of ON. This directly affects the number of feasible samples as the flexibility in the system in the system is lost and constraints are violated, especially (2.6)–(2.10). As the number of false positives increases, this implies that the respective generator *g* in period *t* was identified as ON but, it should be OFF. This affects the solution quality as sub-optimal generators or generators with insufficient capacity may be turned ON.

However, it can also be noted that ML does provide a high number of accurate predictions in each sample. Therefore, identifying a post-procedure may be beneficial to selectively utilize ML solutions that are known in high confidence. To leverage this, probability is a great metric. However, KNN and random forest models are inherently classification only model. This implies that the outcomes belong in one of several classes as generator schedules are grouped together in unique schedule buckets. Hence, these models cannot provide a probability for individual generators being ON/OFF. Models such as LR are inherently probabilistic in nature as the outputs are probability before the decision boundary is utilized to classify the outputs. Similarly, NN can also prove probabilistic outputs when a sigmoid layer is utilized. This implies that LR and NN are more flexible in nature to partially utilize the ML solution for variable reduction. This means that the probability can be construed as a true trained outcome of the ML model. Among the two models, LR results in lower false negative predictions which leads to higher accuracy and fewer infeasible cases and hence chosen as the classification model for further analysis.

5.9.5.2. Comparison between LR and MTLR

Even though ML training is an offline step, while training larger models LR required a high amount of training time. LR is traditionally developed as one vs rest algorithm which implies that the existing packages for LR only performs for each target (generator g in time period t) separately [129]–[130]. This is computationally expensive since this requires training multiple sets of weights for each generator g in each time period t in the test systems. Hence, we proposed the MTLR described in section 5.9.2. In comparison, the proposed MTLR provides outputs for all targets (generators) using single set of weights.

For validation of the proposed MTLR, we compared accuracy using LR from Scikit-learn package [127]. From Table 5.6, as the model size increases, the training time significantly increases as noted in the polish system which requires 6,178 seconds (~1.7 hours) to train. But in MTLR we notice that a minor trade-off in accuracy results in 2.4x speedup over LR on average across all test systems. This results in a significant computational speed-up during offline training in larger test systems. Not only that, LR method from scikit-learn only works if the training set contains both ON/OFF samples for each generator which implies that LR can only be applied for generators showing a flexible trend. In practicality, there can be few generators such as base plants and hydro plants that are ON irrespective of the load profile over the horizon and/or in all data samples. An assumption is required for such generators per the generic trend. In comparison, the proposed MTLR method can handle this certainty in schedules for

147

fixed generators since the true label is a vector of schedules of all generators in each sample and the entire schedule can be unique in nature. Hence, for these reasons, MTLR is used in subsequent results.

Table 5.6. Validation Of MTLR

# Bus	LR Test Accuracy	LR Train Time (s)	MTLR Test Accuracy	MTLR Train Time (s)
24	97.55%	16.19	97.44%	8.18
73	95.39%	374.2	95.96%	176.29
118	95.98%	344.85	95.52%	143.21
500	98.87%	743	98.80%	339.63
2383	98.18%	6,178.33	98.17%	2,445.28

5.9.5.3. MTLR Hyper-parameter Tuning

There are several classification techniques currently available. By utilizing scikit-learn package, we were Each test system is trained using the MTLR model separately by utilizing the respective generated data, M^{train}. During training, the samples are considered as a single full batch for $m \in M^{train}$. The best trained hyper-parameters with highest accuracy will be utilized for further tests. For each test system, the hyper-parameter learning rate (δ) is varied from 0.001–0.05. For each δ, systems

were trained until the cost saturates and then the accuracy was then calculated using (5.5).

During training, the cost vs iterations or epoch is registered to plot learning rate (δ) graph. The δ graph represents the loss/cost with respect to the iteration which provides information about the training when different hyper-parameter is utilized. Here, Fig. 5.12, represents the learning curve for IEEE 24-Bus system when trained for 1000 iterations to show the saturation of the cost. For $\delta \geq 0.03$, the training cost never saturates which implies that the step is too large. For $\delta \leq 0.001$, it is slower to converge in training which implies the step is too small. Between $0.003 \leq \delta \leq 0.01$, the $\delta = 0.01$ is chosen for the IEEE 24-Bus system which provides the highest training accuracy and a strictly decreasing curve for learning rate. In comparison, the scikit-learn models are trained using standard parameters provided by the package which includes an adaptive learning rate and early stopping functionality.
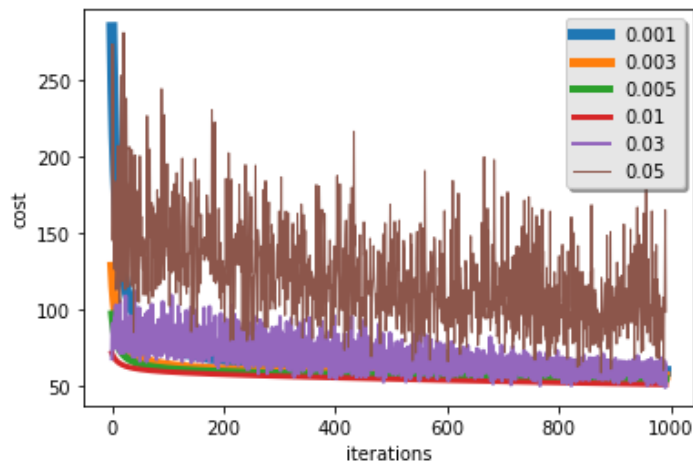
Fig. 5.12. Learning rate (δ) curves for IEEE 24-Bus system ($0.001 \leq \delta \leq 0.05$).

5.9.5.4. Training Summary (Offline)

Each system is trained using both MTLR and NN model using the respective system data, M^{train}, as described in section 5.3. For all test systems, 1500 samples were created, shuffled and split 80% for training and 20% for testing. The training is an offline step performed once for each system.

During training, the samples are considered as a single full batch. For MTLR, the hyper-parameter learning rate (δ) is identified and trained as per section 5.9.5.3. The training and testing accuracy was then calculated using (5.5). Table 5.7 summarizes δ, accuracy and training time for each test system. The MTLR and NN model provides high training and testing accuracy >95% for all the test systems considered in this work. Once the model is trained then the predictions, $u_{m,g,t}^{ML}$ and $P\left(u_{m,g,t}^{ML}\right)$ for each test samples $m \in M^{test}$ are obtained and stored for all test systems.

Table 5.7. MTLR Model Training Summary

# Bus	MTLR Accuracy		NN Accuracy	
	Train	Test	Train	Test
24	97.50%	97.44%	97.48%	97.46%
73	95.97%	95.96%	95.37%	95.30%
118	97.57%	95.52%	97.83%	97.62%
500	98.81%	98.80%	99.06%	99.04%
2383	98.34%	98.17%	98.11%	97.98%

5.9.5.5. Verification Results (Online) & Feasibility Layer Benefits

In order to successfully assist SCUC, we developed the FL and the post-processing technique mentioned in section 5.9.3 and section 5.9.4, respectively. The MTLR and NN based test predictions/outputs, $u_{m,g,t}^{ML}$ and $P(u_{m,g,t}^{ML})$ is verified for feasibility with FL to obtain $u_{m,g,t}^{MF}$ and then post-processed. To address model-reduction, benefits verification is performed for all test samples. The verification is an optimization step based on the ML outputs and therefore is an online step. Since the FL is also an optimization step, the solve time is inclusive of both post-processing and the MILP solve time. The R-SCUC-FL is implemented as per algorithm 5.2 in section 5.9.4. In order to compare the benefits of FL, the R-SCUC (i.e., without FL), is also performed. R-SCUC is implemented by replacing *step 2* and *step 3* in Algorithm 5.2 by:

- *Step II*: for remaining generators after Step 1, $fix\ u_{g,t}^m = 1$ if $P(u_{m,g,t}^{ML}) \geq$ 90%, $fix\ u_{g,t}^m = 0$ if $P(u_{m,g,t}^{ML}) \leq 10\%$ and warm-start $u_{g,t}^m = u_{m,g,t}^{ML}$ if $10\% < P(u_{m,g,t}^{ML}) < 90\%$.

Table 5.8 represents the infeasible problems corrected with R-SCUC-FL by using MTLR and NN based ML outputs respectively. The infeasible problems arise in R-SCUC. Based on our study, we noted that R-SCUC resulted in infeasible problems in many samples since ML mainly cannot distinguish minimum up/down time physical constraint requirement for generators (2.8)–(2.9). It only requires incorrectly

151

identifying one generator g in time period t to result in an infeasible solution for R-SCUC. For example, in IEEE 24-bus system, there are 33 generators and 24 time periods, which implies a total of 792 predictions per sample m to identify commitment schedule. However, we notice that the FL eliminates all infeasible samples in all test systems. Here, NN R-SCUC is more susceptible to infeasible samples in R-SCUC in comparison to MTLR R-SCUC. But, irrespective of the ML model, the FL ensures that the ML outputs adhere to MILP requirements particularly the generator minimum on/off time limit constraints.

Table 5.8. FL Infeasible Problems Elimination

System	IEEE 24-Bus	IEEE 73-Bus	IEEE 118-Bus	SC 500-Bus	Polish 2383-Bus
NN	28	18	4	32	6
MTLR	4	6	0	8	4

Fig. 5.13 represents the solution quality whereas Fig. 5.14 represents the solve time averaged over all test samples for each test system utilizing the MTLR and NN based R-SCUC with and without FL. The objective cost and solve time for reduced models are represented as base-normalized (BN) values averaged over all test samples. The base model is normal SCUC that does not use any ML outputs. From Fig. 5.13, it can also be noted that the solution quality is maintained to a high degree for R-SCUC-

FL without infeasibilities. In the case of IEEE 24-bus system, both MTLR R-SCUC and MTLR R-SCUC-FL result in better cost compared to SCUC. Similarly, the IEEE 73-bus system, NN R-SCUC and NN R-SCUC-FL result in lower cost. This is because model reduction on top of time-saving can also tighten the MIPGAP to a high degree resulting in a better MIPGAP solution in some test systems when compared to SCUC. However, on average across all test systems, the solution quality is maintained to high degree of <0.1 % deviation for MTLR R-SCUC-FL and NN R-SCUC-FL.
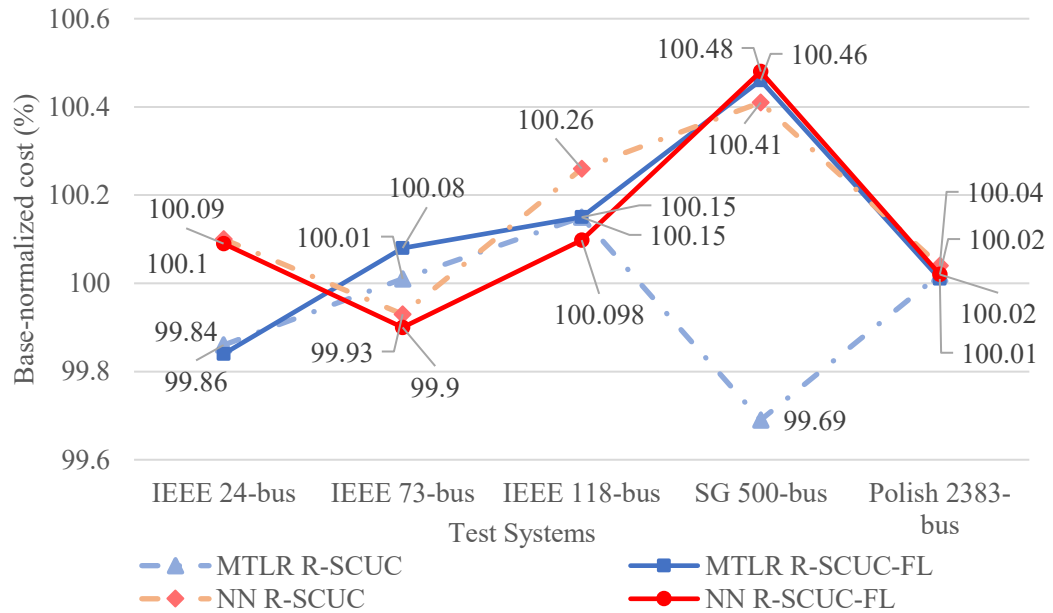
Fig. 5.13. R-SCUC and R-SCUC-FL solution quality.

From Fig. 5.14, the BN solve time shows that R-SCUC-FL requires a minor additional time for ML prediction post-processing as two MILP models are solved when compared with R-SCUC to ensure solution quality and eliminating infeasibility.

MTLR R-SCUC-FL results in a speed-up factor of 1.7x, 3.3x, 2.1x, 2.3x and 8.5x, whereas NN R-SCUC-FL results in a speed-up factor of 1.6x, 3.7x, 1.9x, 2.8x and 6.9x for the IEEE 24-bus, IEEE 73-bus, IEEE 118-bus, SG 500-bus and Polish systems, respectively on average over all testing samples, $m \in M^{test}$, when compared with SCUC. When averaged across all test systems, MTLR R-SCUC-FL results in speed-up factor of 3.6x whereas NN R-SCUC-FL results in a speed-up factor of 3.4x while also ensuring feasibility of all test samples.
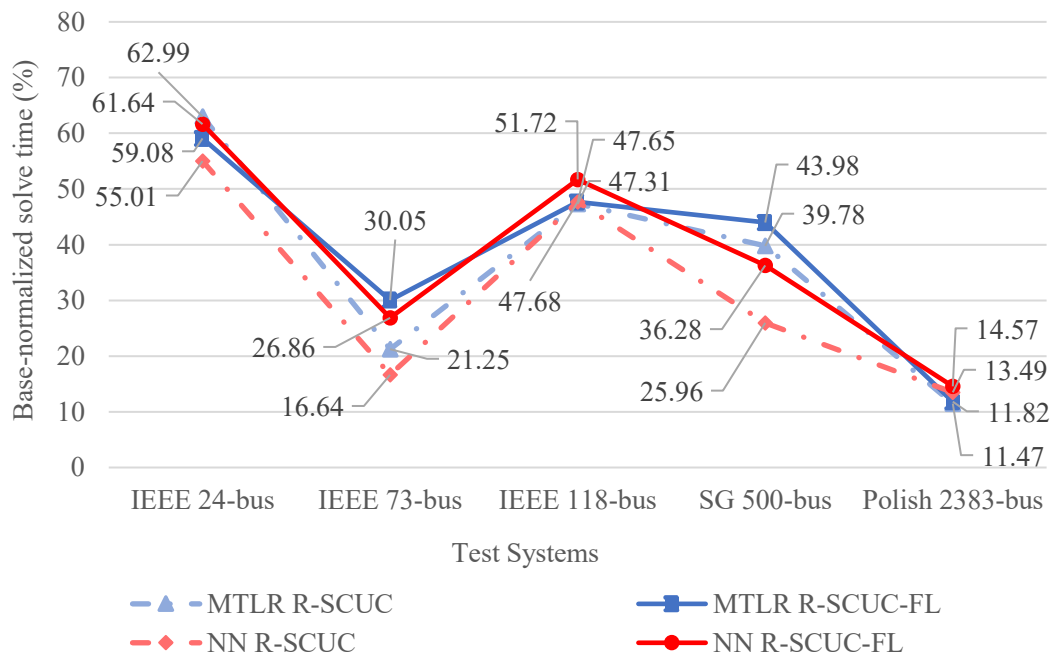
Fig. 5.14. R-SCUC and R-SCUC-FL solve time comparison.

5.9.5.6. Out of Sample Testing

To understand the robustness of the proposed FL, an out-of-sample testing was further performed. The out-of-distribution-sample set consists of 100 samples that were not included in the training or testing samples of the verification process. Here, care was taken to introduce higher variability with $\alpha^m = \pm 25\%$ and $\beta_{n,t}^m = \pm 10\%$ in (5.4) in order to avoid mimicking the original dataset and increase number of infeasible samples.

Table 5.9. Infeasible Problems in Out-of-Distribution-Sample Data

Test System	MTLR R-SCUC	MTLR R-SCUC-FL	NN R-SCUC	NN R-SCUC-FL
IEEE 24-Bus	40	14 (65% ↓)	59	28 (53% ↓)
IEEE 73-Bus	95	54 (41% ↓)	100	74 (26% ↓)
IEEE 118-Bus	63	27 (57% ↓)	78	18 (77% ↓)
SC 500-Bus	82	36 (56% ↓)	100	67 (33% ↓)
Polish 2383-Bus	37	9 (75% ↓)	45	16 (64% ↓)

These samples were never utilized in the offline training phase or online verification phase. Therefore, the trained model might not fare as well in the out-of-sample dataset (with much larger variations) when compared to the original dataset. Despite this, from Table 5.9, we notice a significant reduction in infeasible problems

when the FL was introduced in R-SCUC in all test systems. This resulted in reductions of infeasible samples by 58.8% and 50.6% when averaged across all test systems for MTLR and NN models, respectively.

5.9.5.7. Case Study: Multi-Scenario Renewable Source

As stated in the prior section, the proposed MTLR methods are agnostic to the MILP model. Hence, it can be utilized for both stochastic-SCUC (SSCUC) and deterministic SCUC cases. In a deterministic scenario, renewable profile can be captured through net-load profile. However, renewable energy is unpredictable in nature, the scenarios of wind and solar outputs are often considered. But it can be noted that in SSCUC, a single commitment schedule that satisfies all the scenarios are obtained as outputs. In terms of ML, this only increases the number of inputs, but the targets/outputs remain the same. Therefore, the MTLR and NN models are modified to increase S scenarios of net nodal load as input.

Table 5.10. Modified IEEE 24-bus renewable system results

Metrics	MTLR R-SSCUC FL	NN R-SSCUC FL
Training Accuracy	96.57%	97.01%
Testing Accuracy	94.53%	96.25%
Infeasible samples	0	0
BN cost	100.07%	100.01%
BN Time	43.57%	36.78%

The proposed MTLR R-SCUC FL and NN R-SCUC FL were tested on the modified IEEE 24-Bus renewable test case with two renewable units. Table 5.10 shows the online verification results. It can be noted that the proposed MTLR and NN models can successfully handle stochastic inputs with solution accuracy of 94.53% and 96.25% for test samples. This is marginally lower than the deterministic case. However, utilizing the MTLR and NN solutions, we notice that the Reduced-SSCUC-FL (R-SSCUC) results in higher time savings of 56.43% and 63.22% with respect to SSCUC. In comparison, the deterministic MTLR and NN based R-SCUC-FL only results in a time saving of 40.92% and 38.36% with respect to SCUC. This is because reducing the equivalent number of variables benefits R-SSCUC more since this directly relaxes a higher number of constraints when compared with R-SCUC.

5.9.5.8. Section Remarks

In this section we studied the differences between different classification techniques as an offline step namely, KNN, RF, LR and NN for predicting commitment schedules given the load profile. It was concluded that ML cannot directly replace optimization through SCUC. However, by choosing a confidence level through probabilistic outputs, selective binary variables were reduced in SCUC. LR and NN were more flexible due to the ability to result in probability estimates of commitment status of generators. Not only that, by studying the confusion matrix for ML predictions, both LR and NN led to higher accuracy and resulted in better predictions

157

when compared to KNN and RF. Furthermore, LR was also addressed for computation efficiency through a novel MTLR model. On average, the MTLR model was 2.4x faster than LR during offline training.

The trained models were then introduced for online verification on test samples through post-processing ML solutions with FL. A confidence based variable selection and FL in combination produced desired effects of eliminating infeasible outputs while also maintaining high degree of solution-quality. On average across all test systems, model reductions with the proposed MTLR R-SCUC FL and NN R-SCUC-FL resulted in a speed-up 3.6x and 3.4x, respectively, when compared with SCUC.

On top of this, it was established that the proposed approach is agnostic of MILP models. Therefore, the ML model was also tested on a modified IEEE 24-bus system with three renewable scenarios. The ML outputs were then similarly used for variable reduction in SSCUC. Online verification of MTLR and NN based R-SSCUC-FL resulted in a speed-up of 2.3x and 2.7x, respectively, when compared to SSCUC. In comparison, the deterministic R-SCUC-FL resulted in a speed-up of 1.7x and 1.6x, respectively, when compared to SCUC for the IEEE 24-bus system. It is also worth noting that the proposed model reduction approaches are compatible with any existing optimization/decomposition methods as well as ML methods aiming to remove some unnecessary constraints.

5.10. Advanced ML Models

Most ML techniques work on simple data or flat data therefore only inputs and outputs were studied. However, power system is a connected system with a network topology and a higher resolution can be realized with graphs in GNN. Apart from this, GNN can be utilized to provide additional decision-making tools by studying the network along with nodal information of generation and loads. GNN can enhance reliability of the network and increase SCUC computation by suggesting system re-connection or implement topology reconfiguration as a prediction which can be utilized as a candidate-list input in the stochastic optimization models. The future work for this research considers the use of advanced ML algorithms to understand the data patterns not only between demand profile and commitment schedule but also demand profiles and line loading.

5.10.1. Spatio-Temporal Classification Model

A spatio-temporal (ST) approach is considered for advanced classification models. Since the demand and generators in the system is geographically distributed a special correlation of the data is required to be studied. This is considered using graph neural networks (GNN) where the inputs are represented in the form of graphs which mimic the network structure of power system. Not only that, the temporal correlation of the data can also be studied since SCUC is an optimization for day-ahead 24-hour system operations. Therefore, relationships between various hours of the day are key

since actions in earlier hours are utilized to determine actions performed in the rest of the periods. This is implemented using long short-term memory (LSTM) models in ML.

The GNN layers and LSTM layers together form an advanced ML architecture for ST approach as represented in Fig. 5.15 and Fig. 5.16. In Fig. 5.15, a node-classification ST model is trained to fit inputs of load profile and respective commitment labels where the input is fed through multiple GNN layers with activation and the resulting node embedding is then passed as inputs for the LSTM layer. Multiple GNN layers are utilized since each layer tries to identify the nodal relationship of neighboring nodes and additional layers gather information of nodes multiple hops from each node.
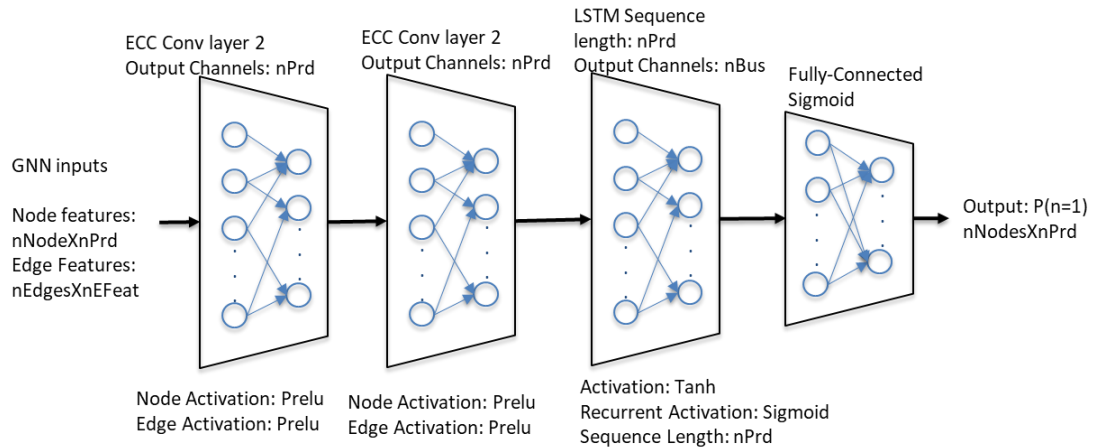
Fig. 5.15. Spatio-temporal ML architecture for node classification.

In Fig. 5.16, edge-classification ST model is trained to fit inputs of nodal load profile and critical lines in the system. Once the models are trained the ML predictions

are utilized not only to reduce binary variables but also reduce redundant constrained to bring about additional time-savings by further reducing the SCUC. In practicality, load profiles are also seasonal, and the consideration of such seasonal profiles seasonal patterns to improve the accuracy of the proposed models.
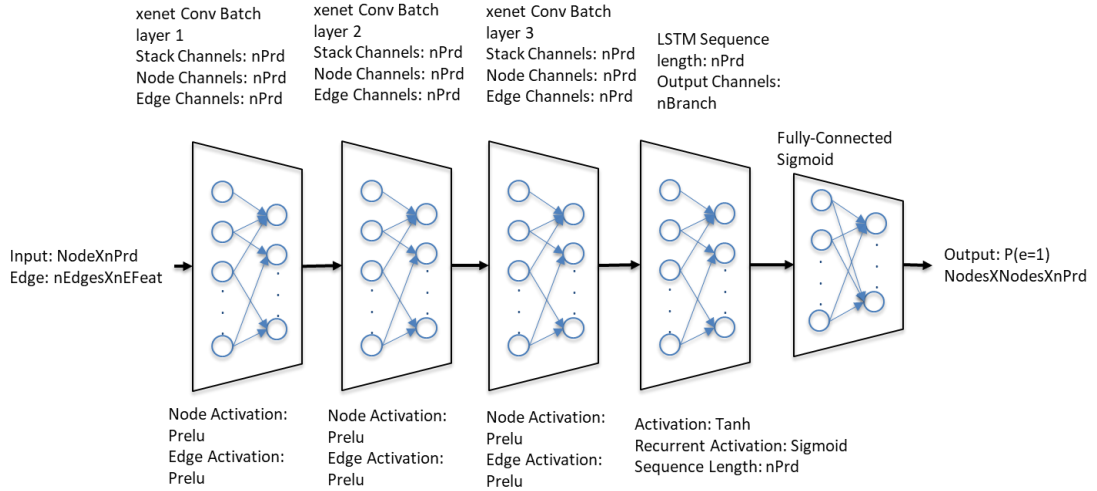
Fig. 5.16. Spatio-temporal ML architecture for edge classification.

5.10.2. Preliminary Node-Classification Results

The mathematical model is formulated in AMPL. The data creation and verification steps are implemented using AMPL and solved using Gurobi solver. For ML step is implemented in Python 3.6. A computer with Intel® Xeon(R) W-2295 CPU @ 3.00GHz, 256 GB of RAM and NVIDIA Quadro RTX 8000, 48GB GPU was utilized. The data collected in section 5.9.5 involved steps for all power system components, [131]. Therefore, this existing SCUC data is also used for studies on advanced ST ML model.

Table 5.11 shows that a proposed ST model outperforms proposed ML models in section 5.8 and section 5.9. The same SCUC model and data from section 5.9 are used for preliminary results to classify generator commitment status. The ST model results in 0.75 – 1.6% increase in testing accuracy when compared to benchmark model which uses deep-neural network (DNN) which is an extension of ML model discussed in section 5.9. Fig. 5.17 and Fig. 5.18 shows the histogram of predictions errors in the test samples for ST and DNN models for the IEEE 73-bus system where ST model results in fewer prediction errors in comparison to DNN model.

Table 5.11. Advanced ML Model Training Summary

System	DNN Accuracy (%)		ST Accuracy (%)	
	train	test	train	test
IEEE 24-Bus	97.16	97.01	98.31 (↑ 1.15)	98.40 (↑ 1.39)
IEEE 73-Bus	95.82	95.65	97.04 (↑ 1.22%)	97.24 (↑ 1.59)
IEEE 118	97.83	97.62	98.96 (↑ 1.13)	98.99 (↑ 1.37)
SC 500	99.06	99.04	99.80 (↑ 0.74)	99.79 (↑ 0.75)
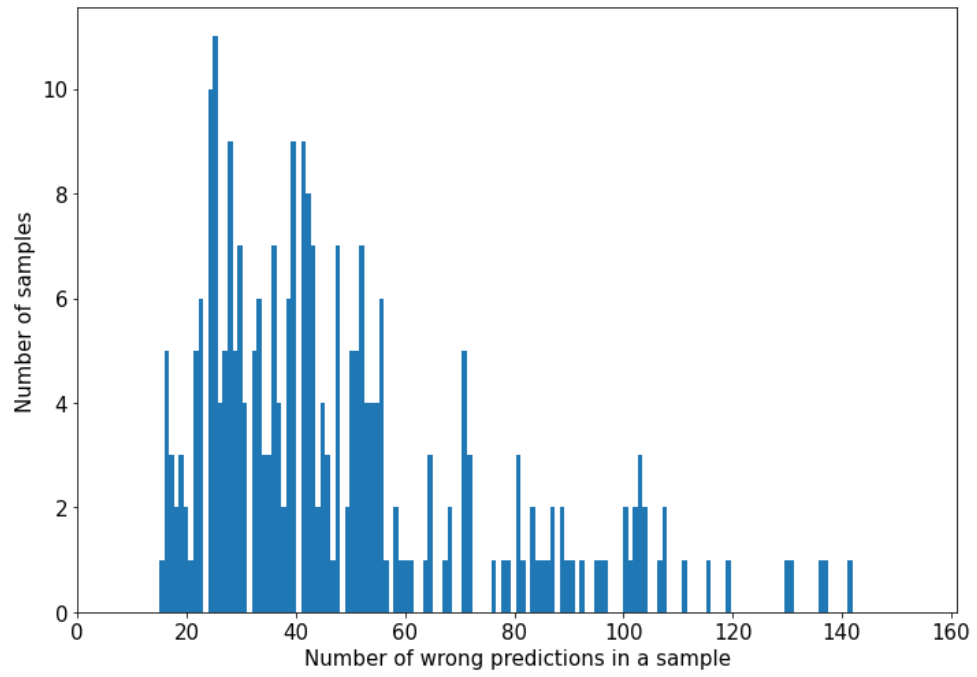
Fig. 5.17. Histogram of predictions (Spatio-Temoporal).
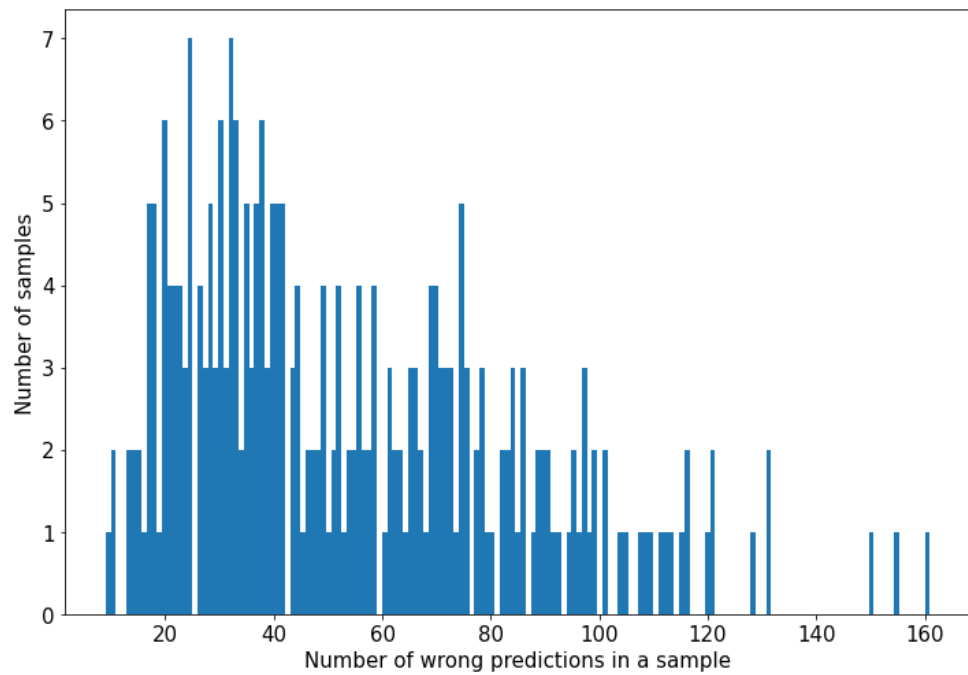
Fig. 5.18. Histogram of predictions (Deep-NN).

Table 5.12 shows the verification results for R-SCUC utilizing advanced ML algorithms. It can be noted that algorithm 5.2 in section 5.9.4 is utilized without FL for the preliminary results. ST model eliminates infeasible problems without the requirement of FL whereas benchmark model still has infeasible problem. On average ST R-SCUC resulted in time savings of 48.05% on average across all test system with superior solution quality whereas DNN R-SCUC results in sub-par solution quality with the absence of FL and only results in time-savings of 39.30%.

Table 5.12. R-SCUC Verification (Generator/Node Classification)

System	Model	Infeasible cases	Avg BN Cost (%)	Avg BN Time saved (%)
IEEE 24-Bus	DNN	0	0	3.92
	ST	0	0.024	34.29
IEEE 73-Bus	DNN	7	0.12	50.83
	ST	0	0.034	44.23
IEEE 118-Bus	DNN	4	0.28	38.72
	ST	0	0.001	36.29
SC 500-Bus	DNN	13	0.13	63.72
	ST	0	0.062	77.40

5.11. Summary

In this chapter various ML models with post-processing techniques were proposed to decrease the computational burden of the SCUC. Initially, the proof-of-concept was implemented on a simplified SCUC model using LR algorithm assisted with post-processing techniques, *P1–P2*. *P1–P2* results in problem size reduction which brings significant time-savings across multiple test systems. B2 provides 95% computational time savings for the large Polish system but is affected by solution quality and/or infeasible problems.

Following this, the work was extended to a SCUC model considering minimum up/down time requirements for generators. Along with this, several ML algorithms, namely LR, NN, RF, MTLR were examined. MTLR and NN were later chosen to be superior in predictions and training time. FL was developed to address infeasibility in ML predictions thereby ensuring that R-SCUC models are always feasible. The proposed MTLR R-SCUC FL and NN R-SCUC-FL outperformed basic classification models by ensuing high solution quality while also resulting significant time reductions. An out-of-sample testing was also performed to showcase the effectiveness of FL.

Finally, a ST model was proposed as an advanced ML model to perform node-classification. The preliminary results with ST model show that ST model can outperform MTLR and NN models in predictions from the model accuracy and

verification results. Additionally, ST model predictions are made by learning the spatial

and temporal correlation of input data, it does not require a FL.

6. CONCLUSIONS AND FUTURE WORK

The work presented in this report addresses three key features, namely, (i) addressing system flexibility with existing components through smart algorithms, (ii) facilitate RES integration and efficient use of ESS, and (iii) scalability of such technologies by enhancing computational ability by reduction of problem complexity without loss of solution quality for day-ahead operations using SCUC. The results presented in this thesis are based on deregulated markets systems. However, SCUC is utilized in both deregulated markets and regulated markets and therefore this work can be feasible in both business scenarios. The contributions of the proposed work in this thesis have extensible reach and several opportunities for industrial adoption. The contributions of each chapter are presented in the following section, and finally the proposed research work for future is detailed at the end of this chapter.

6.1. Contributions

In Chapter 2, technologies such as CNR and CDR are discussed along with mathematical models. Existing power system operations do not use available system flexibility in the form of transmission network or demand response efficiently. However, with the advent of smart grids and two-way communication smarter algorithms can leverage additional savings in the system in day-ahead operations. Therefore, the use of NR and DR were first seen in Chapter 2 along with its constraint

modelling. It can be noted that they are modelled through explicit mathematical models and hence are stable algorithms.

Currently, system operators implement demand response by dispatching controllable loads for economic reasons in day-ahead scheduling and use a static network in day-ahead solutions. Particularly, demand shifting from peak hours when the cost of electricity is higher to non-peak hours to maintain system reliability by flattening the load profile. The power system transmission networks are built with redundancy, but existing ISO practices also implement a static network to meet the supply and demand of electric power. One common reason for disregarding NR or DR in day-ahead operations is that it can cause large disturbance in the network. Therefore, the use of such technologies in response to power system contingencies as a corrective action were proposed since the system flexibility and economic benefits of such action in post-contingency scenarios are not explicitly considered in short-term operations.

The proposed SCUC-CNR and SCUC-CDR mathematical model implementing a dynamic network and/or demand response in the post-contingency scenario as a corrective action provides significant system flexibility in the base-case. It can be noted that corrective solutions are implemented only if a contingency occurs. The presence of these actions also increases the reliability of the SCUC solution in the event of a contingency. Hence, this chapter highlights the benefits of demand response and network reconfiguration solutions as a corrective action for potential post-contingency emergencies in day-ahead scheduling. The proposed models were tested on the IEEE

24-bus system where results demonstrate significant total cost savings in daily operations. Moreover, the results point to better long-term reliability of generators along with the ability to use existing system flexibility, serve higher critical demands in base-case and offers a congestion relief tool along with elimination of congestions cost due to overloaded lines in both the base-case and post-contingency scenarios.

Renewable energy sources (RES) have gained a lot of interest recently. Particularly, the increase in free RES is favorable to reduce carbon emission to reduce the dependence of fossil fuels and to decrease system cost. However, this comes with significant issues resulting from the high penetration of RES and the loss of reliability to the system since RES is unpredictable in nature. To add, the limited transmission capacity serving RES often leads to network congestion since they are located in remote favorable locations. As a result, when poorly scheduled, the intermittent nature of RES may result in high curtailments of the free resource. As a result, it can lead to significant curtailments of the free resource when the network is congested. Therefore, energy storage system (ESS) is considered as a viable solution to store energy and address the intermittent nature of RES though ESS is often distributed and may not be geographically close to RES. Therefore, ESS may also suffer from the limited transmission capacity due to network congestion. Currently, grid operators overlook network flexibility as a congestion management tool in day-ahead scheduling. Considering system flexibility can be an effective solution to address these issues and also facilitate further integration of RES. Therefore, Chapter 3 develops on the idea of

network reconfiguration strategies to use system flexibility and explores the possibility of utilizing network reconfiguration as a corrective action to reduce the transmission congestion and thereby the reduction of RES curtailments in day-ahead scheduling. To facilitate the RES integration in the grid, a multi-scenario stochastic N-1 security-constrained unit-commitment with corrective network reconfiguration (SSCUC-CNR) is modelled. SSCUC-CNR model is studied on a modified IEEE 24-bus system with RES. The simulation results demonstrate that CNR not only leads to a lower cost solution by reducing network congestion but also facilitates RES integration by reducing congestion-induced curtailments in high penetration cases. Emission studies demonstrate that more green generators are committed resulting in reduced carbon emissions when CNR is implemented. Not only that, in Chapter 3 the concept of NR as both preventive and corrective solution provides further validation for efficient use of ESS by providing longevity of batteries.

In most cases, the usage of such tools is deemed complex and hence not readily used in current industry practice. To address these two remedy solutions were proposed, a purely optimization technique through an accelerated-decomposition approach and a machine learning aided technique to reduce problem complexity was studied in Chapter 4 and Chapter 5, respectively.

Firstly, as a purely optimization-based technique, a novel approach of A-SCUC-CNR to handle the computational complexity with fast screening non-critical sub problems was developed using Benders' Decomposition. The proposed approach

provides substantial computational benefits and is also applicable to SCUC. Simulation results on the IEEE 24-bus system show that the proposed methods are substantially faster without the loss in solution quality while the scalability benefits are demonstrated using larger cases: the IEEE 73-bus system, IEEE 118-bus system and Polish system.

Secondly, a reduced-SCUC model is implemented with a novel approach utilizing ML to predict commitment schedules using nodal demand patterns. Additionally, this approach can easily be utilized by any decomposed, heuristic or sped-up algorithms for SCUC. The proposed approaches were validated on several standard test systems namely, IEEE 24-bus system, IEEE 73-bus system, IEEE 118-bus system, synthetic South Carolina 500-bus system and Polish 2383-bus system. Simulation results demonstrate that the proposed post-processing technique ensure selective utilization of ML prediction can reduce the number of variables and constraints in SCUC, which substantially reduces the computing time while maintaining solution quality.

6.2.   Future Work

In chapter 4, scalability of SCUC algorithms were proposed using an accelerated Bender's decomposition algorithm while also addressing system reliability with economic actions by introducing technologies such as CNR. In chapter 5, ML algorithms were leveraged for model-reduction base-case constraints of SCUC thereby increasing the overall computational efficiency. Along with this preliminary case

studies for the proposed model considering multi-scenario SSCUC models were also shown. The future work can be considered in bridging the technologies together encompassing both system reliability constraints, system flexibility, decomposition-algorithms and ML based model-reduction.

Additionally, in Chapter 5, only variable reduction of SCUC were implemented by predicting generator status using ML. This can also be extended to predict constraint reductions by predicting critical lines to monitor in the network by utilizing the advanced ST model. Since ST models leverage layers such as GNN, to topography of the network can be further studied to make predictions and only critical lines require to be modelled. Furthermore, data related weather patterns and scenarios can be studied to predict system reserve limits to address RES outputs for SSCUC.

6.3.   List of Publications

(1) Arun Venkatesh Ramesh and Xingpeng Li, "Security Constrained Unit Commitment with Corrective Transmission Switching," *North American Power Symposium (NAPS)*, Wichita, KS, USA, Oct. 2019.

(2) Arun Venkatesh Ramesh and Xingpeng Li, "Enhancing System Flexibility through Corrective Demand Response in Security-Constrained Unit Commitment," *North American Power Symposium (NAPS)*, Tempe, AZ, USA, Apr. 2021.

(3) Mingjian Tuo, Arun Venkatesh Ramesh, Xingpeng Li, "Benefits and Cyber-Vulnerability of Demand Response System in Real-Time Grid Operations," *IEEE Smart Grid Comm,* Tempe, AZ, USA.

(4) Arun Venkatesh Ramesh and Xingpeng Li, "Reducing Congestion-Induced Renewable Curtailment with Corrective Network Reconfiguration in Day-Ahead Scheduling," *IEEE PES General Meeting 2020,* Montreal, QC, Canada, Jul. 2020.

(5) Arun Venkatesh Ramesh and Xingpeng Li, "Network Reconfiguration Impact on Renewable Energy System and Energy Storage System in Day-Ahead Scheduling," *IEEE PES General Meeting 2021*, Washington, DC, USA, Jul. 2021.

(6) Arun Venkatesh Ramesh, Xingpeng Li and Kory W. Hedman, "An Accelerated-Decomposition Approach for Security-Constrained Unit Commitment with Corrective Network Reconfiguration," *IEEE Transactions on Power Systems*, vol. 37, no. 2, pp. 887–900, Mar. 2022.

(7) Arun Venkatesh Ramesh and Xingpeng Li, "Machine Learning Assisted Model Reduction for Security-Constrained Unit Commitment," *North American Power Symposium (NAPS)*, Salt Lake, UT, Oct. 2022.

(8) Arun Venkatesh Ramesh and Xingpeng Li, "Feasibility Layer aided Machine Learning Approach for Day-Ahead Operations," Available: arXiv:2208.06742, Aug. 2022.

REFERENCES

[1] Makarov, Y. V., Etingov, P. V., Ma, J., Huang, Z., & Subbarao, K., "Incorporating Uncertainty of Wind Power Generation Forecast into Power System Operation, Dispatch, and Unit Commitment Procedures," *IEEE Transactions on Sustainable Energy*, 2(4), 433–442, 2011.

[2] NERC, Transmission System Adequacy and Security, 2005 [Online]. Available: http://www.nerc.com

[3] 2018 Annual Market Report, ISO-NE, [Online]. Available: https://www.iso-ne.com/static-assets/documents/2019/05/2018-annual-markets-report.pdf

[4] 2018 Annual Report on Market Issues and Performance, CAISO, [Online]. Available:http://www.caiso.com/Documents/2018AnnualReportonMarketIssuesandPerformance.pdf

[5] 2018 State of the Market Report for NY-ISO, [Online]. Available: https://www.nyiso.com/documents/20142/2223763/2018-State-of-the-Market-Report.pdf

[6] Energy Market, PJM State of the Market 2019, [Online]. Available: https://www.monitoringanalytics.com/reports/PJM_State_of_the_Market/2019/2019-som-pjm-sec3.pdf

[7] Day-Ahead Market Overview, CA-ISO, [Online]. Available: http://www.caiso.com/Documents/Presentation-Existing-Day-Ahead-Market-Overview.pdf

[8] Manual 11, Day-Ahead Scheduling Manual, NY-ISO, [Online]. Available: https://www.nyiso.com/documents/20142/2923301/dayahd_schd_mnl.pdf/0024bc71-4dd9-fa80-a816-f9f3e26ea53a

[9] Corporate Information, Midwest-ISO, [Online]. Available: https://www.misoenergy.org/about/media-center/corporate-fact-sheet/

[10] X. Ma, H. Song, M. Hong, J. Wan, Y. Chen and E. Zak, "The Security-Constrained Commitment and Dispatch for Midwest ISO Day-Ahead Co-Optimized Energy and Ancillary Service Market," *2009 IEEE Power & Energy Society General Meeting*, Calgary, AB, 2009, pp. 1–8.

[11] Day-Ahead Energy Markets, Introduction to Wholesale Electricity Markets, ISO-NE, [Online]. Available: https://iso-ne.com/static-assets/documents/2019/05/20190916-07-wem101-day-ahead-energy-market.pdf

[12] Module 6: Day-Ahead through Real-Time Operations, ERCOT, [Online]. Available:http://www.ercot.com/content/wcm/training_courses/109600/TRN101_M6_DAM_RT_2017.pdf

[13] Manual 11 update, Day-Ahead Market Timeline, PJM, [Online]. Available:https://www.pjm.com/-/media/committees-

groups/committees/mic/20181107/20181107-item-02a-day-ahead-market-timeline.ashx

[14]   SPP   Integrated   Market   Timeline,   SPP,   [Online].   Available: https://www.spp.org/documents/39257/new%20spp%20marketplace%20timeli nes%20quick%20reference%20card.pdf

[15]   Switching Solutions, PJM, Norristown, PA, USA. (2013). [Online]. Available: http://www.pjm.com/markets-and-operations/etools/oasis/systeminformation/switching-solutions.aspx

[16]   A. Ott, "*VP PJM Norristown PA private communication*, " July 2008.

[17]   ISO-NE   ISO   New   England   Operating   Procedure   no.   19:   Transmission Operations, pp. 7–8, Apr. 2007.

[18]   A. Ott, Personal Communication, "Occasional news: Superstorm Sandy", Oct. 2012.

[19]   K. W. Hedman, S. S. Oren and R. P. O'Neill, "A Review of Transmission Switching and Network Topology Optimization," *2011 IEEE Power and Energy Society General Meeting*, San Diego, CA, 2011, pp. 1–7.

[20]   E. B. Fisher, R. P. O'Neill and M. C. Ferris, "Optimal Transmission Switching," *IEEE Transactions on Power Systems*, vol. 23, no. 3, pp. 1346–1355, Aug. 2008.

[21]   Koglin, and Müller, "Corrective Switching: A New Dimension in Optimal Load Flow," *International Journal of Electrical Power and Energy Systems*, 4.2 (1982): 142–49.

[22] A.A. Mazi, B.F. Wollenberg, M.H. Hesse, "Corrective Control of Power System Flows by Line and Bus-Bar Switching," *IEEE Transactions on Power Systems*, 1986, 1, (3), pp. 258–264

[23] Wei Shao and V. Vittal, "Corrective Switching Algorithm for Relieving Overloads and Voltage Violations," *IEEE Transactions on Power Systems*, vol. 20, no. 4, pp. 1877–1885, Nov. 2005.

[24] Arun Venkatesh Ramesh, Xingpeng Li, "Security Constrained Unit Commitment with Corrective Transmission Switching," *North American Power Symposium*, Wichita, KS, USA, October 2019.

[25] J. C. Villumsen, G. Brønmo and A. B. Philpott, "Line Capacity Expansion and Transmission Switching in Power Systems with Large-Scale Wind Power," *IEEE Transactions on Power Systems*, vol. 28, no. 2, pp. 731–739, May 2013.

[26] T. Lan and G. M. Huang, "Transmission Line Switching in Power System Planning with Large Scale Renewable Energy," *2015 First Workshop on Smart Grid and Renewable Energy (SGRE)*, Doha, 2015, pp. 1–6.

[27] Nikoobakht, A., Mardaneh, M., Aghaei, J., Guerrero-Mestre, V., Contreras, J., & Nikoobakht, A., "Flexible Power System Operation Accommodating Uncertain Wind Power Generation using Transmission Topology Control: An Improved Linearized AC SCUC Model," *IET Generation, Transmission and Distribution*, *11*(1), 142–153, 2017.

[28] F. Qiu and J. Wang, "Chance-Constrained Transmission Switching with Guaranteed Wind Power Utilization," in *IEEE Transactions on Power Systems*, vol. 30, no. 3, pp. 1270–1278, May 2015.

[29] Xingpeng Li and Qianxue Xia, "Stochastic Optimal Power Flow with Network Reconfiguration: Congestion Management and Facilitating Grid Integration of Renewables," *IEEE PES T&D Conference & Exposition*, Chicago, IL, USA, Apr. 2020.

[30] J. Hetzer, D. C. Yu and K. Bhattarai, "An Economic Dispatch Model Incorporating Wind Power," *IEEE Transactions on Energy Conversion*, vol. 23, no. 2, pp. 603–611, June 2008.

[31] M. Vrakopoulou, K. Margellos, J. Lygeros and G. Andersson, "A Probabilistic Framework for Reserve Scheduling N-1 Security Assessment of Systems With High Wind Power Penetration," *IEEE Transactions on Power Systems*, vol. 28, no. 4, pp. 3885–3896, Nov. 2013.

[32] A. Nikoobakht, J. Aghaei and M. Mardaneh, "Optimal Transmission Switching in the Stochastic Linearised SCUC for Uncertainty Management of the Wind Power Generation and Equipment Failures," in *IET Generation, Transmission & Distribution*, vol. 12, no. 17, pp. 4060–4060, 30 9 2018.

[33] O. Ziaee and F. Choobineh, "Optimal Location-Allocation of TCSCs and Transmission Switch Placement Under High Penetration of Wind Power," *IEEE Transactions on Power Systems*, vol. 32, no. 4, pp. 3006–3014, July 2017.

[34]   J. Shi and S. S. Oren, "Stochastic Unit Commitment with Topology Control Recourse for Power Systems with Large-Scale Renewable Integration," *IEEE Transactions on Power Systems*, vol. 33, no. 3, pp. 3315–3324, May 2018.

[35]   Sang and M. Sahraei-Ardakani, "Stochastic Transmission Impedance Control for Enhanced Wind Energy Integration," *IEEE Transactions on Sustainable Energy*, vol. 9, no. 3, pp. 1108–1117, Jul. 2018.

[36]   X. Dui, G. Zhu and L. Yao, "Two-Stage Optimization of Battery Energy Storage Capacity to Decrease Wind Power Curtailment in Grid-Connected Wind Farms," *IEEE Transactions on Power Systems*, vol. 33, no. 3, pp. 3296–3305, May 2018.

[37]   C. Su and D. Kirschen, "Quantifying the Effect of Demand Response on Electricity Markets," *IEEE Transactions on Power Systems*, vol. 24, no. 3, pp. 1199–1207, Aug. 2009.

[38]   M. H. Albadi and E. F. El-Saadany, "A Summary of Demand Response in Electricity Markets," *Electric Power System Research*, vol. 78, no. 11, pp. 1989–1996, Nov. 2008.

[39]   L. R. Ferreira, L. C. Siebert, A. R. Aoki and T. S. P. Fernandes, "Load Shedding through Optimal Power Flow to Support Self-Healing Actions in Distribution Feeders," *IEEE PES Transmission & Distribution Conference and Exposition - Latin America (PES T&D-LA)*, Medellin, 2014, pp. 1–6.

[40]   H. Wu, M. Shahidehpour, and A. Al-Abdulwahab, "Hourly Demand Response in Day-Ahead Scheduling for Managing the Variability of Renewable Energy,"

IET Generations, Transmission and Distribution, vol. 7, no. 3, pp. 226–234, 2013.

[41] Reliability Primer, Federal Energy Regulatory Commission [Online]. Available:https://www.ferc.gov/legal/staff-reports/2016/reliability-primer.pdf

[42] A.L.A. Syrri, P. Mancarella, "Reliability and Risk Assessment of Postcontingency Demand Response," in *Smart Distribution Networks, Sustainable Energy Grids Networks*, 7 (2016) 1–12.

[43] Xingpeng Li, P. Balasubramanian, M. Sahraei-Ardakani, M. Abdi-Khorsand, K. W. Hedman and R. Podmore, "Real-Time Contingency Analysis with Corrective Transmission Switching," *IEEE Transactions on Power Systems*, vol. 32, no. 4, pp. 2604–2617, July 2017.

[44] K. E. Van Horn, A. D. Domínguez-García and P. W. Sauer, "Measurement-Based Real-Time Security-Constrained Economic Dispatch," *IEEE Transactions on Power Systems*, vol. 31, no. 5, pp. 3548–3560, Sep. 2016.

[45] Demand Response Strategies, PJM [Online]. Available: https://www.pjm.com/markets-and-operations/demand-response.aspx

[46] Load Resource Participation in the ERCOT Markets, ERCOT [Online]. Available: http://www.ercot.com/services/programs/load/laar

[47] Demand Response and Load Participation, CAISO [Online]. Available: http://www.caiso.com/participate/Pages/Load/Default.aspx

[48] Schedule 30 FERC Electric Tariff Emergency Demand Response Initiative Schedules 36.0.0, MISO [Online]. Available: https://cdn.misoenergy.org/Schedule%2030109703.pdf

[49] Demand Response, NYISO [Online]. Available: https://www.nyiso.com/demand-response

[50] ISO New England Transmission Equipment Outage Coordination 2018 [Online]. Available: https://www.iso-ne.com/static-assets/documents/2019/04/2018-iso-ne-transmission-equipment-outage-coordination.pdf

[51] Annual US Transmission Data Review, March 2018 [Online]. Available: https://www.energy.gov/sites/prod/files/2018/03/f49/2018%20Transmission%20Data%20Review%20FINAL.pdf

[52] R. Deng, Z. Yang, M. Chow and J. Chen, "A Survey on Demand Response in Smart Grids: Mathematical Models and Approaches," in *IEEE Transactions on Industrial Informatics*, vol. 11, no. 3, pp. 570-582, June 2015.

[53] J. S. Vardakas, N. Zorba and C. V. Verikoukis, "A Survey on Demand Response Programs in Smart Grids: Pricing Methods and Optimization Algorithms," in *IEEE Communications Surveys & Tutorials*, vol. 17, no. 1, pp. 152–178, Firstquarter 2015.

[54] Kun-Yuan Huang and Yann-Chang Huang, "Integrating Direct Load Control with Interruptible Load Management to Provide Instantaneous Reserves for

Ancillary Services," in *IEEE Transactions on Power Systems*, vol. 19, no. 3, pp. 1626-1634, Aug. 2004.

[55]　N. Ruiz, I. Cobelo and J. Oyarzabal, "A Direct Load Control Model for Virtual Power Plant Management," in *IEEE Transactions on Power Systems*, vol. 24, no. 2, pp. 959–966, May 2009.

[56]　D. Huang and R. Billinton, "Impacts of Demand Side Management on Bulk System Reliability Evaluation Considering Load Forecast Uncertainty," *2011 IEEE Electrical Power and Energy Conference*, Winnipeg, MB, 2011, pp. 272–277.

[57]　H. Wu, M. Shahidehpour, A. Alabdulwahab and A. Abusorrah, "Demand Response Exchange in the Stochastic Day-Ahead Scheduling with Variable Renewable Generation," in *IEEE Transactions on Sustainable Energy*, vol. 6, no. 2, pp. 516–525, April 2015

[58]　Mingjian Tuo, Arun Venkatesh Ramesh, Xingpeng Li, "Benefits and Cyber-Vulnerability of Demand Response System in Real-Time Grid Operations," *IEEE Smart Grid Comm,* Tempe, AZ, USA.

[59]　Xingpeng Li and K. W. Hedman, "Enhanced Energy Management System with Corrective Transmission Switching Strategy — Part I: Methodology," *IEEE Transactions on Power Systems*, vol. 34, no. 6, pp. 4490–4502, Nov. 2019.

[60] Xingpeng Li and K. W. Hedman, "Enhanced Energy Management System with Corrective Transmission Switching Strategy — Part II: Results and Discussion," *IEEE Transactions on Power Systems*, vol. 34, no. 6, pp. 4503–4513, Nov. 2019.

[61] E. A. M. Ceseña and P. Mancarella, "Distribution Network Reinforcement Planning Considering Demand Response Support," *2014 Power Systems Computation Conference*, Wroclaw, 2014, pp. 1–7.

[62] A. L. A. Syrri and P. Mancarella, "Reliability Evaluation of Demand Response to Increase Distribution Network Utilization," *2014 International Conference on Probabilistic Methods Applied to Power Systems (PMAPS)*, Durham, 2014, pp. 1–6.

[63] C. Grigg, P. Wong, P. Albrecht, R. Allan, M. Bhavaraju, R. Billinton, Q. Chen, C. Fong, S. Haddad, S. Kuruganty, W. Li, R. Mukerji, D. Patton, N. Rau, D. Reppen, A. Schneider, M. Shahidehpour, C. Singh, "The IEEE Reliability Test System-1996. A report prepared by the Reliability Test System Task Force of the Application of Probability Methods Subcommittee," *IEEE Transactions on Power Systems*, vol. 14, no. 3, pp. 1010–1020, Aug. 1999.

[64] Paris Agreement, 2030 Climate and Energy Framework, [Online]. Available: https://ec.europa.eu/clima/policies/strategies/2030

[65] M. Milligan, "Wind Power Myths Debunked," *IEEE Power Energy Magazine*, vol. 7, no. 6, pp. 89–99, Nov./Dec. 2009

[66] H. Glavitsch, "State of the art review: switching as means of control in the power system," *International Journal Electric. Power Energy System*, vol. 7, no. 2, pp. 92–100, Apr 1985.

[67] A. Nasri, A. J. Conejo, S. J. Kazempour, and M. Ghandhari, "Minimizing Wind Power Spillage using an OPF with FACTS Devices," *IEEE Transaction Power System*, vol. 29, no. 5, pp. 2150–2159, Sep. 2014.

[68] X. Dui, G. Zhu and L. Yao, "Two-Stage Optimization of Battery Energy Storage Capacity to Decrease Wind Power Curtailment in Grid-Connected Wind Farms," *IEEE Transactions on Power Systems*, vol. 33, no. 3, pp. 3296-3305, May 2018.

[69] N. Li and K. Hedman, "Economic Assessment of Energy Storage in Systems with High Levels of Renewable Resources," *IEEE Transactions on Sustainable Energy*, vol. 6, no. 3, pp. 1103–1111, Jul. 2015.

[70] J. C. Villumsen, G. Brønmo and A. B. Philpott, "Line Capacity Expansion and Transmission Switching in Power Systems with Large-Scale Wind Power," *IEEE Transactions on Power Systems*, vol. 28, no. 2, pp. 731–739, May 2013.

[71] N. Li, C. Uçkun, E. M. Constantinescu, J. R. Birge, K. W. Hedman and A. Botterud, "Flexible Operation of Batteries in Power System Scheduling with Renewable Energy," in *IEEE Transactions on Sustainable Energy*, vol. 7, no. 2, pp. 685–696, April 2016.

184

[72] K. W. Hedman, R. P. O'Neill, E. B. Fisher and S. S. Oren, "Optimal Transmission Switching with Contingency Analysis," *IEEE Transactions on Power Systems*, vol. 24, no. 3, pp. 1577–1586, Aug. 2009.

[73] G. Ayala and A. Street, "Energy and Reserve Scheduling with Post-Contingency Transmission Switching," *Electric Power Systems Research*, 2014.

[74] Arun Venkatesh Ramesh, Xingpeng Li, Kory W. Hedman, "An Accelerated-Decomposition Approach for Security-Constrained Unit-Commitment with Corrective Network Reconfiguration," *IEEE Transactions on Power Systems*, vol. 37, no. 2, pp. 887–900, Mar. 2022.

[75] R. Saavedra, A. Street, and J. M. Arroyo, "Day-Ahead Contingency-Constrained Unit Commitment with Co-Optimized Post-Contingency Transmission Switching," *IEEE Transactions on Power Systems*, 2020.

[76] Arun Venkatesh Ramesh and Xingpeng Li, "Reducing Congestion-Induced Renewable Curtailment with Corrective Network Reconfiguration in Day-Ahead Scheduling," *IEEE PES General Meeting*, Montreal, QC, Canada, August 2020.

[77] Nikoobakht, A., Mardaneh, M., Aghaei, J., Guerrero-Mestre, V., Contreras, J., & Nikoobakht, A., "Flexible Power System Operation Accommodating Uncertain Wind Power Generation Using Transmission Topology Control: An Improved Linearized AC SCUC Model," *IET Generation, Transmission and Distribution*, *11*(1), 142–153, 2017.

[78] J. Fuller, R. Ramasra, A. Cha, "Fast Heuristics for Transmission-Line Switching," *IEEE Trans. Power Syst.*, 2012, 27, (3), pp. 1377–1386.

[79] C. Liu, J. Wang, J. Ostrowski, "Heuristic Prescreening Switchable Branches in Optimal Transmission Switching," *IEEE Transactions on Power Systems*, 2012, 27, (4), pp. 2289–2290

[80] M. Soroush, J. Fuller, "Accuracies of Optimal Transmission Switching Heuristics based on DCOPF and ACOPF," *IEEE Transactions on Power Systems*, 2014, 29, (2), pp. 924–932.

[81] A. Papavasiliou, S.S. Oren, Z. Yang, P. Balasubramanian and K. Hedman, "An Application of High Performance Computing to Transmission Switching," *IREP Symposium Bulk Power System Dynamics and Control-IX*, Security and Control of the Emerging Power Grid, 2013, pp. 1–6.

[82] C. Barrows and S. Blumsack, "Transmission Switching in the RTS-96 Test System," *IEEE Transaction on Power Sysem.*, 2012, 276, (2), pp. 1134–1135

[83] G. Schnyder and H. Glavitsch, "Security Enhancement Using an Optimal Switching Power Flow," *IEEE Transactions on Power Systems*, vol. 5, no. 2, pp. 674–681, May 1990.

[84] A. Khodaei and M. Shahidehpour, "Transmission Switching in Security-Constrained Unit Commitment," *IEEE Transactions on Power Systems*, vol. 25, no. 4, pp. 1937–1945, Nov. 2010.

[85] C. Liu, M. Shahidehpour and L. Wu, "Extended Benders Decomposition for Two-Stage SCUC," *IEEE Transactions on Power Systems*, vol. 25, no. 2, pp. 1192–1194, May 2010.

[86] Y. Fu and M. Shahidehpour, "Fast SCUC for Large-Scale Power Systems," *IEEE Transactions on Power Systems*, vol. 22, no. 4, pp. 2144–2151, Nov. 2007.

[87] Yunfeng Wen, Chuangxin Guo, H. Pandzic, and D. Kirschen, "Enhanced Security-Constrained Unit Commitment with Emerging Utility-Scale Energy Storage," *IEEE Transactions on Power Systems*, vol. 31, no. 1, 652–662, Jan. 2016.

[88] M. Abdi-Khorsand, M. Sahraei-Ardakani and Y. M. Al-Abdullah, "Corrective Transmission Switching for N-1-1 Contingency Analysis," *IEEE Transactions on Power Systems.*, vol. 32, no. 2, pp. 1606–1615, March 2017.

[89] Khodayifar, S., Raayatpanah, M., Rabiee, A., Rahimian, H., & Pardalos, P., "Optimal Long-Term Distributed Generation Planning and Reconfiguration of Distribution Systems: An Accelerating Benders' Decomposition Approach," *Journal of Optimization Theory and Applications*, 179(1), 283–310, 2018.

[90] Rodríguez, J., Anjos, M., Côté, P., & Desaulniers, G., "Accelerating Benders decomposition for short-term hydropower maintenance scheduling," *European Journal of Operational Research*, 289(1), 240–253, 2021.

[91] Saberi, H., Amraee, T., Zhang, C., & Dong, Z., "A Heuristic Benders-Decomposition based Algorithm for Transient Stability Constrained Optimal

Power Flow," *Electric Power Systems Research*, 185, 106380, 2020

[92]   Wu, L., & Shahidehpour, M., "Accelerating the Benders Decomposition for Network-Constrained Unit Commitment Problems," *Energy Systems* (Berlin. Periodical), 1(3), 339–376, 2010.

[93]   R. D. Zimmerman, C. E. Murillo-Sanchez, and R. J. Thomas, "MATPOWER: Steady-State Operations, Planning, and Analysis Tools for Power Systems Research and Education," *IEEE Transactions on Power Systems*, vol. 26, no. 1, pp. 12–19, 2011.

[94]   Mingjian Tuo and Xingpeng Li, "Security-Constrained Unit Commitment Considering Locational Frequency Stability in Low-Inertia Power Grids," arXiv:2110.11498, Oct. 2021.

[95]   Jin Lu and Xingpeng Li, "The Benefits of Hydrogen Energy Transmission and Conversion Systems to the Renewable Power Grids: Day-ahead Unit Commitment," arXiv:2206.14279, Jun. 2022.

[96]   Arun Venkatesh Ramesh, Xingpeng Li, "Network Reconfiguration Impact on Renewable Energy System and Energy Storage System in Day-Ahead Scheduling," *2021 IEEE Power & Energy Society General Meeting (PESGM)*, 2021, pp. 1–5, doi: 10.1109/PESGM46819.2021.9638033.

[97]   Cunzhi Zhao and Xingpeng Li, "Microgrid Day-Ahead Scheduling Considering Neural Network based Battery Degradation Model," arXiv:2112.08418, Feb. 2022.

[98] Vasudharini Sridharan, Mingjian Tuo and Xingpeng Li, "Wholesale Electricity Price Forecasting using Integrated Long-term Recurrent Convolutional Network Model," arXiv:2112.13681, Dec. 2021.

[99] Thuan Pham and Xingpeng Li, "Neural Network-based Power Flow Model," *IEEE Green Technologies Conference*, Houston, TX, USA, Mar. 2022.

[100] Mingjian Tuo and Xingpeng Li, "Long-term Recurrent Convolutional Networks-based Inertia Estimation using Ambient Measurements," *IEEE IAS Annual Meeting*, Detroit, MI, USA, Oct. 2022.

[101] Thuan Pham and Xingpeng Li, "Reduced Optimal Power Flow Using Graph Neural Network," arXiv:2206.13591, Jun. 2022.

[102] V. Nair, S. Bartunov, F. Gimeno, I. von Glehn, P. Lichocki, I. Lobov, B. O'Donoghue, N. Sonnerat, C. Tjandraatmadja, P. Wang, R. Addanki, T. Hapuarachchi, T. Keck, J. Keeling, P. Kohli, I. Ktena, Y. Li, O. Vinyals, Y. Zwols, "Solving Mixed Integer Programs using Neural Networks," arXiv:2012.13349, Dec 2020.

[103] X. Lin, Z. J. Hou, H. Ren and F. Pan, "Approximate Mixed-Integer Programming Solution with Machine Learning Technique and Linear Programming Relaxation," *2019 3rd International Conference on Smart Grid and Smart Cities (ICSGSC)*, 2019, pp. 101–107, doi: 10.1109/ICSGSC.2019.00-11.

[104] J. Qin, N. Yu and Y. Gao, "Solving Unit Commitment Problems with Multi-Step

Deep Reinforcement Learning," *2021 IEEE International Conference on Communications, Control, and Computing Technologies for Smart Grids (SmartGridComm)*, 2021, pp. 140–145, doi: 10.1109/SmartGridComm51999.2021.9632339.

[105] F. Li, J. Qin and W. X. Zheng, "Distributed Q-Learning-Based Online Optimization Algorithm for Unit Commitment and Dispatch in Smart Grid," in *IEEE Transactions on Cybernetics*, vol. 50, no. 9, pp. 4146–4156, Sept. 2020, doi: 10.1109/TCYB.2019.2921475.

[106] Y. Yang, X. Lu, and L Wu. "Integrated Data-Driven Framework for Fast SCUC Calculation, " *IET Generation, Transmission & Distribution*, vol. 14, no. 24, pp. 5728-5738, Dec. 2020.

[107] S. Pineda, J. M. Morales, and A. Jiménez-Cordero, "Data-Driven Screening of Network Constraints for Unit Commitment," *IEEE Transactions on Power Systems*, vol. 35, no. 5, pp. 3695–3705, Sept. 2020.

[108] G. Dalal, E. Gilboa, S. Mannor, and L. Wehenkel, "Unit Commitment using Nearest Neighbor as a Short-Term Proxy," in *Proceedings on 20th Power System Computing Conference*, 2018, doi: 10.23919/PSCC.2018.8442516.

[109] F. Mohammadi, M. Sahraei-Ardakani, D. N. Trakas and N. D. Hatziargyriou, "Machine Learning Assisted Stochastic Unit Commitment During Hurricanes with Predictable Line Outages," in *IEEE Transactions on Power Systems*, vol. 36, no. 6, pp. 5131–5142, Nov. 2021.

[110] F. Mohammadi, M. Sahraei-Ardakani, D. N. Trakas and N. D. Hatziargyriou, "Machine Learning Assisted Stochastic Unit Commitment: A Feasibility Study," *2020 52nd North American Power Symposium (NAPS)*, 2021, pp. 1–6, doi: 10.1109/NAPS50074.2021.9449789.

[111] A. Porras, S. Pineda, J. M. Morales and A. Jimenez-Cordero, "Cost-driven Screening of Network Constraints for the Unit Commitment Problem," in *IEEE Transactions on Power Systems*, doi: 10.1109/TPWRS.2022.3160016.

[112] S. Zhang, H. Ye, F. Wang, Y. Chen, S. Rose and Y. Ma, "Data-Aided Offline and Online Screening for Security Constraint," in *IEEE Transactions on Power Systems*, vol. 36, no. 3, pp. 2614–2622, May 2021, doi: 10.1109/TPWRS.2020.3040222.

[113] Y. Yang, Z. Yang, J. Yu, K. Xie and L. Jin, "Fast Economic Dispatch in Smart Grids Using Deep Learning: An Active Constraint Screening Approach," in *IEEE Internet of Things Journal*, vol. 7, no. 11, pp. 11030–11040, Nov. 2020, doi: 10.1109/JIOT.2020.2993567.

[114] F. Hasan and A. Kargarian, "Topology-aware Learning Assisted Branch and Ramp Constraints Screening for Dynamic Economic Dispatch," in *IEEE Transactions on Power Systems*, doi: 10.1109/TPWRS.2022.3142957.

[115] S. Schmitt, I. Harjunkoski, M. Giuntoli, J. Poland and X. Feng, "Fast Solution of Unit Commitment Using Machine Learning Approaches," *2022 IEEE 7th International Energy Conference (ENERGYCON)*, 2022, pp. 1–6, doi:

10.1109/ENERGYCON53164.2022.9830191.

[116]	T. Iqbal, H. U. Banna, A. Feliachi and M. Choudhry, "Solving Security Constrained Unit Commitment Problem Using Inductive Learning," *2022 IEEE Kansas Power and Energy Conference (KPEC)*, 2022, pp. 1–4, doi: 10.1109/KPEC54747.2022.9814780.

[117]	T. Iqbal, H. U. Banna and A. Feliachi, "AI-Driven Security Constrained Unit Commitment Using Eigen Decomposition and Linear Shift Factors," *2021 North American Power Symposium (NAPS)*, 2021, pp. 1–6, doi: 10.1109/NAPS52732.2021.9654579.

[118]	Arun Venkatesh Ramesh and Xingpeng Li, "Machine Learning Assisted Model Reduction for Security-Constrained Unit Commitment," *North American Power Symposium (NAPS)*, Salt Lake, Utah, 2022.

[119]	A.S. Xavier, F. Qiu, S. Ahmed, "Learning to Solve Large-Scale Security-Constrained Unit Commitment Problems," *INFORMS Journal on Computing*, 2020.

[120]	Y. Zhou, Q. Zhai, L. Wu and M. Shahidehpour, "A Data-Driven Variable Reduction Approach for Transmission-Constrained Unit Commitment of Large-Scale Systems," in *Journal of Modern Power Systems and Clean Energy*, doi: 10.35833/MPCE.2021.000382.

[121]	T. Wu, Y. -J. Angela Zhang and S. Wang, "Deep Learning to Optimize: Security-Constrained Unit Commitment with Uncertain Wind Power Generation and

BESS," in *IEEE Transactions on Sustainable Energy*, vol. 13, no. 1, pp. 231–240, Jan. 2022, doi: 10.1109/TSTE.2021.3107848.

[122] M. Li, W. Wei, Y. Chen, M. -F. Ge and J. P. S. Catalão, "Learning the Optimal Strategy of Power System Operation with Varying Renewable Generations," in *IEEE Transactions on Sustainable Energy*, vol. 12, no. 4, pp. 2293–2305, Oct. 2021, doi: 10.1109/TSTE.2021.3088951.

[123] T. Xu; A. B. Birchfield; K. S. Shetye; T. J. Overbye, "Creation of Synthetic Electric Grid Models for Transient Stability Studies," *2017 IREP Symposium Bulk Power System Dynamics and Control,* Espinho, Portugal, 2017.

[124] F. Pedregosa, G. Varoquaux, A. Gramfort, V. Michel, B. Thirion, O. Grisel, M. Blondel, P. Prettenhofer, R. Weiss, V. Dubourg, J. Vanderplas, A.Passos, D. Cournapeau, M. Brucher, M. Duchesnay, "Scikit-learn: Machine learning in Python," in *Journal of Machine Learning Research* 12 (2011): 2825–2830.

[125] K-Nearest Neighbors Model, SCIKIT, [Online]. Available: https://scikit-learn.org/stable/modules/generated/sklearn.neighbors.KNeighborsClassifier.html

[126] Random Forest Model, SCIKIT, [Online]. Available: https://scikit-learn.org/stable/modules/generated/sklearn.ensemble.RandomForestClassifier.html

[127] Logistic Regression Model, SCIKIT, [Online]. Available: https://scikit-learn.org/stable/modules/generated/sklearn.linear_model.LogisticRegression.ht

ml

[128] Multi-Layer Perceptron Model, SCIKIT, [Online]. Available: https://scikit-learn.org/stable/modules/generated/sklearn.neural_network.MLPClassifier.html

[129] Lecture on Supervised Learning, Machine Learning Course, Andrew NG [online]. Available: http://cs229.stanford.edu/materials.

[130] A.Y. Ng and M.I. Jordan, "On Discriminative vs. Generative Classifiers: A Comparison of Logistic Regression and Naive Bayes," *Advances in Neural Information Processing Systems,* pp. 841–848, 2002.

[131] Arun Venkatesh Ramesh and Xingpeng Li, "Feasibility Layer aided Machine Learning Approach for Day-Ahead Operations," Available: arXiv:2208.06742, Aug. 2022.